CEDIM Forensic Disaster Analysis (FDA) Group

Heat wave June 2026 | Western and Central Europe

Report No. 1

Information as of 07 July 2026

DOI: 10.5445/IR/1000195086

Authors: Susanna Mohr[1], Susanne Benz[1], Denise Böhnke[1], Hüseyin Çakmak[1], Jan Cermak[1], Haozhen Cheng[1], Ines Dillerup[1], Uwe Ehret[1], Gabriel Fink[2], Jannick Fischer von zur Gathen[1], Sarah Ho[1], Julian Hoffmann[1], Emma Holmberg[3], Tatiana Klimiuk[1], Alexander Lemburg[1], Patrick Ludwig[1], Bernhard Mühr[4], Joaquim Pinto[1], Sonja Rosenberg[1], Andrew Ross[5], Andreas Schäfer[1,6], Johannes Schuhmacher[1], Christian Sperka[1], Michael Kunz[1]

[1] *Karlsruhe Institute of Technology (KIT)*
[2] *Landesanstalt für Umwelt Baden-Württemberg (LUBW)*
[3] *University of Bern*
[4] *EWB Wetterberatung GmbH*
[5] *Forschungszentrum Jülich (FZJ)*
[6] *Risklayer GmbH*

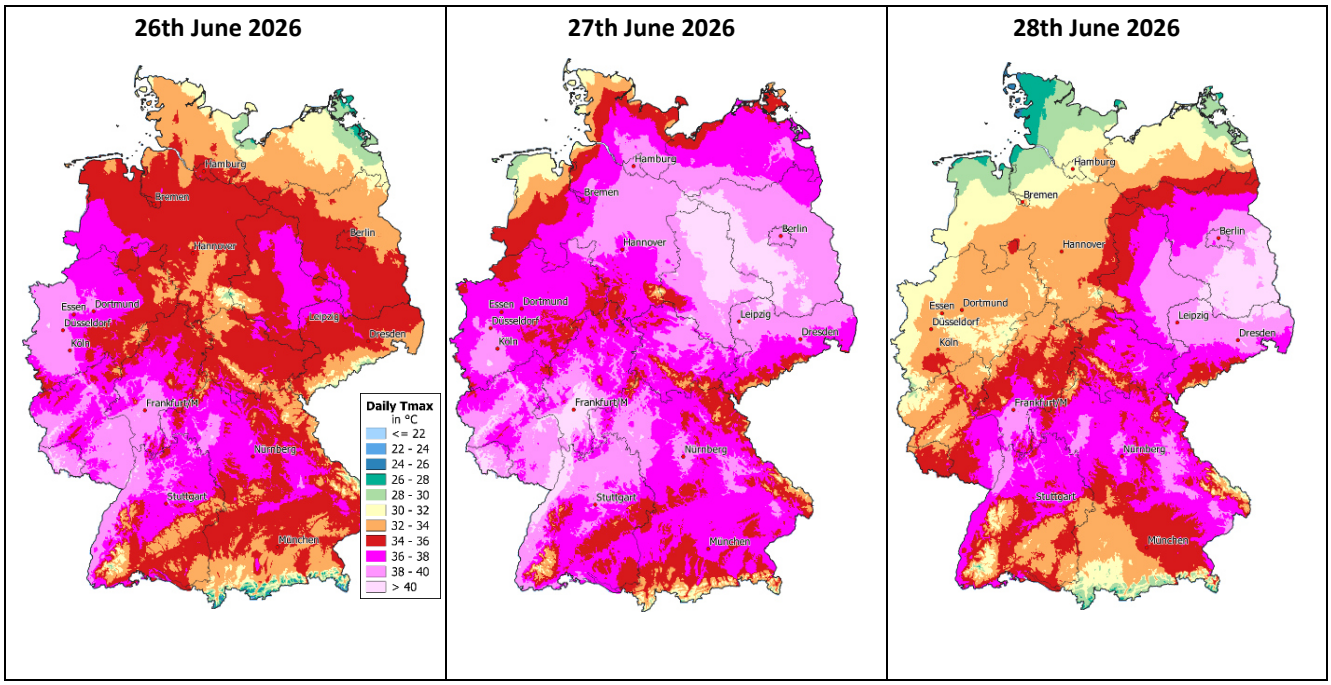

Fig. 1: Daily maximum temperatures during the peak of the June 2026 heat wave in Germany (26th to 28th June 2026; Data: HYRAS, DWD).

Table of content

1. Summary

The June 2026 heat wave was one of the most exceptional heat events ever observed in Europe. It affected large parts of Western, Central and Southern Europe between 13 and 29 June and was characterized by record-breaking daytime temperatures, exceptionally warm nights and prolonged heat exposure. The event developed under a **blocking-dominated circulation**, including an omega-blocking phase, which disrupted the westerly flow and enabled repeated advection of very warm subtropical air into Europe. Although the blocking was sufficient to sustain the heat wave, it was less persistent and less stable than classical high-latitude blocking events.

Across Europe, numerous countries recorded new June or all-time **temperature records**. New national all-time records were reported, with some still subject to official verification, in countries such as Germany (41.8 °C), Denmark (37.0 °C), Poland and the Czech Republic, while several other countries, including Austria, Hungary and the Netherlands, experienced unprecedented June temperatures. France was particularly affected by the duration of the event, with almost ten consecutive days exceeding 40 °C in parts of the country. Germany experienced three consecutive days above 40 °C, while exceptionally warm nights culminated in a new national minimum-temperature record of 29.4 °C. Long-term analyses show that the June 2026 event established new daytime temperature records across an exceptionally large fraction of Europe, while nighttime temperatures were likewise historically extreme.

In addition to the large-scale circulation, elevated Mediterranean **sea surface temperatures** likely contributed to atmospheric moisture availability and the broader heat-stress environment. During the event, sea surface temperatures intensified markedly, with local anomalies exceeding 8 K in parts of the western and central Mediterranean. Although **atmospheric moisture anomalies** were less exceptional than the temperature anomalies, the combination of extreme heat and elevated humidity substantially increased human heat stress. **Thunderstorms**, while widespread and frequent, were mostly small and poorly organized, resulting in localized and short-lived severe weather rather than long-lived high-impact systems, with a few exceptions of large hail and severe wind gusts.

Beyond meteorological records, the heat wave produced widespread **impacts across multiple sectors**. **Hydrologically**, exceptionally high river water temperatures occurred unusually early in the year, reflecting both the acute heat event. Low groundwater levels and historically low lake levels, particularly in southern Germany, further highlighted increasing hydrological stress. In addition, **soil moisture deficits** and moisture-limited land-atmosphere coupling likely amplified near-surface heating in affected regions. River temperatures reached record values that pose growing risks for aquatic ecosystems, industrial cooling and energy infrastructure.

The heat wave also had pronounced effects on the German **energy system**. Meteorological conditions during the event were characterized by substantially increased surface solar irradiance (+31.2 %) and land surface temperatures (+5.4 K), combined with persistently weak winds (-28.6 %). This led to a marked shift in the renewable generation mix: photovoltaic (PV) generation increased by approximately 31 %, more than compensating for potential efficiency losses caused by elevated PV module temperatures, while wind power generation declined substantially over an extended period. Despite the exceptional heat, total electricity demand in Germany increased by only 1.8 %, indicating that cooling demand currently plays a comparatively minor role in determining German summer peak loads. Other countries, especially France, showed a stronger cooling-related load response.

Nevertheless, the heat wave placed noticeable stress on **electricity markets**. During the late afternoon and evening, declining solar generation coincided with persistently low wind power output and elevated cooling-related electricity demand, resulting in steeper residual-load ramps and temporary electricity price spikes across interconnected European markets. Beyond renewables, high river and air temperatures also affected thermal generation: French **nuclear output** was temporarily reduced because of river-temperature constraints, while several **gas-fired power plants** in the United Kingdom faced cooling-related restrictions.

The June 2026 heat wave had substantial implications for **human health**, as prolonged extreme temperatures exposed large parts of the European population to severe heat stress. A multi-scale assessment combining urban

observations, population exposure analyses, building simulations, labor-productivity estimates and the current understanding of heat-related mortality demonstrates that impacts extended far beyond outdoor air temperatures alone. In Karlsruhe, persistent **heat exposure** was amplified by pronounced nighttime urban warming, with densely built-up areas experiencing the longest periods of thermal stress and limited nocturnal recovery. At the continental scale, hundreds of millions of people were exposed to temperatures above critical thresholds for several days, with the longest and most intense exposures concentrated across Southern and Western Europe.

Building simulations further showed that even modern residential buildings may experience severe overheating during prolonged heat waves without effective heat mitigation strategies, highlighting the importance of solar protection, ventilation and adaptive building operation. Extreme heat conditions also reduced potential **labor productivity**, particularly for outdoor and physically demanding work. Reliable **mortality** estimates were not yet available at the time of reporting, but the early-season timing, prolonged exposure and high nocturnal temperatures indicate a substantial risk of excess heat-related mortality, especially among vulnerable populations. Overall, the event illustrates the growing importance of heat adaptation strategies across urban planning, buildings, workplaces, healthcare systems and early warning services.

The heat wave also affected **transport infrastructure** across Europe. Germany experienced the most severe road damage, with thermal expansion causing blow-ups of older concrete motorway pavements and requiring motorway closures and emergency repairs. Rail transport was disrupted in several countries, including Germany, France, Belgium and the United Kingdom, due to track deformation, overheating of technical systems and precautionary speed restrictions.

Overall, the June 2026 heat wave illustrates how sufficiently persistent blocking-like circulation patterns can trigger compound impacts across natural and human systems. The event combined record-breaking daytime temperatures, limited nocturnal cooling and widespread societal impacts, providing another clear indication that extreme heat is becoming an increasingly important climate risk for Europe. Continued adaptation of infrastructure, buildings, water management, healthcare systems and early warning services will therefore be essential to reduce future heat-related impacts.

2. Meteorological information

2.1. Analysis of large-scale pressure pattern

2.1.1. Onset of the heat wave: 13rd to 15th June 2026

At the 500 hPa geopotential level, a ridge began to slowly form on 13rd June 2026. Initially, it extended - still not very pronounced - from the Iberian Peninsula across the Bay of Biscay to the area west of Ireland. Figure 2 (left) shows the geopotential pattern at the 500 hPa level, averaged over the period 13rd to 15th June 2026. The ridge is flanked by an area of low geopotential over the sea south of Greenland. An upper-level trough over northeastern Europe appears significantly stronger; its axis extends from Scandinavia across the central Baltic Sea to the Baltic States and on to Ukraine. Along its western flank, cold maritime air extends far to the south, resulting in below-average temperatures across large parts of Central Europe, including Germany. Figure 2 (right) illustrates the anomaly in the geopotential pattern at the 500 hPa level for the averaged period of June 13–15, 2026. The upper-level low in the west and the upper-level trough in the east each stand out distinctly as areas where the geopotential is 12 to 16 gpdam lower than during the 1991–2020 reference period. The upper-level ridge arching over southwestern Europe is accompanied by a positive geopotential anomaly of 8 to 12 gpdam in the three-day average.

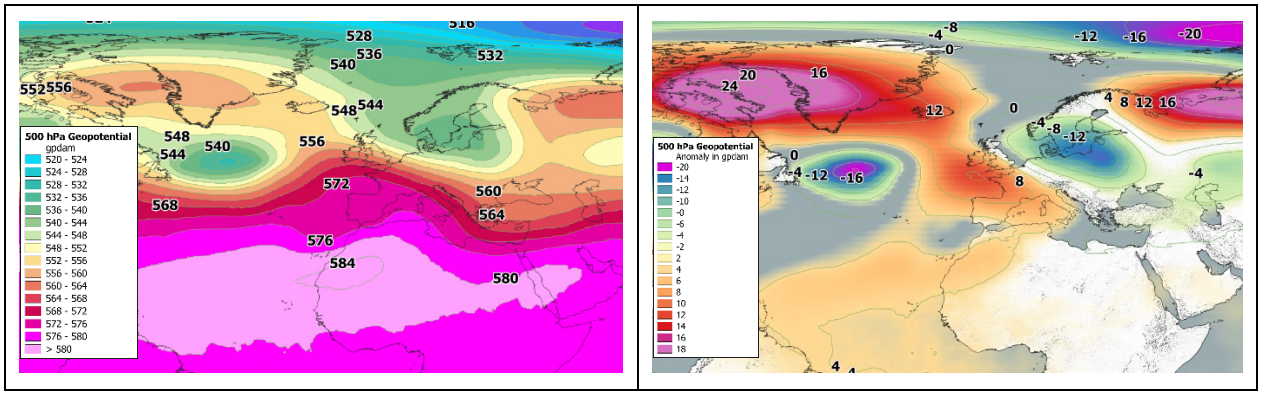

Fig. 2: Analysis of the 500 hPa geopotential height at the start of the heat wave. 3-day average of the 00Z analyses from **13rd to 15th** *June 2026 (left). Deviation of the 500 hPa geopotential height from the 1991 to 2020 long-term average (right; Data: https://cds.climate.copernicus.eu/).*

2.1.2. Timeline and peak of the heat wave: 16th to 29th June 2026

Figure 3 (left) strikingly shows a broad and powerful ridge for the averaged period from 16th to 26th June 2026. The fact that the ridge is so clearly visible even when averaged over a period of nearly two weeks demonstrates its persistence and minimal tendency to shift. The ridge arches with its axis extending from the central Mediterranean region through France and Germany to southern Sweden. To the west of the ridge, a well-defined trough appears off the coast of the Iberian Peninsula. Another trough is located over southeastern Europe, with its axis extending from the Black Sea to the Aegean Sea and into the eastern Mediterranean region. The large-scale geopotential pattern, consisting of a massive central ridge and two flanking troughs, proved to be exceptionally stable in its basic features. It can also be described as an “Omega” pattern (see further details in Section 2.3). A geopotential pattern of this nature, duration, and intensity is otherwise only observed in winter. Over Germany, France, the Benelux countries, Denmark, and the southern North Sea, the anomalies in the 500-hPa geopotential level reached values of more than 16 gpdam over a wide area (Figure 3, right). Between the axis of the trough in front of the Iberian Peninsula and the ridge, a strong southerly flow allowed the hot African air to enter France and Central Europe.

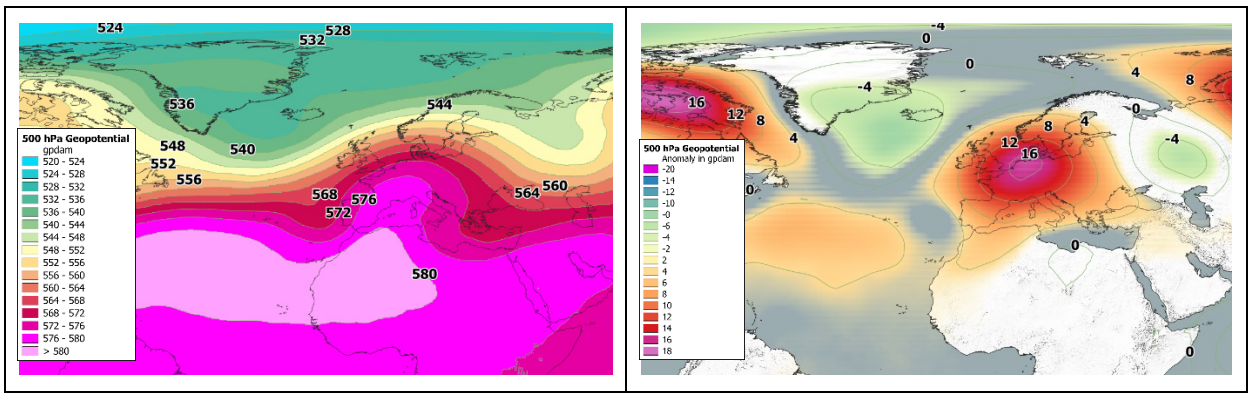

Fig. 3: Analysis of the 500 hPa geopotential height during the heat wave. 14-day average of the 00Z analyses from **16th to 29th** *June 2026 (left). Deviation of the 500 hPa geopotential height from the 1991 to 2020 long-term average (right; Data: https://cds.climate.copernicus.eu).*

2.2. Analyses of air masses at the 850 hPa geopotential level

Distinctive pressure areas always result in significant air mass transport. Over Central Europe from 13rd to 15th June 2026, the initial air mass was cold maritime air, accompanied by temperatures at the 850 hPa level of less than 10 °C (Fig. 4). On 15th June, air temperature anomalies over parts of Germany and Poland were below -5 K. A first warm-air surge manifested itself on 13rd and 14th June, with temperatures exceeding 20 °C at the 850 hPa level over the Iberian Peninsula. This corresponded to temperatures 5 to 10 K above seasonal norms over western France and northern Spain. Over the next two days, the 20-degree isotherm shifted toward Algeria, allowing slightly cooler air to briefly prevail in southwestern Europe.

On 17th to 19th June, temperatures over Spain and southwestern France at an altitude of about 1,500 meters were again in the range of 20 to 22 °C. However, the transport of warm air really gained momentum starting on 20th June, when a new and massive bubble of warm air began moving northward from North Africa. By 23rd June, the area with 850 hPa temperatures of 25 to 30 °C had spread across all of Spain, the Bay of Biscay, and northwestern France. On 24th June, the warm-air bubble began to detach from the North African reservoir and, as an independent system, slowly moved eastward along the upper-level ridge while gradually cooling. On 26th June, the area with 850 hPa temperatures of 20 to 25 °C covered central France, southern England, and western Germany. By 28th June, its center had shifted to eastern Germany, and it finally turned toward southeastern Europe on 29th June. Figure 4 shows the analysis of temperatures at the 850 hPa level (approximately 1,500 meters) for each day of the period from 13rd to 29th June. The dark red and purple areas indicate regions with a temperature of at least 24 °C.

Figure 5 illustrates the deviation of the temperature at the 850 hPa level from the 1991 to 2020 long-term average. It shows the air temperature anomalies for the period 13rd to 29th June 2026, at 00 UTC and relative to the 1991 to 2020 reference period. However, only those areas where the deviation from the norm exceeds ±3 K are shown. The deviations in the 850 hPa air temperature become increasingly larger as the warm air bubble shifts northward and eastward, penetrating into areas that are normally significantly colder, such as northern France, Germany, England, or Denmark. If the deviation of the 850 hPa temperature from the norm is used as a measure of the heat wave's intensity, then the heat wave peaked from 23rd to 28th June. On these days, air temperature anomalies at an altitude of approximately 1,500 meters exceeded +15 K in some areas.

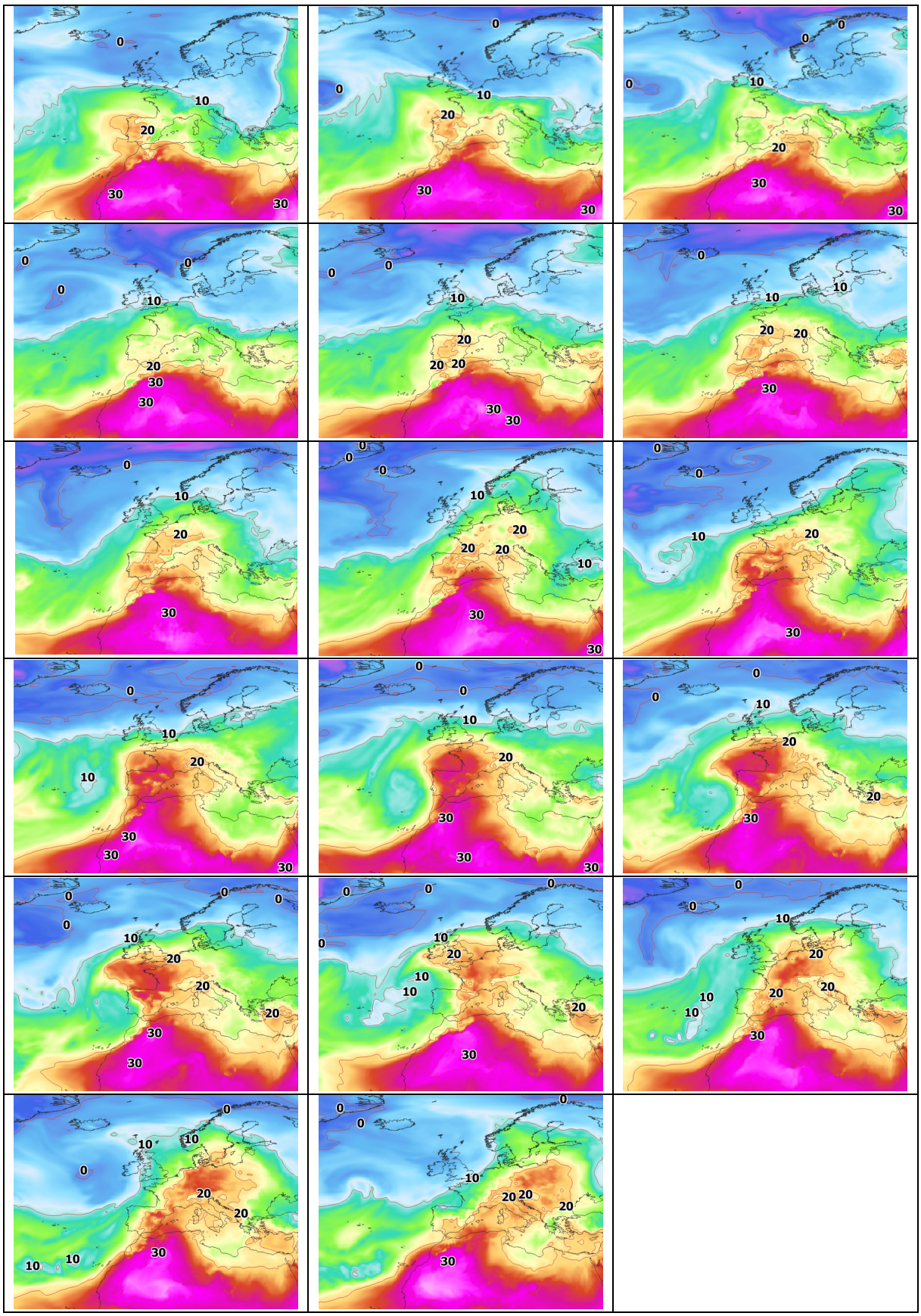

Fig. 4: Analysis of temperature at 850 hPa (Period: 13rd to 29th June 2026, at 00 UTC; Data: ERA5. Data source: https://cds.climate.copernicus.eu).

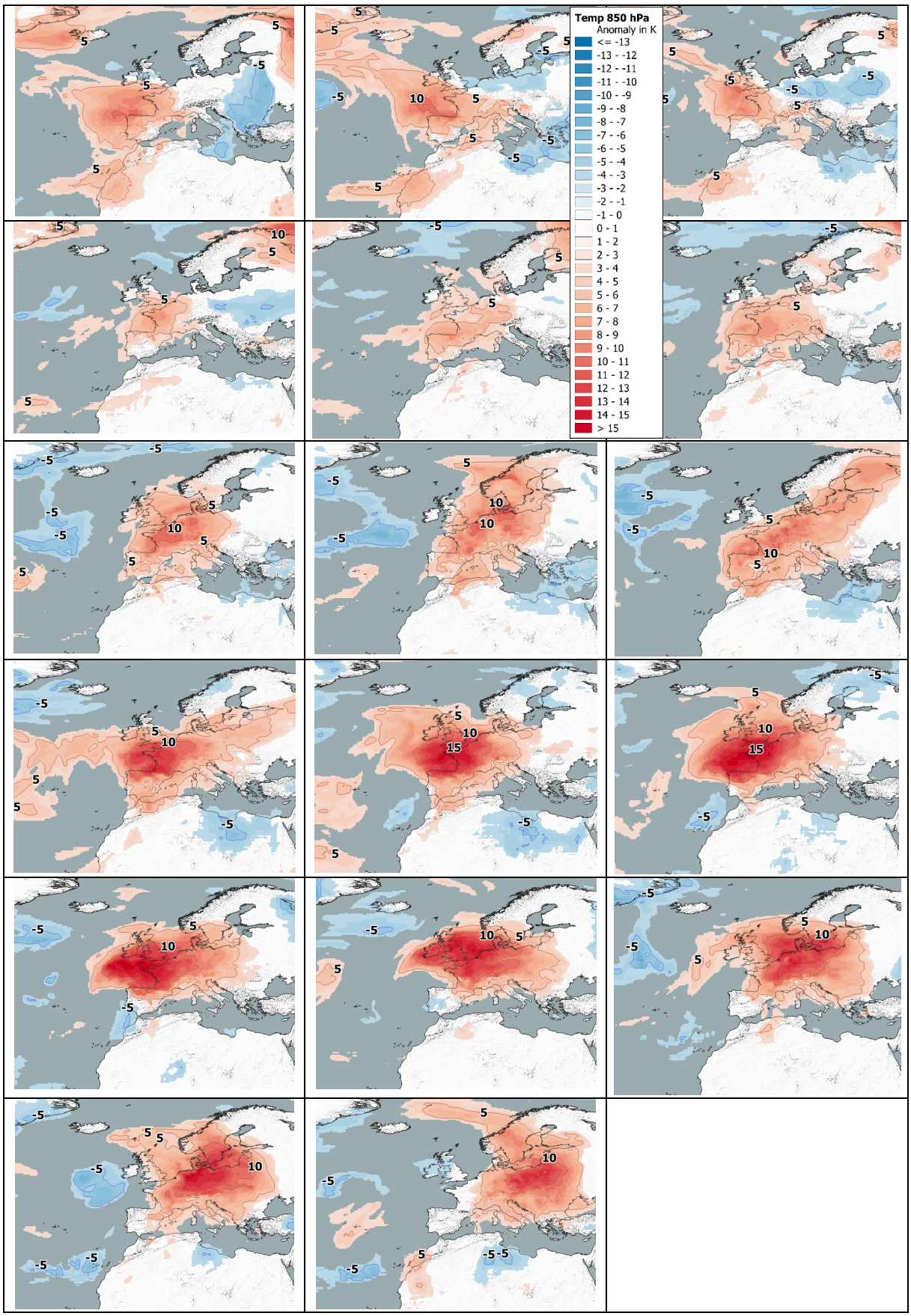

Fig. 5: Analysis of the deviation of the temperature at 850 hPa from the 1991 to 2020 long-term average. Only temperature anomalies greater than ±3 K are shown (Period: 13rd to 29th June 2026, at 00 UTC*; Data: ERA5. Data source: https://cds.climate.copernicus.eu*).

2.3. Evolution of the large-scale atmospheric circulation

At the beginning of the second half of June, the large-scale atmospheric circulation over the North Atlantic and Europe thus slowly shifted towards an anomalous state, which increasingly favored the development of a heat wave over Western and Central Europe. While on the 14th and 15th June a pronounced trough over Eastern Europe was still causing rather cool and humid weather conditions over large parts of Central Europe (see Fig. 2), a ridge begins to amplify over western Europe two days later (Fig. 6, red contours). On the 19th June, this atmospheric ridge further amplified and evolved into a rather persistent Omega blocking, which is often referred to in the media as "heat dome" (Fig. 3 and Fig. 6, green contours). This large-scale circulation pattern is characterized by a strong anticyclone often flanked by low-pressure systems to the west and the east, resulting in a poleward displacement of the jet stream and persistent atmospheric conditions (e.g., Kautz et al., 2022; see their Fig. 2b).

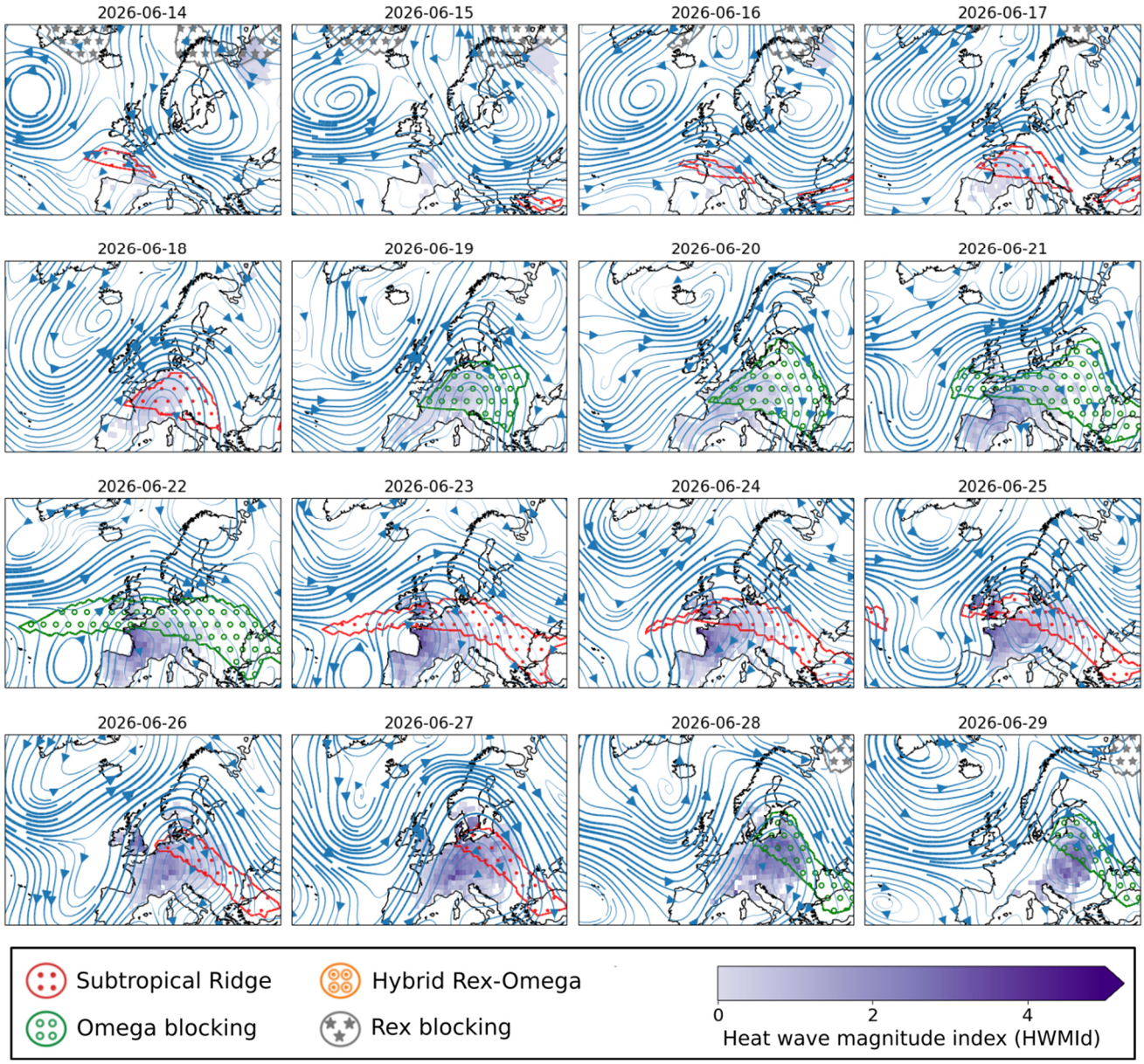

Fig. 6: Relationship between the heat wave over Western and Central Europe and the large-scale atmospheric circulation from mid- to late June 2026. The streamlines show the atmospheric circulation at the 500 hPa pressure level (approximately 5500 m altitude). Areas with anomalous circulation detected by an objective algorithm (Lima et al., 2026; based on earlier work by Sousa et al., 2021) are highlighted by different colors of hatching (see legend). The purple color shading highlights grid points where heat waves are recorded by means of the Heat Wave Magnitude Index daily (HWMId; Russo et. al, 2015) metric (the darker the color, the more intense the heat). The analyses are based on 500 hPa zonal and meridional wind, 500 hPa geopotential and 2 m maximum temperature data from the ERA5 reanalysis. Due to the normal delay in reanalysis production, data from the ECWMF IFS analysis was used for the days of 27th to 29th June.

In the areas influenced either by a pronounced ridge or Omega blocking, there is a strongly increased likelihood of above-average temperatures (e.g., Kautz et al., 2022). The anomalous warming of air masses is attributable to the combined effects of air mass transport, subsidence, intense solar radiation, and soil moisture depletion. (Kautz et a., 2022, Lemburg et al., 2026). While the horizontal transport of air from climatologically warmer regions may play a role, in most cases the vertical movement of air masses is more important. As air masses are dynamically forced to descend within a high-pressure system, they are warmed substantially by adiabatic compression. Moreover, the warming of the subsiding air masses also results in clear skies and, consequently, increased solar radiation at the surface. Especially when soils are dry and most of the net radiative energy is partitioned into sensible heat, more and more heat is accumulated in the overlaying air masses.

Over the next few days, the Omega blocking remains mostly stationary, continuously affecting large parts of Western and Central Europe. A rather remarkable development is the pinching off of a trough over the North Atlantic, leading to the formation of a rather stagnant cut-off low west of Iberia which may have amplified warm air advection and fostered the blocking over the European continent. The used objective algorithm tends to switch back and forth between classifying the large-scale circulation anomaly either as a subtropical ridge or an Omega blocking. This is a consequence of the fact that the northward displacement of the jet stream was rather limited in this case, which also kept large parts of Scandinavia unaffected by this heat wave.

The heat wave culminated in magnitude around the 27th and 28th June -- during a time, when the large-scale weather patterns first began to become less stagnant again. The ridge, formerly centered on France, began to move eastwards, shifting the heat wave peak from France to Eastern Germany. On the final day of June, the ridge has propagated further eastward, allowing westerly winds to finally terminate the heat wave in most parts of Europe.

2.4. Weather regimes and atmospheric persistence

A complementary way to describe the atmospheric circulation is to classify each day's large-scale weather pattern into one of seven characteristic weather regimes, following the classification of Grams (2026) spatial fields are displayed in Figure 7. If the atmospheric circulation does not closely resemble any of these seven patterns, it is assigned to the "no regime" category.

During the June heat wave, the atmospheric circulation underwent a transition through a series of distinct weather regimes (Fig. 8). At the onset of the heat wave, the atmospheric circulation was dominated by the Greenland Blocking regime, characterized by a high-pressure anomaly over Greenland and a lower-latitude jet stream that remained only weakly disrupted over Central Europe. At the same time, the Atlantic Trough regime, a more transient pattern featuring a low-pressure system near the British Isles, was also present, thereby supporting the development of a ridge over Europe until around 19th June. Consequently, the initial phase of the heat wave developed under atmospheric conditions that were not particularly stagnant.

Around 20th June, the formation of a cut-off low marked a transition toward a more typical omega blocking pattern. This was reflected by the dominance of the European Blocking regime, in which the westerly winds are strongly disrupted. From 24th June onward, the Zonal regime became increasingly mixed with the European Blocking regime. While the Zonal regime also features a northward displacement of the westerlies, this disruption is weaker than during European Blocking. By the peak and final stage of the heat wave, the Zonal regime had become the dominant circulation pattern.

The atmospheric persistence shown in Figure 9, describes how long an atmospheric circulation pattern remains similar to itself and sticks around in a very similar way (Faranda et al., 2024). Consistent with the weather regime evolution, persistence during the heat wave was generally not exceptional. Only around June 21st, when the European omega blocking was most pronounced, the atmosphere exhibited unusually persistent atmospheric conditions.

Overall, the atmospheric circulation during the June heat wave was characterized by a disruption of the westerly winds associated with blocking. However, the blocking remained relatively far south and did not extend into the high latitudes, making it less persistent and less stable than is typical of long-lived, high-latitude blocking events.

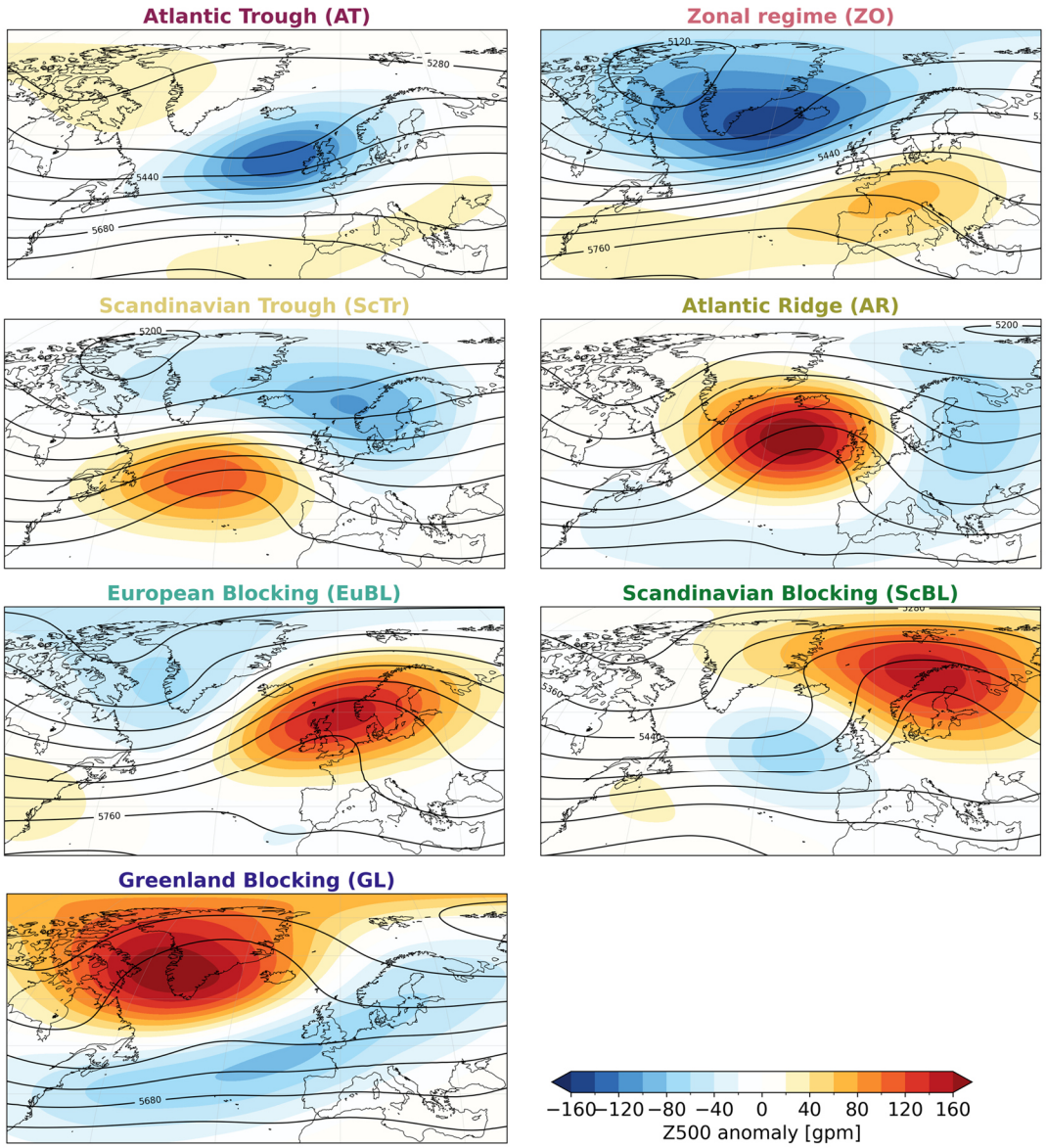

Fig. 7: The seven weather regime clusters (Grams, 2026). Together, these characteristic circulation patterns represent most of the variability of the mid-tropospheric atmospheric circulation (500 hPa). Black contours show the geopotential height, while shading indicates geopotential height anomalies (positive anomalies (red) correspond to a high-pressure system and negative anomalies (blue) to a low-pressure system.

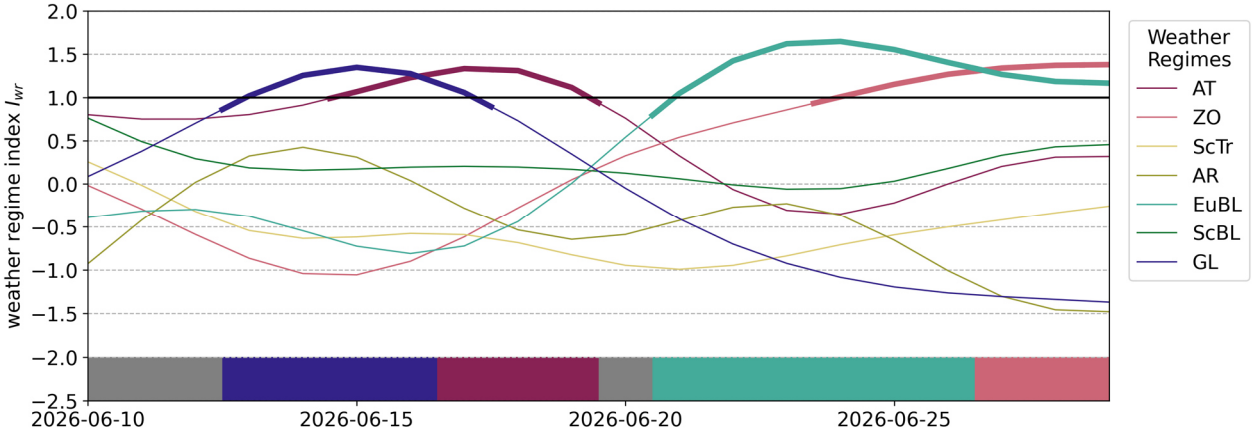

Fig. 8: Classification of the atmospheric circulation during the heat wave into the closest matching weather regime (see Fig. 7). The weather regime index measures how closely the daily atmospheric circulation resembles each of the seven weather regime clusters. Values greater than 1 indicate a close match to the corresponding weather regime. The colored bar at the bottom shows the dominant weather regime for each day. Days for which none of the weather regimes is dominant are classified as no regime. The computation is based on 500hPa geopotential data from the ERA5 reanalysis. Due to the normal delay in reanalysis production, data from the ECWMF IFS analysis was used for the days of 27th - 29th June.

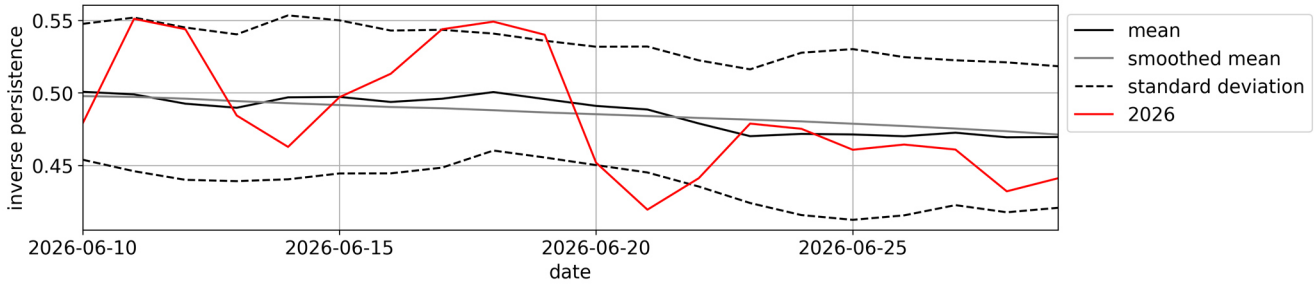

Fig. 9: Inverse persistence of the atmospheric circulation during the June 2026 heat wave compared with the climatology. Smaller values indicate that the atmospheric circulation remains more similar to itself over time and is therefore more persistent. The climatology is based on the daily mean for 1950–2025 (solid black line), smoothed using a running window (grey line). The dashed black lines show one standard deviation around the climatological mean. The red line shows the inverse persistence during the 2026 heat wave. The computation is based on 500hPa zonal and meridional wind data from the ERA5 reanalysis. Due to the normal delay in reanalysis production, data from the ECWMF IFS analysis was used for the days of 27th to 30th June.

2.5. Analyses of sea surface temperature at the start of and during the heat wave

On the first day of the heat wave, 13rd June, sea surface temperatures (SSTs) across much of the Mediterranean were already above average. SSTs reached around 24 °C in the central and eastern Mediterranean, while the western Mediterranean was slightly cooler, with temperatures below 20 °C near the Rhône estuary (Fig. 10, top). Relative to the 1991 to 2020 climatology, most of the basin exhibited positive SST anomalies of 1 to 3 K, with only localized negative anomalies in parts of the Aegean Sea, around Cyprus, and near the Rhône mouth.

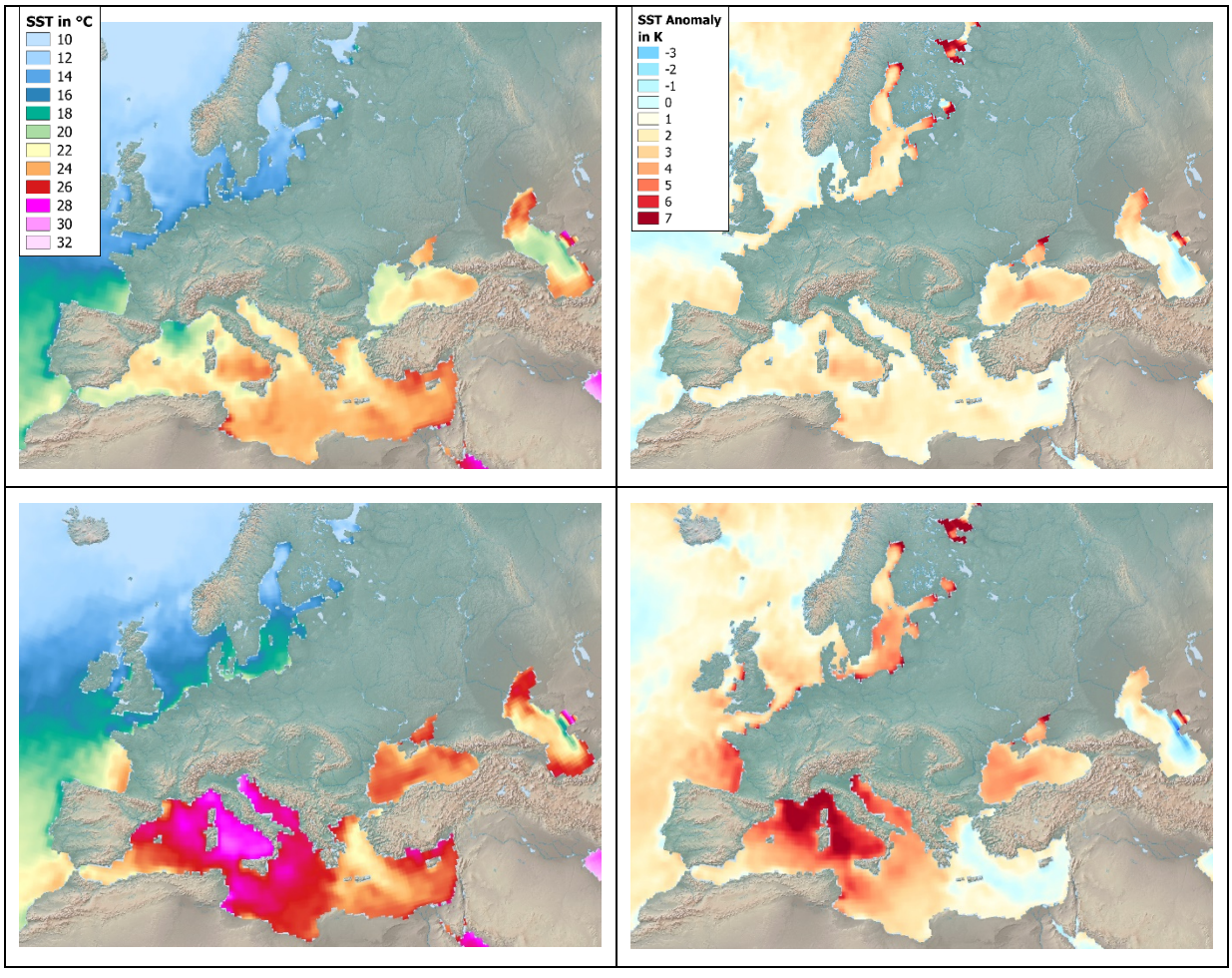

Fig. 10: Analysis of the sea surface temperature (left) and the deviation from the 1991 to 2020 long-term average (right). Shown at the start of the heat wave on 13rd June (top) and during the heat wave on 26th June 2026 (bottom; Data: https://www.ncei.noaa.gov).

Although these moderately elevated SSTs may have supported the development of the heat wave, the persistent high air temperatures and intense solar radiation during the following two weeks caused a rapid warming of the Mediterranean Sea itself. At the peak of the heat wave in Central Europe (Fig. 10 below), exceptionally high SSTs were observed across the western and central Mediterranean. Temperatures exceeded 28 °C in the Tyrrhenian Sea, between the Balearic Islands and Corsica, and in the northern Adriatic, corresponding to local anomalies of more than 8 K above the 1991 to 2020 average

In contrast, the eastern Mediterranean experienced markedly different conditions (Fig. 10 below). A quasi-stationary upper-level trough (see Fig. 6) maintained relatively cool and unsettled weather, while northerly flow associated with a low-pressure system advected cooler air into the region. Increased cloud cover and reduced incoming solar radiation limited surface warming and even led to declining SSTs in some areas. Consequently, the eastern Mediterranean, extending from the Aegean Sea to Cyprus and parts of the Egyptian coast, exhibited locally negative SST anomalies during the same period

2.6. The heat wave in Germany in June 2026

In Germany, the heat wave reached its peak between 26th and 28th June 2026. During this period maximum temperatures exceeded 40 °C across several regions. On 26th June, the hottest conditions extended from the southern Emsland region to Upper Franconia, with temperatures above 36 °C also occurring in Saxony-Anhalt and western Brandenburg (Fig. 11, left). Temperatures exceeding 40 °C were initially confined to relatively small areas in southwestern Germany, particularly the Saarland and the northern Upper Rhine Valley. On that day, the Saarbrücken-Burbach weather station recorded 41.3 °C, setting a new national temperature record.

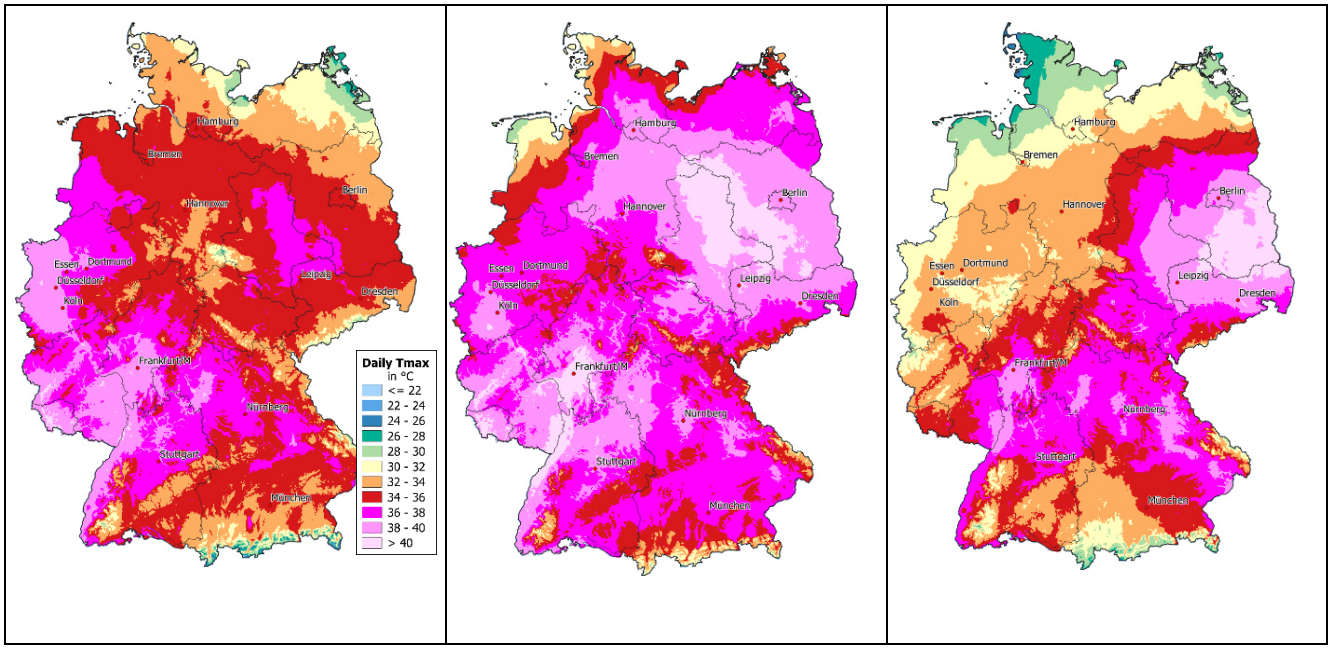

Fig. 11: Analysis of the distribution of daily maximum temperatures at the peak of the heat wave in Germany on 26th (left), 27th (middle), and 28th June 2026 (right; Data: HYRAS, DWD).

On 27th June, the extreme heat expanded across almost the entire country. With the exception of the immediate coastal regions, the northern Emsland, and the higher elevations of the low mountain ranges and the Alps, maximum temperatures exceeded 36 °C nationwide. A total of 47 stations within the German Weather Service (DWD) network recorded temperatures of at least 40 °C, more than during any previous event. The most intense heat affected the Upper Rhine Valley, the Rhine-Main region, and large parts of eastern Saxony-Anhalt and western Brandenburg (Fig. 11, centre). At Möckern-Drewitz (Saxony-Anhalt), a maximum temperature of 41.8 °C established a new German all-time heat record, although its official confirmation was still pending at the time of writing (DWD, 2026b). Overall, 215 of the 492 DWD stations recorded new all-time maximum temperature records on 27th June.

By 28th June, the focus of the most extreme heat had shifted eastwards towards Brandenburg. Cooler air had already spread across northwestern Germany and the far south, although maximum temperatures still exceeded 30 °C across much of these regions (Fig. 11, right). The previous day's national record remained unbeaten, with the station at Neißemünde-Coschen reaching 41.7 °C, only 0.1 °C below the value recorded at Möckern-Drewitz. Table 1 lists the 14 hottest stations in Germany during the period 26th to 28th June 2026; all recorded new all-time maximum temperature records.

Nighttime temperatures were equally exceptional. Record-breaking high minimum temperatures were observed across large parts of Germany, highlighting the limited nocturnal cooling during the event. New all-time records for daily minimum temperature were set at 51 DWD stations on the night of 26th/27th June and at 85 stations on the following night. The highest nighttime minimum temperature was recorded at Kubschütz (district of Bautzen), where the temperature remained at 29.4 °C on 28th June. A local foehn effect associated with the Ore Mountains (Erzgebirge) prevented further nocturnal cooling.

Table 1: List of the 14 hottest locations in Germany at the peak of the heat wave from 26th to 28th June 2026. Daily maximum temperature readings from official stations of the German Weather Service (Data: DWD, mtwetter.de).

Station	Altitude	Federal State	Records	Date
Möckern-Drewitz	30 m	Saxony-Anhalt	41.8 °C	27.06.2026
Neißemünde-Coschen	39 m	Brandenburg	41.7 °C	28.06.2026
Bad Muskau	127 m	Saxony	41.5 °C	28.06.2026
Seehausen	22 m	Saxony-Anhalt	41.4 °C	27.06.2026
Waghäusel-Kirrlach	105 m	Baden-Wuerttemberg	41.4 °C	27.06.2026
Saarbrücken-Burbach	190 m	Saarland	41.4 °C	27.06.2026
Genthin	35 m	Saxony-Anhalt	41.3 °C	27.06.2026
Bad Nauheim	149 m	Hesse	41.3 °C	27.06.2026
Frankfurt/Main-Westend	121 m	Hesse	41.2 °C	27.06.2026
Andernach	75 m	Rhineland-Palatinate	41.1 °C	27.06.2026
Frankfurt/Main	100 m	Hesse	41.1 °C	27.06.2026
Holzdorf-Bernsdorf	78 m	Brandenburg	41.1 °C	27.06.2026
Trier-Zewen	132 m	Rhineland-Palatinate	41.1 °C	27.06.2026
Schipkau-Klettwitz	128 m	Brandenburg	41.1 °C	28.06.2026

2.6.1. Historical perspective based on the Karlsruhe temperature series

While the previous section describes the spatial evolution and peak intensity of the heat wave across Germany, long-term station observations are required to assess how exceptional the event was in a historical context. Using one of Germany's longest instrumental temperature records from Karlsruhe (Kunz et al., 2022), we quantified two June heat-wave indices: TS30 and TM18. These indices are defined as the cumulative exceedance of daily maximum temperature (Tmax) above 30 °C and daily minimum temperature (Tmin) above 18 °C, respectively; that is, the temperature excess above the corresponding threshold is summed over all days in June within a given year. By combining the duration and intensity of threshold exceedances, both indices provide an integrated measure of heat-wave severity.

The two indices, shown in Fig. 12, exhibit substantial interannual variability. Elevated values occurred during the first half of the nineteenth century, followed by a period of generally lower values between approximately 1880 and 1930. Since around 2000, both indices have increased markedly, particularly TS30. Nevertheless, the values observed in 2026 are unprecedented within the entire record dating back to 1779. While TS30 established a new record, TM18 was even more exceptional: in 2026, TM18 reached 28.4 K, whereas the previous maximum, recorded in 1826, was only 12.0 K. Thus, the 2026 value exceeded the former record by more than 16 K. Besides the record-breaking daytime temperatures, this indicates a substantial heat stress by limited cooling during nighttime.

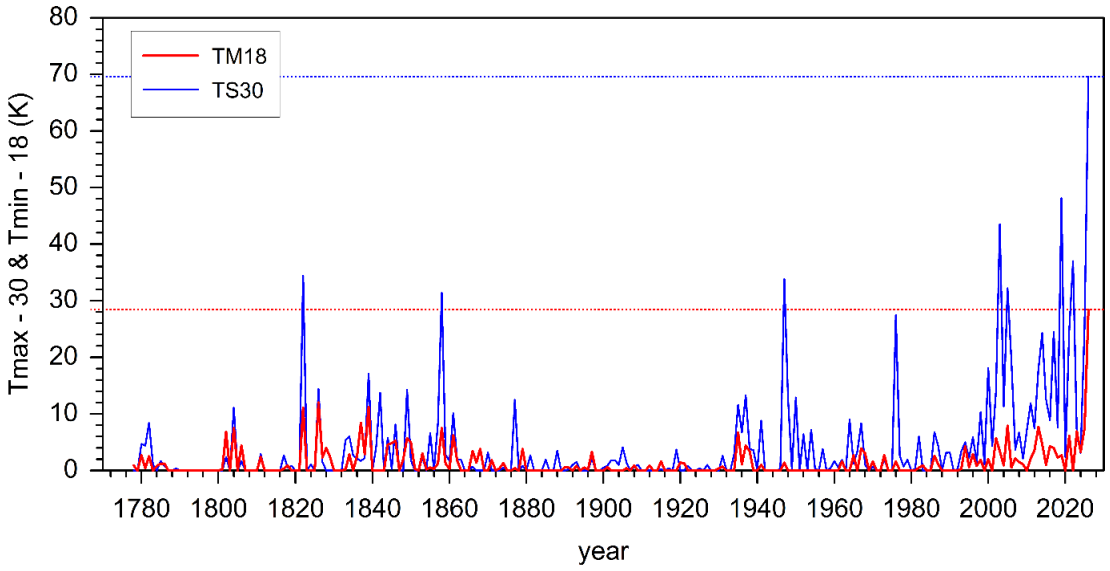

Fig. 12: June heat wave indices TS30 (blue), defined as the cumulative exceedance of daily maximum temperature (Tmax) above 30 °C, and TM18 (red), defined as the cumulative exceedance of daily minimum temperature (Tmin) above 18 °C, derived from the long-term Karlsruhe temperature series of Kunz et al. (2022). Tmax and Tmin data for 1779 to 2009 are based on the homogenized Karlsruhe series. For 2010 to 2022, data from the Mannheim and Rheinstetten stations (DWD) were homogenized and adjusted to the Karlsruhe reference series. For 2026, temperatures were obtained exclusively from the Rheinstetten station and were not further adjusted.

2.7. The heat wave in Europe in June 2026

2.7.1. Observed temperature records during the June 2026 heat wave

In many European countries, the June 2026 heat wave set new monthly maximum temperature records and, in several cases, new national all-time records. Although some of these records were still subject to official verification at the time of writing, the event clearly ranks among the most exceptional heat waves ever observed across Western and Central Europe.

France was particularly affected. While summer temperatures around 35 °C are not uncommon, the persistence of temperatures exceeding 40 °C for almost ten consecutive days represents an extraordinary event even by French standards. In most other countries of Western and Central Europe, temperatures above 35 or even 40 °C occurred only for a few days. Germany, for example, experienced three consecutive days with maximum temperatures exceeding 40 °C (see Fig. 11). Table 2 summarizes the highest daily temperatures recorded in selected European countries between 13rd and 29th June 2026.

During the event, numerous national and regional temperature records were broken:

- **Austria:** Vienna recorded its hottest June day on record with **40.0 °C**.
- **Czech Republic:** The national all-time record increased from 40.9 °C to **41.9 °C** on **27 June**.
- **Denmark:** A new national all-time record of **37.0 °C** was measured on **27 June** at both Beldringe (north of Odense) and Odum (north of Aarhus), surpassing the previous record of 36.4 °C from August 1975.
- **France:** Although the national all-time record of **45.9 °C**, measured at Gallargues-le-Montueux on **28 June 2019**, was not exceeded, many stations established new June records and several regions experienced exceptionally persistent temperatures above 40 °C.
- **Germany:** A new national all-time record of **41.8 °C** was recorded at Möckern-Drewitz (Saxony-Anhalt) on **27 June**. In total, **252 stations** within the German Weather Service (DWD) network established new all-time maximum temperature records.
- **Hungary:** A new national June record of **40.7 °C** was measured near Budapest**.**
- **Netherlands:** Numerous stations established new June records, with one station reaching a new national June record of **39.4 °C**.
- **Poland:** A new national all-time record of **40.5 °C** was recorded.

- **Spain:** Spain experienced its hottest June days on record on **23 and 24 June**. Numerous stations set new June records, including Bilbao with **42.7 °C**, its highest temperature ever recorded in June.
- **United Kingdom:** An all-time maximum temperature of **39.3 °C** was recorded on **25 June** at St. Helier (Jersey, Channel Islands), surpassing the previous national record of 37.9 °C from July 2022. On the British mainland, Lingwood (Norfolk) reached **37.7 °C** on **27 June**, exceeding its previous June record by 2.1 °C.

2.7.2. Spatiotemporal evolution of the June 2026 heat wave from ERA5

While station observations document the exceptional temperatures recorded at individual locations, ERA5 reanalysis provides a spatially consistent picture of the evolution and propagation of the heat wave across Europe. Figure 13 shows the daily maximum 2 m air temperature (Tmax) from 13rd to 30th June 2026 based on ERA5 reanalysis (Hersbach et al., 2023), illustrating the onset, intensification, and eastward progression of the event. Between 13rd and 15th June, Tmax values exceeding 34 °C are mostly confined to the Iberian Peninsula and southwestern France, while the rest of the continent remains close to or even below seasonal norms. From 16th June onward, the warm air mass expands north-eastward into France and intensifies rapidly: by 19th to 21st June, a broad corridor of Tmax above 34 °C stretches from southern tip of the Iberian Peninsula toward southwestern Germany, while the UK, Scandinavia, and eastern Europe stay comparatively cool. The event peaks around 22nd and 24th June in France, when a large area in the west of the country exceeds maximum temperatures of 40 °C, with several grid points even reaching daily highs of 42 to 44 °C. Over the next few days, the core of the heat wave starts to shift eastward into Germany, the Benelux countries, and the Alpine-Balkan region, as Iberia and western France begin to cool. By 29th to 30th June, the heat retreats further east, concentrating over south-eastern Europe.

Note: As ERA5 has a native resolution of 0.25° and represents grid box averages, it inherently smooths sub-grid-scale extremes and cannot be directly compared to individual station observations, which can record substantially higher local peak temperatures. Therefore, products based on station observations, like the one in Figure 11, show slightly different values.

Table 2: Selection of the highest daily maximum temperatures at official weather stations in various countries in Central and Western Europe during the period June 13–29, 2026. Data: meteociel.fr, mtwetter.de, dwd.de

2026	Frankreich	England	Belgien	Niederlande	Luxemburg	Deutschland	Schweiz	Österreich
13.06.	38.3 Durban-Corbières	22.6 Bournemouth Ap	21.5 Buzenol	20.1 Maastricht Ap	22.2 Luxembourg	29.2 Ohlsbach	31.1 Visp	29.9 Villach
14.06.	37.3 Durban-Corbières	25.4 St. Helier	19.3 Charleroi/Gosselies	19.0 Ell	19.0 Luxembourg	27.4 Müllheim	30.6 Cevio	Dellach 29.4
15.06.	39.1 Argeliers	23.5 Almondsbury	20.7 Kleine Brogel	20.5 Ell	20.0 Luxembourg	27.3 Müllheim	30.1 Locarno-Magadino	26.6 Innsbruck Ap
16.06.	36.5 Moulès-et-Baucels	27.1 London Heathrow	26.4 Kleine Brogel	26.3 Maastricht Ap	25.5 Luxembourg	30.9 Müllheim	31.4 Visp	28.2 Hartberg
17.06.	38.4 Villariès	26.6 London Heathrow	27.4 Dourbes	27.1 Ell	26.7 Luxembourg	32.7 Müllheim	33.0 Visp	31.1 Feldkirch
18.06.	42.6 Pruniers	26.8 Marham	33.0 Kleine Brogel	32.4 Ell	32.0 Luxembourg	35.6 Saarbrücken-Burbach	35.4 Visp	32.6 Landeck
19.06.	40.4 Pruniers	30.9 Weybourne	34.7 Kleine Brogel	35.1 Ell	34.4 Luxembourg	38.5 Kitzingen	35.7 Schaffhausen	35.1 Mayrhofen
20.06.	39.8 Pruniers	27.2 Saint Helier	32.1 Kleine Brogel	32.4 Ell	33.7 Luxembourg	37.5 Saarbrücken-Burbach	35.3 Basel/Binnigen	35.6 Tulln
21.06.	44.2 Pruniers	31.8 London Heathrow	32.6 Buzenol	30.7 Maastricht Ap	34.2 Luxembourg	37.2 Regensburg	36.6 Psi Wuerenlingen	36.1 Ranshofen
22.06.	45.2 Pruniers	33.7 Jersey Ap	31.9 Buzenol	29.7 Ell	33.7 Luxembourg	37.5 Müllheim	36.6 Basel/Binnigen	34.1 Landeck
23.06.	44.7 Les Herbiers	37.2 Saint Helier	30.9 Oostende Ap	30.4 Wilhelminadorp	31.5 Luxembourg	36.8 Müllheim	36.4 Basel/Binnigen	32.8 Landeck
24.06.	44.6 Chatonnay	35.8 Saint Helier	36.8 Chièves	36.1 Woensdrecht	35.2 Luxembourg	37.5 Perl-Nennig	Visp 36.8	33.8 Bregenz
25.06.	45.0 Pruniers	39.3 Saint Helier	36.6 Kleine Brogel	35.2 Woensdrecht	36.3 Luxembourg	39.0 Waghäusel-Kirrlach	38.0 Basel/Binnigen	36.4 Bregenz
26.06.	42.7 Mussy_sur_Seine	36.9 Wittisham	39.9 Kleine Brogel	39.4 Ell	38.2 Luxembourg	41.3 Saarbrücken-Burbach	38.8 Basel/Binnigen	37.4 Mistelbach
27.06.	43.2 Vassincourt	32.1 Tibenham Airfield	38.3 Buzenol	36.3 Ell	37.8 Luxembourg	41.8 Möckern-Drewitz	39.0 Basel/Binnigen	38.7 Wien/City
28.06.	41.8 °C Les Arcs	27.2 London Heathrow	31.0 Kleine Brogel	30.9 Twenthe	31.4 Luxembourg	41.7 Coschen	37.5 Buchs/Aarau	40.0 Wien/City
29.06.	39.4 Villevieille	24.7 London Heathrow	28.5 Charleroi/Gosselies	27.8 Hupsel	26.7 Luxembourg	34.4 Regensburg	34.2 Stabio	39.9 Mistelbach

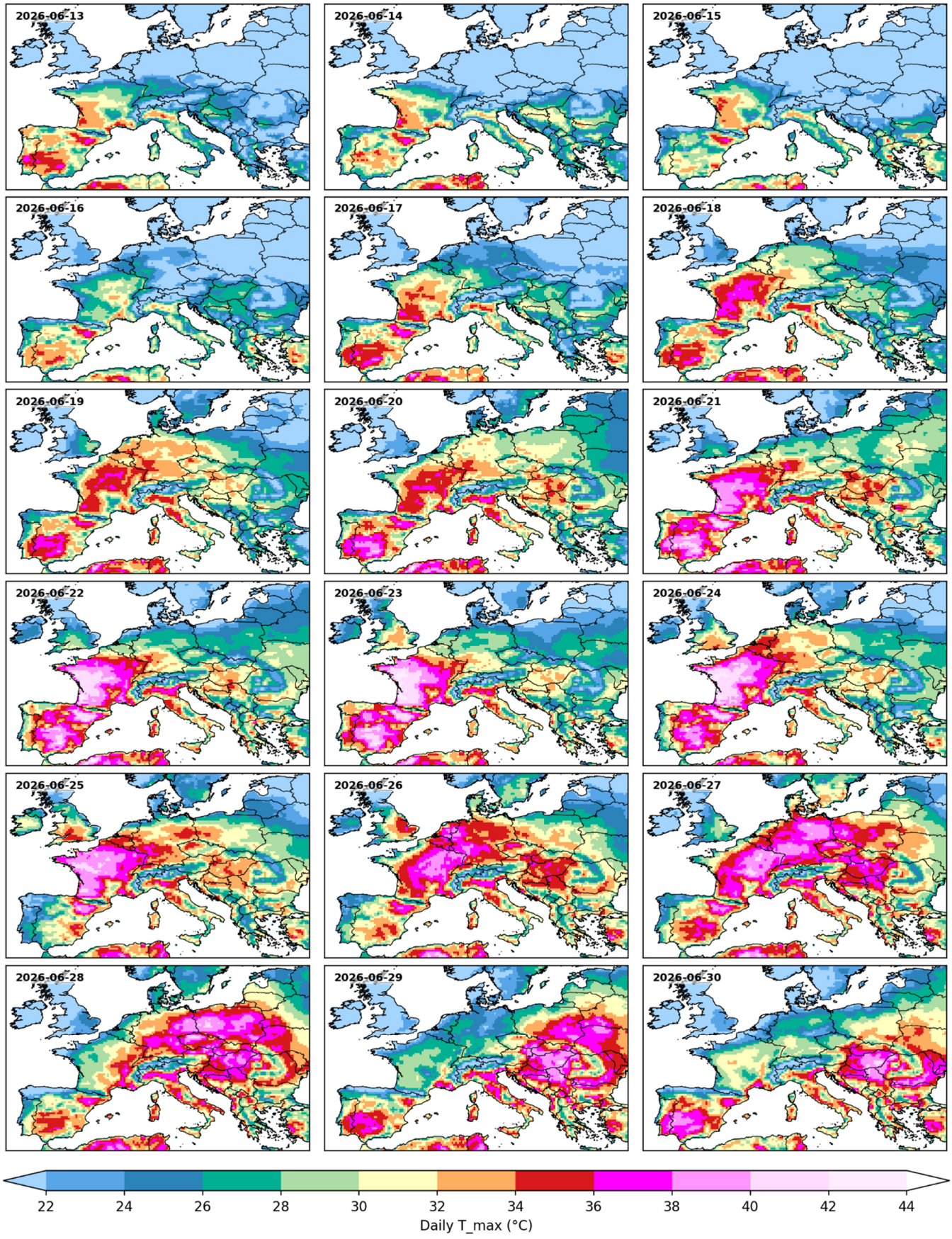

Fig. 13: Daily maximum 2 m air temperature (Tmax) over Europe for 13rd to 30th June 2026, at 0.25° × 0.25° horizontal resolution. Ocean grid points are masked (Data: ERA5 reanalysis; Source: https://cds.climate.copernicus.eu).

2.8. Comparison with previous heat waves in Europe based on ERA5

2.8.1. Historical ranking of the heat wave in June 2026

Additional heat wave metrics were derived from hourly 2 m air temperature (T) and 2 m dew point temperature (Td) data from the ERA5 reanalysis (Hersbach et al., 2023) over the European domain (approximately 35 – 60°N, 11°W –20 °E) at a horizontal resolution of 0.25°. These metrics were calculated for the months of May through September each year from 1940 to 2025, as well as up to June 30 (16:00 UTC) in 2026. For each grid point and year, the hourly values were resampled to determine the daily maximum air temperature (Tmax), daily minimum air temperature (Tmin), and daily maximum dew point temperature (Tdmax).

A day was classified as a heat wave day for a given metric if it exceeded a fixed threshold: 30°C for Tmax, 18 °C for Tmin, and 18 °C for Tdmax (see Section 2.6.1). For each day exceeding this threshold, the excess, i.e. the amount by which the daily value surpassed the threshold, was retained. Consecutive heat wave days were grouped into discrete runs, and for each run the excess values of its constituent days were summed to give that run's total excess sum. To facilitate a meaningful comparison between the 2026 heat wave event and other heat waves, two distinct time periods are utilized in the analysis. The period of the first analysis includes only the month of June, whereas the second analysis used the entire warm season period from May to September, in order to investigate how the June heat wave compares to the strongest heat wave in all summer. Rather than aggregating exceedances across an entire time period, we isolated, for each grid point and period, the single run with the largest cumulative excess. This run is then termed "strongest heat wave" of that period and weaker warm spells that may also have occurred in the same period are discarded. This procedure was applied independently to each of the three variables, yielding three strongest-heat wave excess fields per grid point and time period.

For each grid point, we then identified the year in which this strongest-heat wave metric reached its historical maximum, once using the 1940 to 2025 archive and again with June 2026 included (Fig. 14). Ocean grid points were excluded using Natural Earth land polygons, restricting the analysis to land areas. For each of the two periods, the ten years holding the per-grid point record most often (by grid point count) were retained and assigned distinct colors. The remaining years were pooled into a residual "other years" category (black), and grid points that never exceeded the relevant threshold in any year were left unclassified (white). A shared color assignment was used across the "before" and "after" panels so that a given year retains the same color in both, allowing years common to both top-10 lists to be visually tracked across the comparison.

Before the inclusion of June 2026, the per grid point record for the highest Tmax excess in June was most often held by 2019 (882 grid points), followed by 2022, 2021, 2025, and 1976. Once June 2026 is included, it takes the record at 3682 grid points — more than four times the previous leading year and more than ten times the new second-place year (2017, 343 grid points). Almost every other year in the top 10 loses a substantial share of its previously record-holding area (e.g. 2019 falls from 882 to 161, 2022 from 557 to 165), while 2013, 2000, 1976 and 1947 are displaced from the top 10 entirely. This indicates that in June 2026, new all-time daytime heat records were set over a large fraction of the land grid points across most of Europe, including several countries where the records were nearly continuous. Additionally, the June 2026 heat wave expanded the Tmax excess metric to grid points that had never previously recorded positive values, for example, in parts of the British Isles and Denmark.

The pattern of the highest overnight heat, as quantified by Tmin, is qualitatively similar but slightly less extreme: 2026 becomes the new record-holder overall (2745 grid points, versus 1947's previous lead of 751), but its footprint is visibly less dominant and more concentrated over France, the British Isles, the Low Countries, Czechia and parts of Germany, Denmark, Austria and Poland. Similar to Tmax, most other years in the previous top 10 exhibit dramatic losses and the historic heat wave ranking is significantly shuffled. This suggests June 2026's overnight warmth, while still historically extreme in aggregate, was less universally record-breaking than its daytime heat.

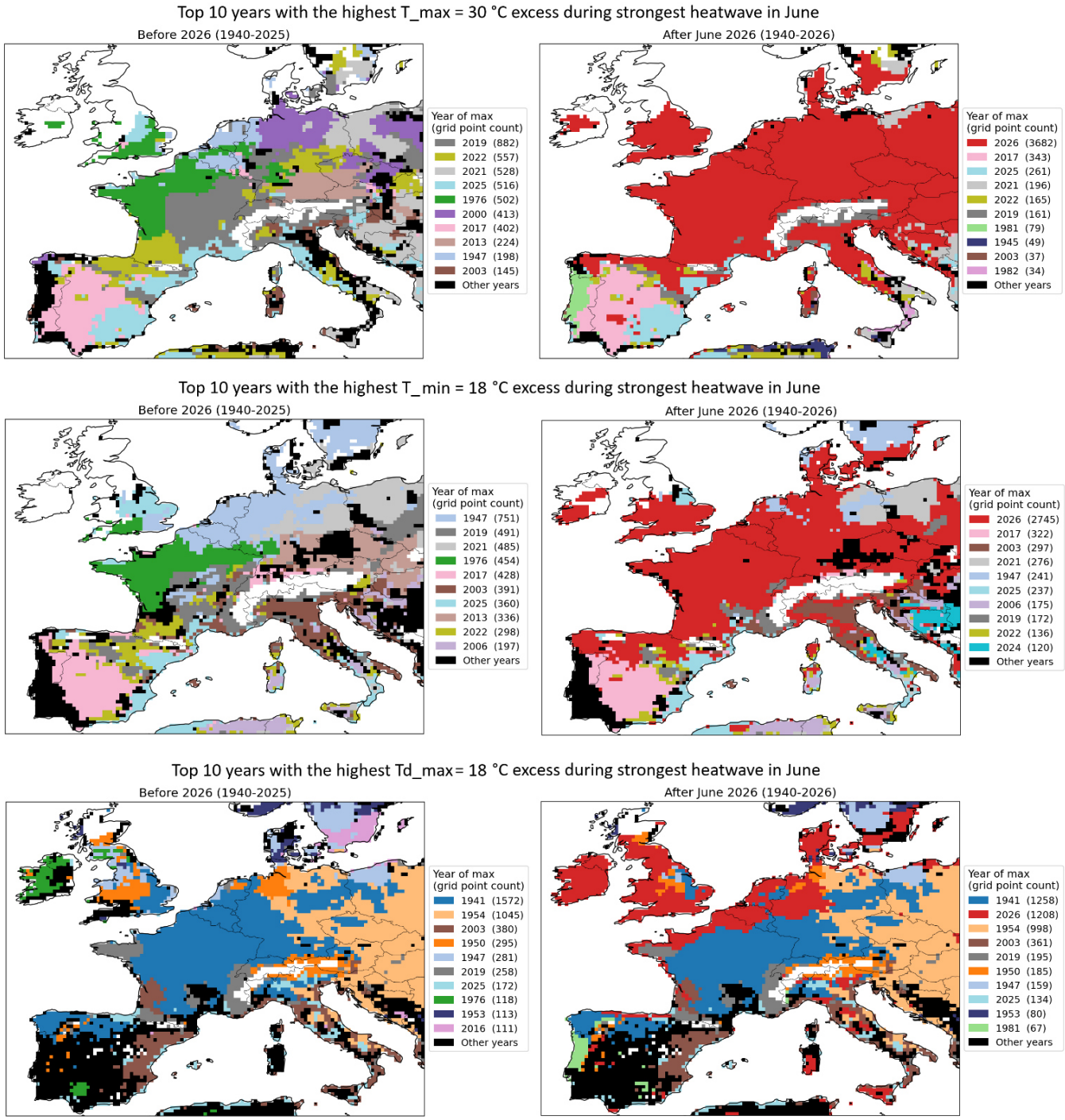

Fig. 14: Spatial distribution of the years holding the record for the strongest June heat wave in maximum temperature (top row, Tmax > 30°C excess), minimum temperature (middle row, Tmin > 18°C excess), and maximum dewpoint temperature (bottom row, Td_max > 18°C excess) per grid point, based on ERA5 reanalysis over Europe at 0.25° resolution. For each grid point and year, the metric represents the cumulative excess above threshold summed over the single strongest consecutive-day heat wave in June of that year (weaker warm spells in the same month are excluded). Left column: record year computed from 1940–2025; right column: record year recomputed with June 2026 included. Only the ten years holding the most grid-point records are shown individually (colored, ranked by grid point count in parentheses); all remaining years are pooled as "Other years" (black). White indicates ocean grid points (masked) or land grid points that never exceeded the relevant threshold in any year.

The maximum dewpoint Tdmax excess is the most notable departure from the other metrics. Rather than taking over the record, June 2026 (1208 grid points) enters in second place, behind 1941 with 1258 grid points (down from 1572 before 2026 was added), and 1954 drops to third place with almost 1000 grid points still left. The footprint of the 2026 heat wave for this metric is concentrated mainly over Ireland, the British Isles, and parts

of the Low Countries and Germany, which fits well to the numerous observed severe weather reports in these locations (see Section 2.8.3). Meanwhile, 1941 continues to dominate central and western Europe, and 1954 dominates parts of eastern Europe and the Balkans. Comparing the top 10 list with previous metrics reveals big differences, with several new years appearing in the top 10 (e.g. 1941, 1954, 1950). Therefore, it is impressive that 2026 is ranked second place in this metric, while other years that are notably absent (e.g. 2017, 2021, 2022) featured probably more dry heat.

When considered collectively, the three metrics point to June 2026 being an exceptional heat that was on a smaller scale also a combined heat-and-humidity extreme. The June 2026 heat wave overwhelmingly dominates the daytime temperature record and in slightly reduced form also the overnight temperature records. However, for dewpoint-based moisture excess it does not surpass the extent of the historical 1941 event. Since combined heat-and-humidity conditions are generally associated with greater physiological heat stress than dry heat of comparable air temperature, including moisture records is relevant for interpreting the health impact of the 2026 event relative to historical extremes with often smaller moisture components.

2.8.2. Limitations of the June-based analysis

One caveat applies to the grid point counts reported in the legends: because the analysis uses a regular latitude–longitude grid, a grid cell's physical area decreases with increasing latitude. Grid point counts are therefore a reasonable proxy for spatial extent within a given panel, but should not be read as directly proportional to land area, particularly when comparing footprints across different latitude bands.

The analysis domain was deliberately restricted to the area west of roughly 20°E. This cutoff was chosen based on the pre-2026 climatology: across all three metrics, there exists already a significant number of residual grid points in black for years other than the top 10. Consequently, it can be deduced that an expansion of the domain would have likely led to an expansion of these residual grid points. In the Tmax and Tmin panels, the 2026 record-holding area now visibly reaches the eastern edge of the domain. This edge effect only became apparent with the inclusion of the final days of the month, indicating that the spatial extent of the record-breaking heat was still expanding eastward at the time the analysis was cut off. The grid point counts and mapped extent for June 2026 reported here should therefore be interpreted as a lower bound on the true areal extent of the event.

2.8.3. June 2026 in the context of the full warm season

Additionally, it should be noted that the strict focus on June underestimates heat waves that started at the end of June and lasted into July. To address this issue and compare the 2026 June heat wave to the most extreme heat waves in full summer, the same methodology for Tmax > 30 °C and Tmin > 18 °C was recomputed using the full May–September window for each year from 1940–2026 (Fig. 15). Because ERA5 data for 2026 currently extend only through 30 June, the 2026 value reflects at most a May–June heat wave. Any warm spell that might still be ongoing or yet to occur later in the 2026 season is not included, so the 2026 result should be read as a preliminary, partial-season figure rather than a final seasonal total. This is especially relevant for very hot areas, like southern Spain, that can often exceed the temperature thresholds for several months during summer.

Across the full season, 2003 holds the per grid point record for Tmax over by far the largest area (1156 grid points), spanning a broad swath of France, Germany, and Italy – consistent with the well-documented August 2003 European heat wave. June 2026 places second (717 grid points), with its record-holding area concentrated over Ireland, the British Isles, France, the Low Countries, and Germany – closely mirroring the spatial footprint already identified in the June-only analysis. 2022 follows closely in third (674 grid points, mainly over the UK, Ireland, and the Iberian Peninsula), with 1994, 2015, 2024, 2023, 1975, 2025, and 2019 rounding out the remainder of the top 10 at successively smaller areas.

The Tmin ranking exhibits a similar structural pattern: 2003 once again occupies the leading position (891 grid points), 2026 places second (550 grid points), and 2024 emerges as a close third (541 grid points). The years 2015, 2022, 1941, 1994, 2018, 2023, and 2020 complete the top 10, with the first four of them also being present in the Tmax top 10. As with Tmax, the record-holding area for overnight heat in 2026 is concentrated over the same northwestern European region (Ireland, Britain, France, the Low Countries) identified in the June-

restricted analysis. Similar to the June only ranking, the Tdmax metric exhibits the lowest amount of record-breaking grid points in comparison to the other two metrics. Nevertheless, this is sufficient for sixth place in the full season analysis, with the majority of grid points concentrated along the coastlines of the British Isles, France and Belgium (not shown).

When evaluated against the entire warm season as opposed to June alone, the June 2026 heat wave no longer holds the uncontested record — 2003 remains the more extreme occurrence in both metrics across the full five-month period, reflecting the exceptional duration and magnitude of the August 2003 heat wave rather than any weakening of the June 2026 signal itself. However, utilizing just two of the five months included in the analysis period (May and June), 2026 has already secured second place. In contrast, all other years in the ranking have benefited from the entire May–September period to generate their most intense heat waves. This asymmetry indicates that the current second-place ranking for 2026 is a conservative, lower-bound estimate. It is possible that should a further significant heat wave occur later in the 2026 season (July–September), 2026's ranking could rise further, potentially even surpassing 2003, once the full season is available for comparison. Consequently, these results should be regarded as preliminary and utilized data might change in further quality controls.

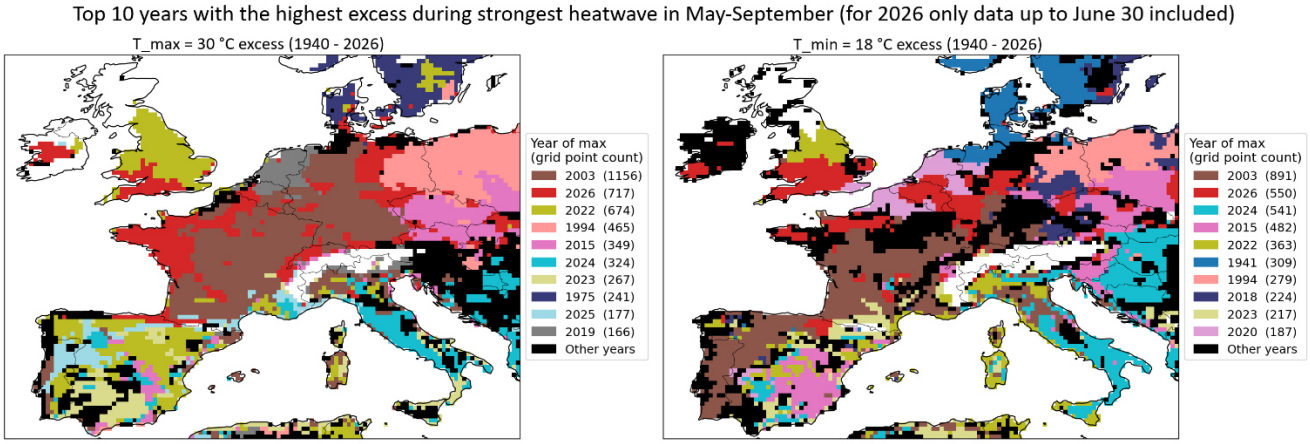

Fig. 15: **Spatial distribution of the years holding the record for the strongest heat wave during May – September in maximum temperature (left, Tmax > 30°C excess) and minimum temperature (right, Tmin > 18°C excess) per grid point, based on ERA5 reanalysis over Europe at 0.25° resolution. For each grid point and year, the metric represents the cumulative excess above threshold summed over the single strongest consecutive-day heat wave in that year (weaker warm spells in the same year are excluded). Only the ten years holding the most grid-point records are shown individually (colored, ranked by grid point count in parentheses); all remaining years are pooled as "Other years" (black). White indicates ocean grid points (masked) or land grid points that never exceeded the relevant threshold in any year.**

2.9. Convective environment and severe weather impacts during the heat wave

The synoptic weather pattern described above enabled continuous northward moisture transport along the western flank of the blocking ridge (e.g., Mohr et al., 2019). The presence of unusually high SSTs over the Mediterranean and Eastern Atlantic (see Fig. 10) likely contributed to the large moisture content (e.g., Lebeaupin et al. 2006, Miglietta et al. 2017). Consequently, large areas spanning Northern France, the UK, the Benelux, and Germany observed dew points around 20 °C (Fig. 14) or more and Convective Available Potential Energy (CAPE) values exceeding 1000 J/kg – with peak values surpassing 3000 J/kg – especially from 18th June to 29th June. However, the severity of convection was hindered by several limiting factors:

i. Despite the high absolute moisture, the low relative humidity due to the extreme temperatures led to elevated Lifted Condensation Levels (LCL) and, in some regions, also to high Convective Inhibition (CIN).
ii. The lack of significant forcing mechanisms, such as fronts or upper-level disturbances, further limited Convective Initiation (CI).
iii. Weak to moderate wind shear constrained thunderstorm organization.

As a result, most convection remained localized (Fig. 16), forming primarily over orography and convergence boundaries. Furthermore, the limited wind shear led to thunderstorms exhibiting single to multi-cell characteristics, mostly preventing the formation of supercells or Mesoscale Convective Systems (MCS). Given

the large CAPE values, severe weather hazards were still reported daily across Western and Central Europe, but they were generally localized and limited to small hail, downburst winds, or intense lightning activity (Fig. 16). To further illustrate this point, Figure 17 shows accumulated precipitation over Germany from 13th to 29th June. Several areas with over 100 mm stand out. These maxima were produced over short periods on individual days with slow-moving or back-building orographic storms, but to the authors knowledge only produced very localized and short-term flash floods.

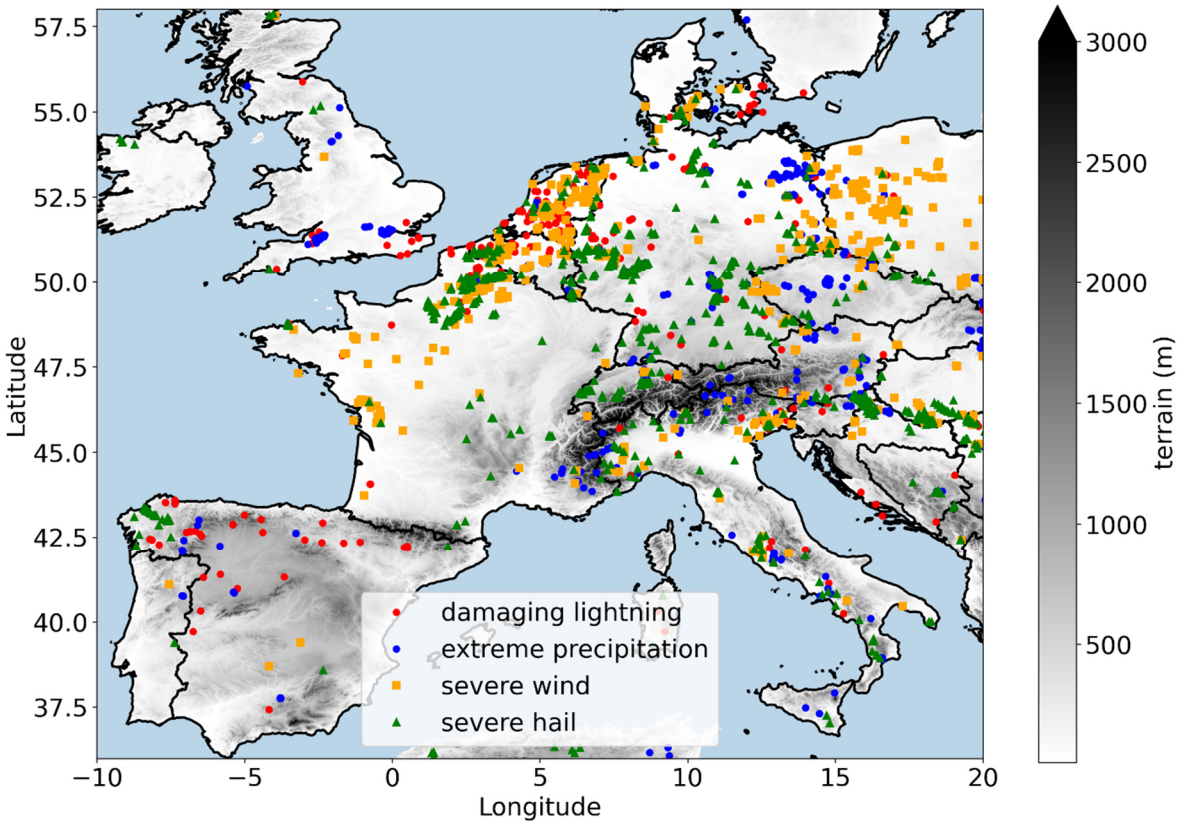

Fig. 16: **Verified severe weather reports in the European Severe Weather Database (ESWD) between 13rd to 29th June 2026 (see eswd.eu for details on reporting criteria for each hazard*).***

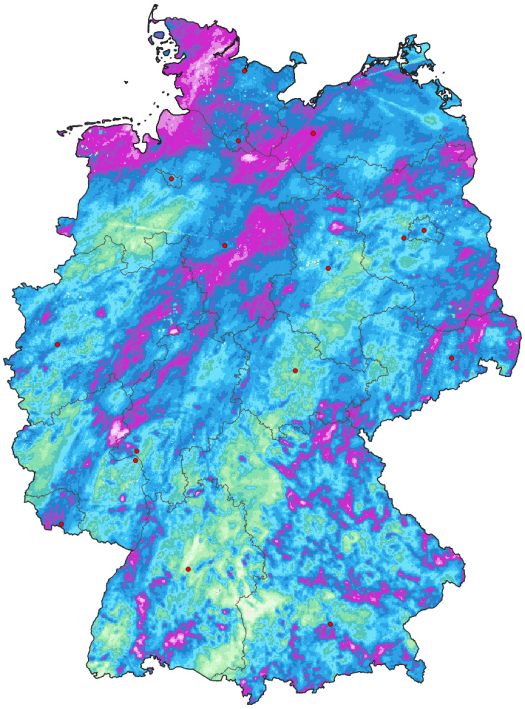

Fig. 17: Radar-derived precipitation amount accumulated from 13rd to 29th of June 2026 using the German Weather Service radar network (Data: RADOLAN, DWD).

Notable exceptions with more severe weather included several events of hail greater than 4 cm with isolated supercells in Northern France on 18/19 June, Spain on 24 June, France and Benelux on 27/28 June, Switzerland on 19 June, Germany on 21 June, and Italy on 27 June. These events were often associated with orographic storms that briefly developed supercell characteristics in areas of moderate wind shear, likely aided by local boundaries and enhanced shear near lower mountain ranges (e.g., Fischer et al., 2025). A short-wave trough moving from northern Spain to northern Germany from 27 to 29 June also contributed to these events by increasing wind shear and large-scale ascent. With this trough, a bow-echo mesoscale convective system produced widespread severe wind gusts over Benelux on 27 June (Fig. 16). The combination of weak low-level shear and high LCLs also resulted in the absence of major tornadoes throughout the heat wave.

In short, the thunderstorms, while widespread and frequent, were predominantly small and unorganized, leading to localized and short-lived severe weather events rather than long-lived, high-impact systems. A more detailed impact assessment will require damage data that were not yet available for this report.

3. Hydrological information

This section provides an overview on the hydrological aspects of the heat wave, including precipitation, water balance, streamflow quantity and temperature, lake and groundwater levels. The heat wave occurred as a short-term extreme event on top of a long-term trend of increasing water deficit. The first resulted in record breaking river water temperatures, the second led to extremely low water levels in Lake Constance and groundwater levels especially in Southeast Germany. It is also striking how early in the year this heat wave occurred. Long-term analyses of river water temperatures reveal that this is a trend rather than an exception.

3.1. Precipitation and climatic water balance

In Germany, the cumulative precipitation from the beginning of the year 2026 until the onset of the heat wave was well below average and comparable to the precipitation deficit during the drought years 2003 and 2022 (BFG, 2026; see Fig. 18). Similarly, for Baden-Württemberg, the NIZ (2026) report states that the climatic water balance (the difference between precipitation input and potential evapotranspiration output) for the current hydrological year (1st October 2025 to 31st May 2026) is at an all-time low compared to values in the 1991 to 2026 reference period. On average, the value is 277 mm; for the current period, however, it is only 63 mm (input data source: German Weather Service).

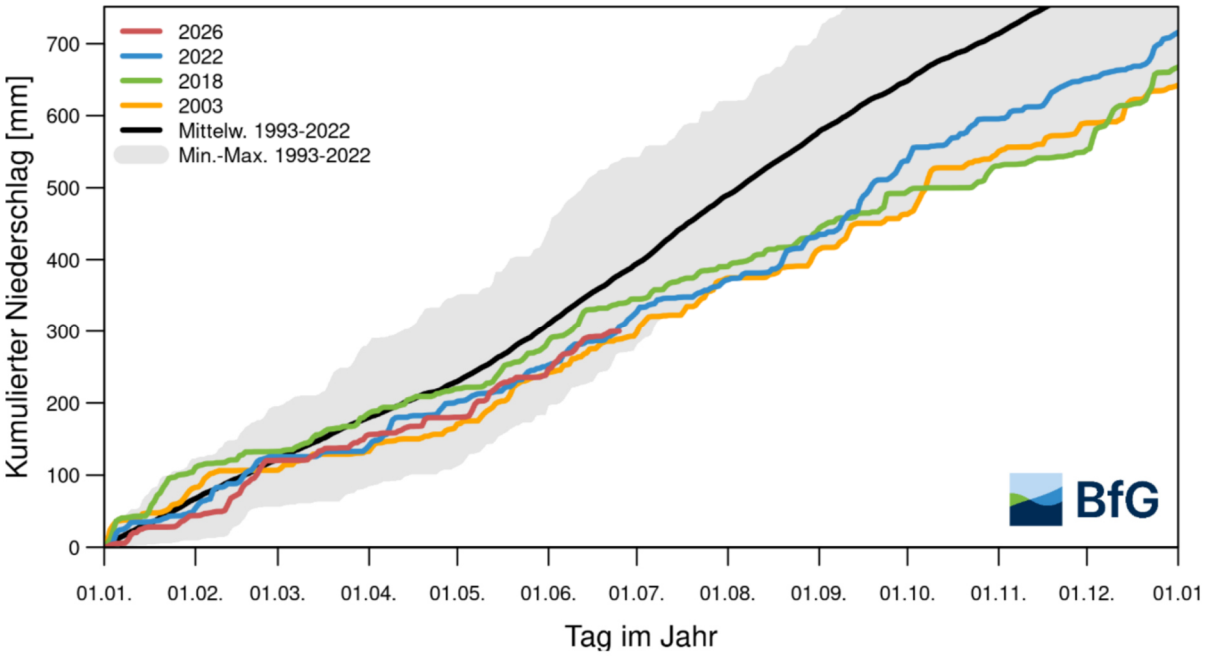

Fig. 18: Cumulative precipitation sums averaged over major middle European river basins for years 2026, 2022, 2018, 2003 and related mean, minimum and maximum values of 30-year period 1993 to 2022 (Data sources: German Weather Service and Meteorological Services of Neighboring countries; figure taken from BFG, 2026).

3.2. Streamflow

BFG (2026) reports generally low and locally very low stream water levels in Germany (see Fig. 19). In southern Germany, streamflow was generally much lower: For Bavaria, NID (2026) reported that 91 % of all gauges show low flow, and at some gauges flow approached all-time daily averages (NQ). For Baden-Württemberg, NIZ (2026) reported that 34 % of all gauges showed extremely low water levels, additionally 43% showed very low water levels. Extremely low water levels occurred mainly in South-East Baden-Württemberg, especially at rivers Riß, Schussen and Argen, and Danube (Fig. 20). At gauge Hundersingen/Danube, on 28th June, the lowest ever daily average flow for this day of the year was recorded (3.98 m^3/s, average flow is 26.6 m^3/s). This is exceptional, as annual low flow at this gauge usually occurs later in the season (September and October).

Fig. 19: River gauge map for Germany at 25th June 2026. Orange markers indicate water levels below the mean annual low water level (MNW). Green markers indicate water levels above MNW. Grey markers indicate technical problems. (Data source: GeoPortal. WSV; Figure taken from BFG, 2026).

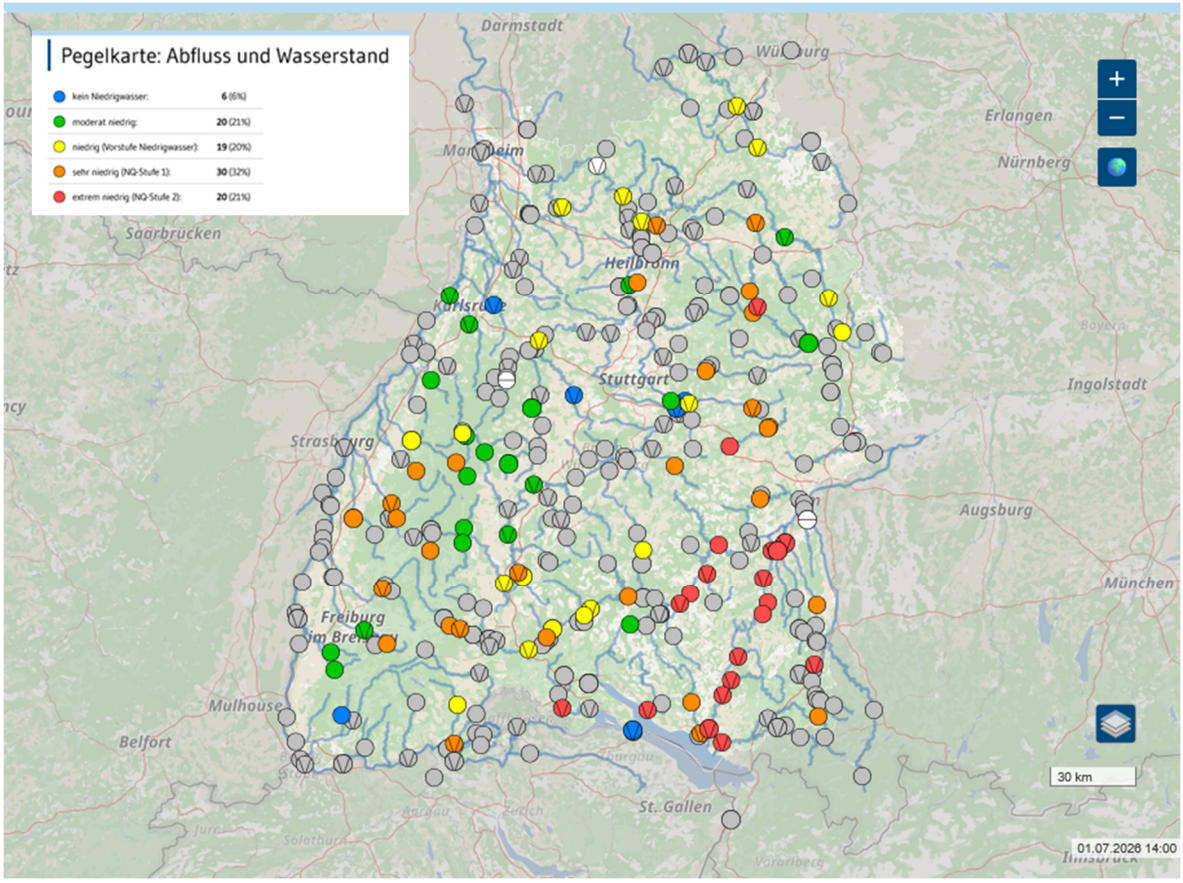

Fig. 20: Flow situation at gauges in Baden-Württemberg at 1st July 2026 (Figure taken from NIZ, 2026).

3.3. Stream water temperature

Hydrologically, the most striking aspect of this heat wave was the very high stream water temperatures. The analysis of heat wave-induced impacts on water temperatures of surface waters extends beyond the identification of record values or historical classification. Exceptionally high-water temperatures can have substantial ecological, economic, and societal consequences.

Rising water temperatures reduce the solubility of dissolved oxygen, exacerbating outgassing effects, while oxygen-consuming processes—such as microbial degradation of organic matter—persist within aquatic systems. Concurrently, ectothermic organisms like fish experience increased metabolic rates at elevated temperatures, intensifying their oxygen demand. The cumulative effect of these processes can drive dissolved oxygen concentrations below the critical threshold of approximately 3 mg O_2 L^{-1}, leading to physiological stress and potentially catastrophic fish mortality events. Documented impacts from the June 2026 heat wave include dissolved oxygen concentrations as low as 2.6 mg O_2 L^{-1} in the upper Mosel (near Palzem, district Trier-Saarburg), large-scale fish mortality in a lake near Munich-Allach (Bavaria), and localized fish kills in a fishing pond with water temperatures reaching 33 °C in Gensingen (Mainz-Bingen district). In Rhineland-Palatinate, warning level 2 was issued due to daily mean water temperatures exceeding 28 °C in both the Mosel and Rhine.

For Germany, BFG (2026) reported widespread very high river temperatures exceeding 25°C (Fig. 21). An exemplary example from the Rhine basin (gauge Koblenz) is shown in Figure 22. In the Figure, it is clearly visible how measurements in June 2026 exceed the upper limits of the 30-year reference period 1993 to 2022. For Baden-Württemberg, NIZ (2026) also reported widespread high-water temperatures (see Fig. 23), and reported that at many gauges all-time water temperature records were broken.

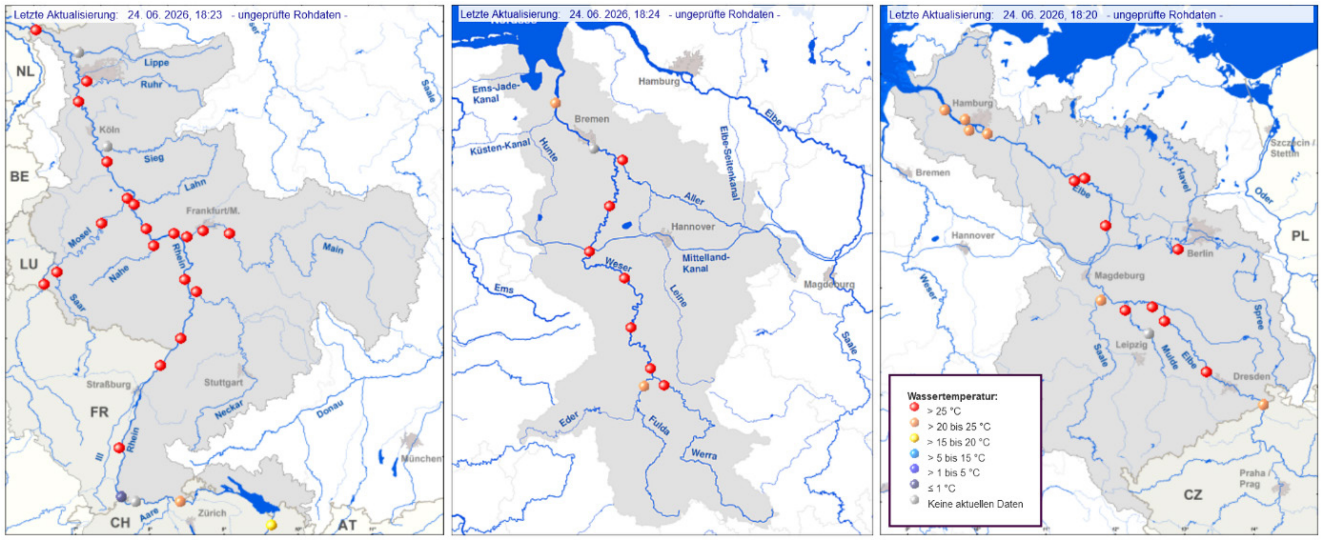

Fig. 21: River water temperatures in major river basins in Germany (Rhine, Weser, Elbe) at 24th June 2026. Red dots indicate temperatures exceeding 25 °C (see legend; Figure taken from BFG, 2026).

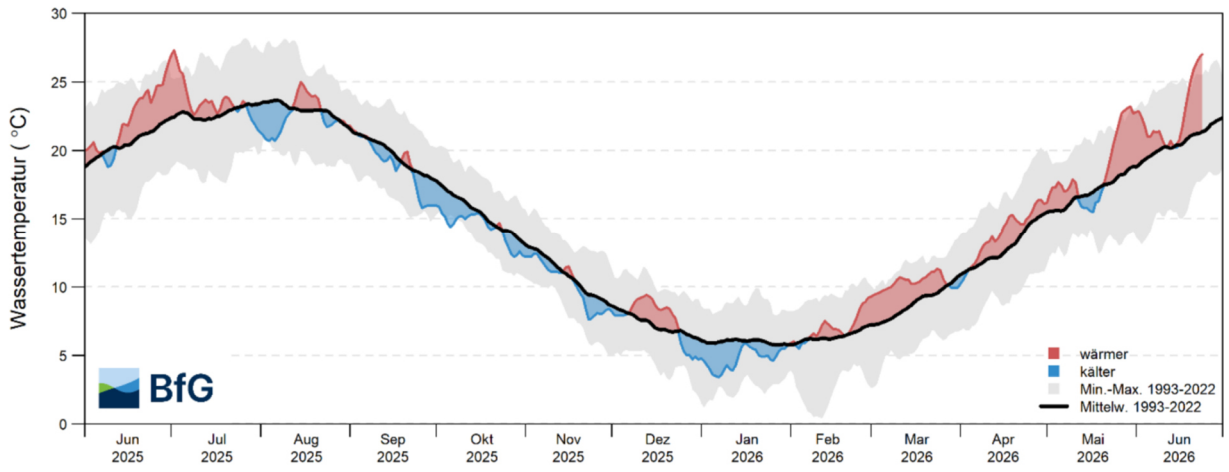

Fig. 22: Daily mean water temperature (°C) at gauge Koblenz/Rhine in period 1st June 2025 to 23rd June 2026. The black line is long-year averages (1993 - 2022), red-blue line are current values, grey area indicates range of long-year values (1993 to 2022; Data Source: BfG, Figure taken from BFG, 2026).

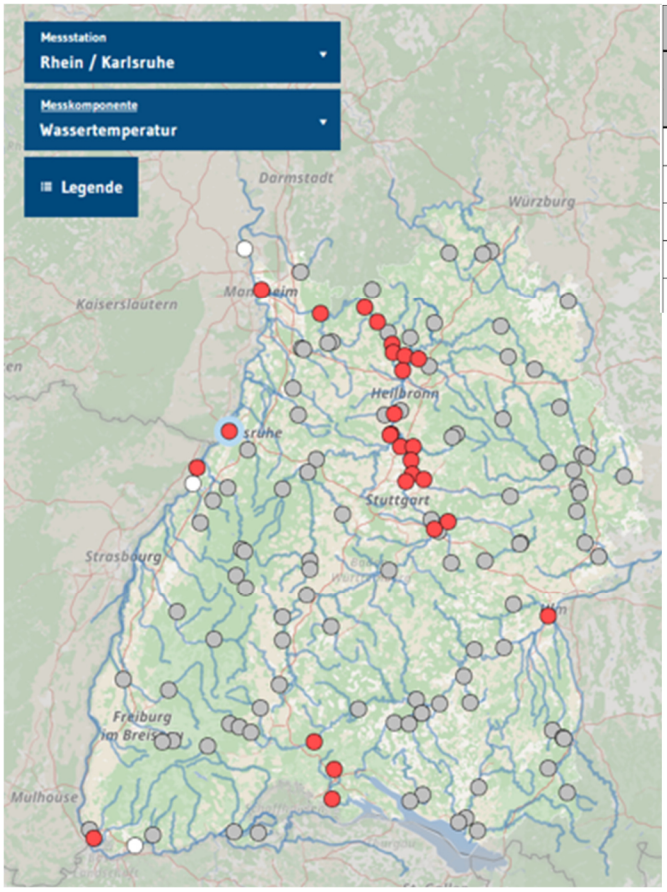

Klassifizierung der Wassertemperatur in Fließgewässern

	Bezeichnung	Statistischer Wert	Erläuterung
	Datenbezug ist jeweils der aktuelle Stundenmittelwert der Wassertemperatur		
	kühl bis mittel	< P75	Die Wertebereiche stellen die Unterschreitungs-Perzentile der Wassertemperatur [°C] dar, berechnet aus den langjährigen Stundenmittelwerten zur jeweiligen Stunde am Tag im Jahr der verfügbaren Zeitreihe der betreffenden Station.
	moderat warm	< P90	
	warm	< P95	
	sehr warm	< P99	
	extrem warm	≥ P99	

Fig. 23: River water temperatures at gauges in Baden-Württemberg at 27th June 2026. Red colors indicate temperatures above the 99th percentile of the observed records (Figure taken from NIZ, 2026).

The impacts of the June 2026 heat wave on the mean water temperatures of surface waters are in the following assessed in a historical context using Baden-Württemberg (Germany) as a case study. The analysis includes the large river system Rhine (monitoring station Karlsruhe), its major tributary Neckar (stations Hofen and Mannheim)—both classified as federal waterways according to the German Federal Waterways and Shipping Administration (BAW)—as well as the upper Danube (Donau) at the stations Immendingen and Ulm-Wiblingen. The available observational time series, which vary in length depending on the start of measurements at each station, extend to 28th June 2026 and range from a maximum of 49 years (Mannheim, March 1977) to a minimum of 31 years (Ulm-Wiblingen, December 1994).

From a historical perspective, the June 2026 heat wave was evaluated with respect to the highest ever recorded daily mean water temperatures at each river (Fig. 24). By 28 June 2026, the heat wave had already reached

rank 1 at three monitoring stations, rank 2 at four stations, and other high-ranking positions within the record temperature statistics. Traditionally, such extreme temperatures have occurred in the peak summer months of July or August (e.g., 1998, 2003, 2006, 2018, 2022, 2023, and 2025). Only in 2022 and 2026 were these extremes observed as early as June. Furthermore, an increasing trend in the frequency of these extreme events is evident during the 2020s, a pattern that is very likely to persist in the latter half of the decade.

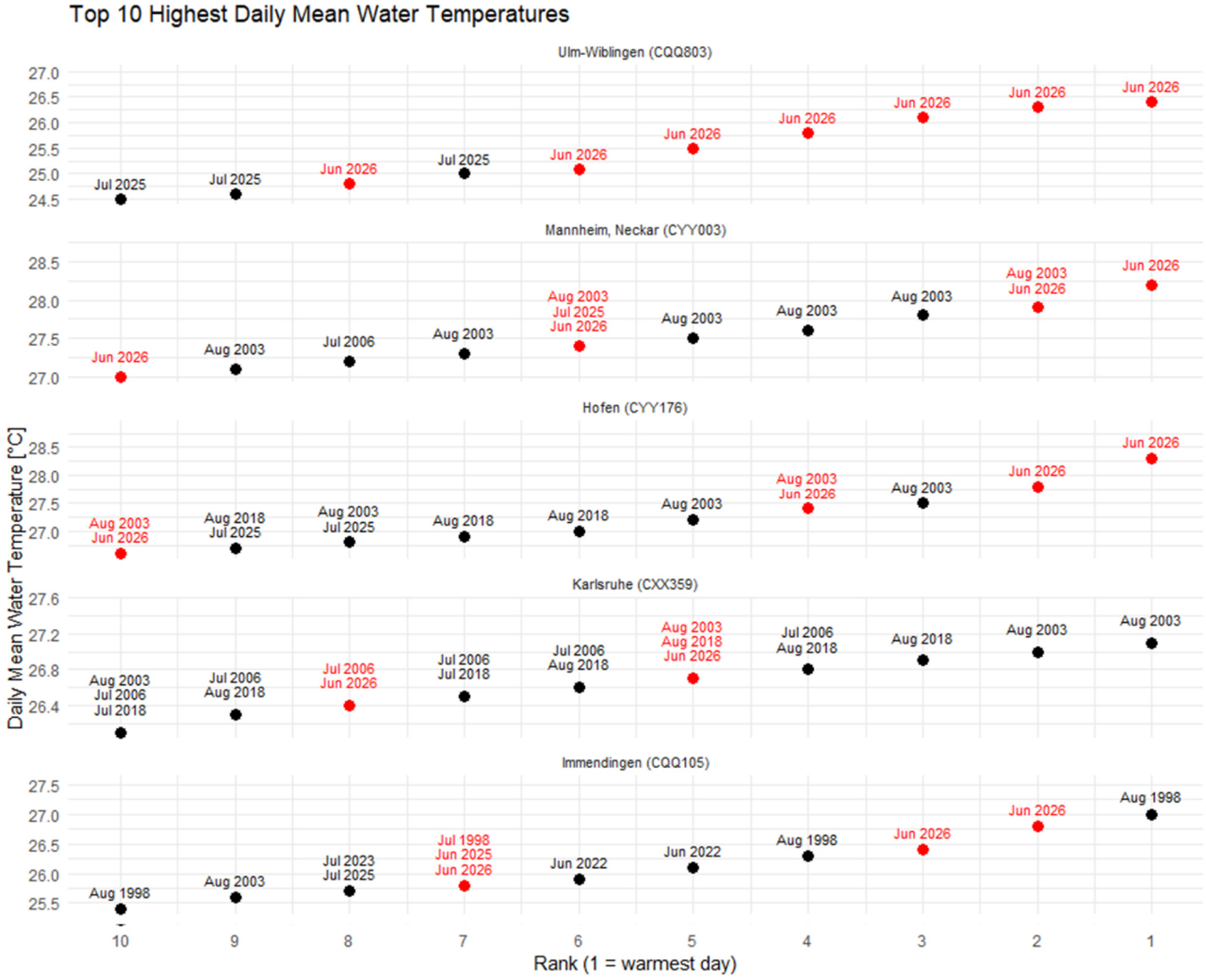

Fig. 24: Ranking of the highest recorded daily mean water temperatures from LUBW monitoring stations on the Rhine (Karlsruhe), Donau (Immendingen, Ulm Wiblingen), and Neckar (Mannheim, Hofen near Stuttgart; Data sourced from the Baden Württemberg State Institute for the Environment, LUBW).

3.3.1. Trend analysis of extreme water temperatures and their temporal shift

As the year 2026 has not yet concluded, a final classification of 2026 extreme-temperature days per year within the long-term context is currently not feasible. However, a first long-term comparison provides critical insights into the thermal evolution of these river systems over the past 31 to 49 years.

The long-term analysis of the annual number of days on which the daily mean water temperature exceeds the 90th percentile (P90) of the respective full daily temperature record reveals a clear increase at all monitoring stations (Fig. 25). For the 90th percentile, statistically significant to highly significant trends are observed at all stations except Hofen (Neckar), ranging from approximately +0.5 to +1.3 days per year. The Danube at Ulm exhibits the strongest warming trend since the beginning of observations in 1994, with an increase of 1.25 days per year – corresponding to a cumulative increase of approximately 40 days per year up to the June 2026 heat wave.

Trends for the 95th percentile (P95), representing exceptionally extreme values, are, as expected, lower and more variable over time, ranging from +0.2 to +0.9 days per year. The high interannual variability, particularly for P95, results in individual years without exceedances. However, a decline in such “zero years” and an increasing frequency of years with numerous extreme-temperature days is evident for P90. The longest time series (Neckar) indicates that “zero years” were still common during the 1980s; however, since the late 1980s, a marked increase in mean water temperatures and a complete disappearance of such years can be observed. Overall, the distribution of daily mean water temperatures has systematically shifted toward higher values since the beginning of the respective observation periods.

Parallel to the observed increase in extreme water temperatures, the analysis of the earliest occurrence of these events (i.e., exceedance of P90 threshold temperatures) indicates a clear temporal shift toward earlier dates within the year (Fig. 26). Linear trends range from approximately −0.2 to −1.1 days per year, with highly significant developments recorded at Karlsruhe (−1.06 days/year), Rheinfelden (−0.90 days/year), and Immendingen (−0.72 days/year). At the Rhine station Karlsruhe, such extreme temperature events now occur, statistically, approximately 35 days earlier in the year compared to the start of observations in 1993.

In summary, extreme water temperatures in the rivers studied are not only occurring more frequently, but are also occurring earlier in the year. This trend will likely be reflected in many other water bodies in Germany and Central Europe. Against this backdrop, more frequent occurrences of extreme water temperatures in the future could pose increasing challenges for fish populations and aquatic ecosystems, as well as for industrial operations and energy supply infrastructure.

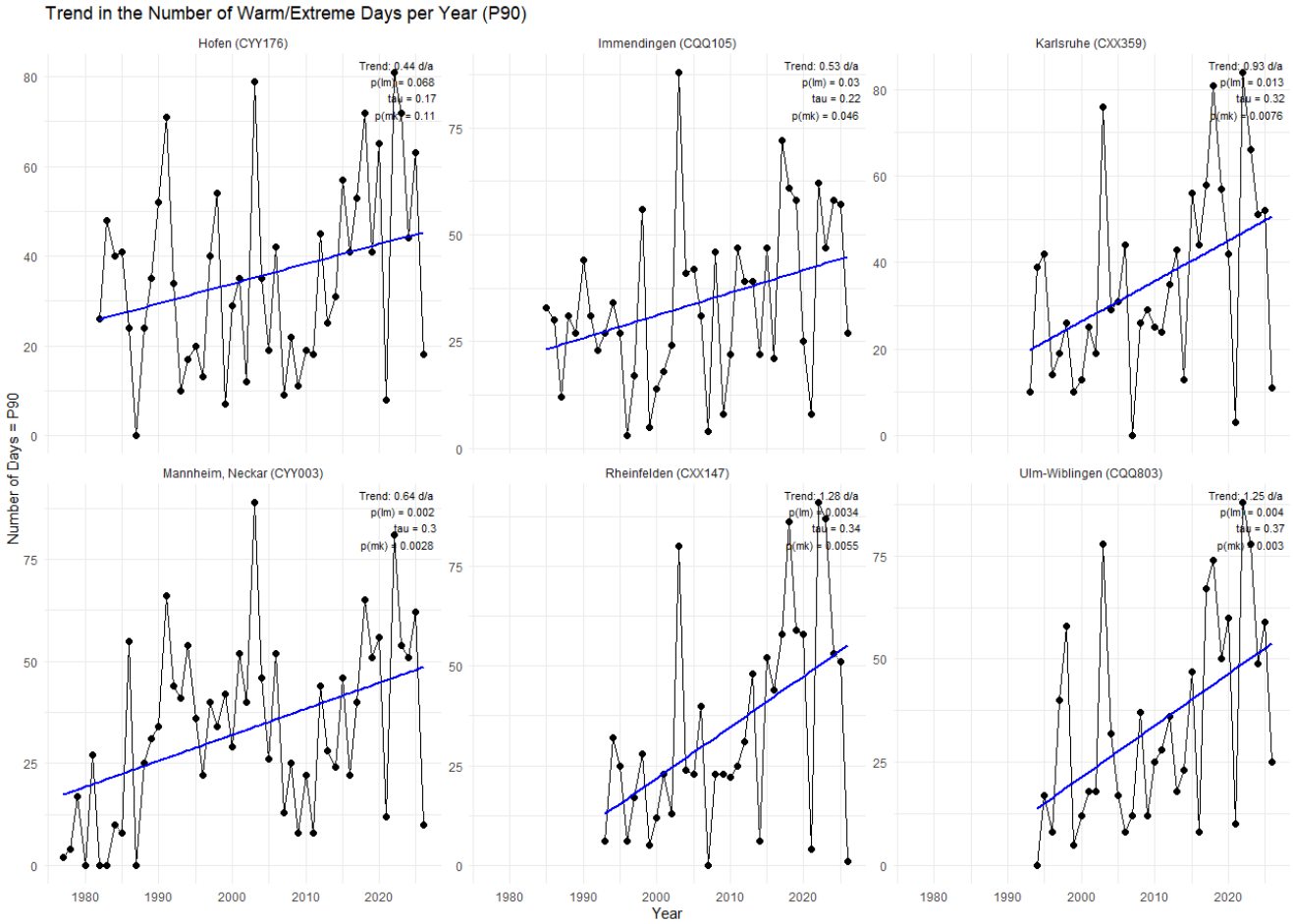

Fig. 25: Trends in the number of days with warm river water temperatures at selected gauges in Baden-Württemberg.

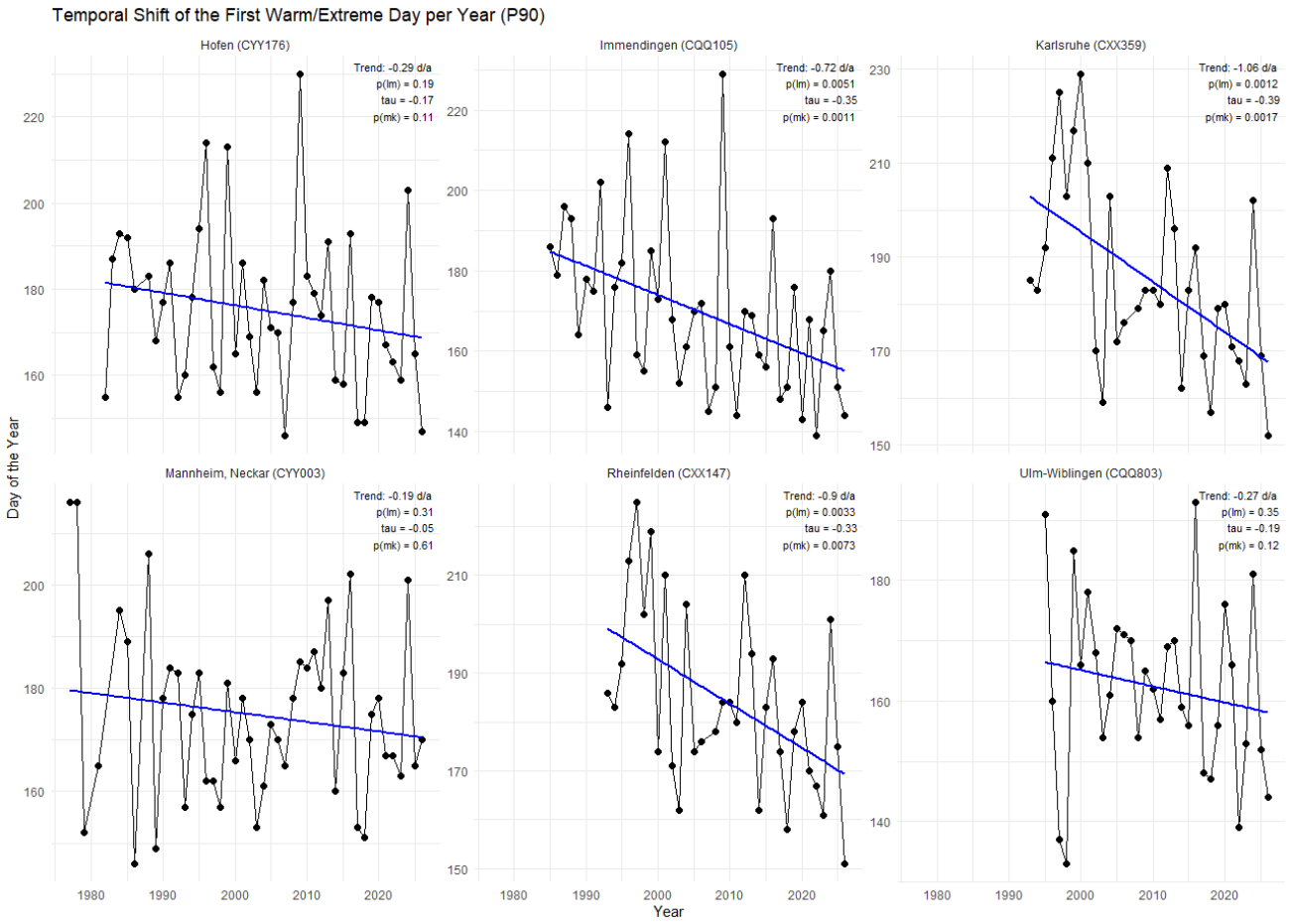

Fig. 26: Trends in the first occurrence of warm river water temperatures at selected gauges in Baden-Württemberg.

3.4. Lake water levels

Lakes in southern Germany generally exhibit low water levels, mainly as a consequence of the increasing climatic water deficit (see Section 3.1). If they are fed by alpine rivers, the low water levels are also due to low snow cover and melt. Lake Constance, Germany's largest lake, is a striking example (Fig. 27). According to NIZ (2026), on 30th June, the lake's water level was 326 cm, 81 cm below the 30-year average (1991-2020) of 407 cm for this date. Among the long-term records since 1850, only 28th June 1865, had a lower value (322 cm).

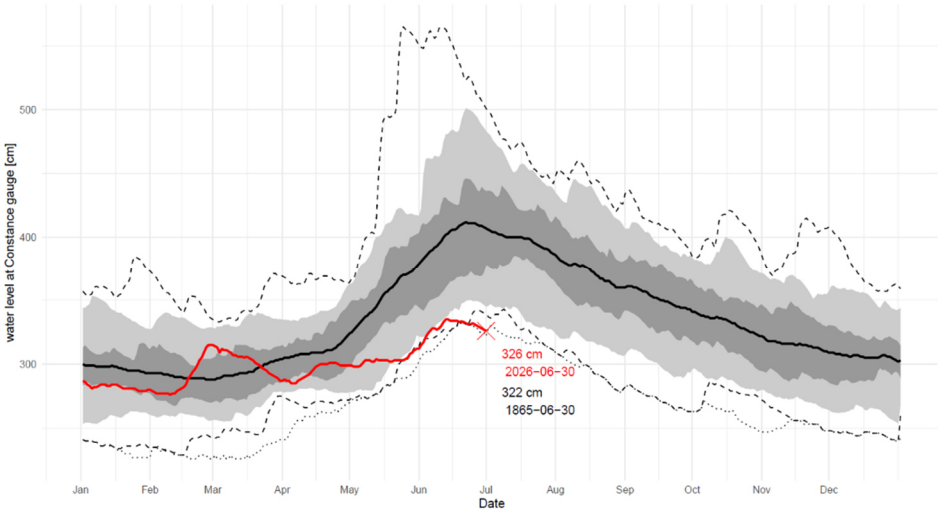

Fig. 27: Lake Constance water levels year-to-date compared with the average annual course (Reference period: 1991 to 2020). Dark grey: 90 % Interval, light grey: 50 % interval, black line: mean, dashed lines: max/min, dotted line: lowest values ever recorded. Since 1865, 2nd-lowest water level at 30 June.

3.5. Groundwater

Similar to the trends in lake water levels (see Section 3.4), and due to the same causes, groundwater levels in Southwest Germany are on a long-term decline (Fig. 28). NID (2026) report that at the time of the heat wave, 80 % of all shallow groundwater wells and 74% of all deep groundwater wells showed low to very low values, and occasionally, new all-time lows were recorded in southern Bavaria (see Fig. 29).

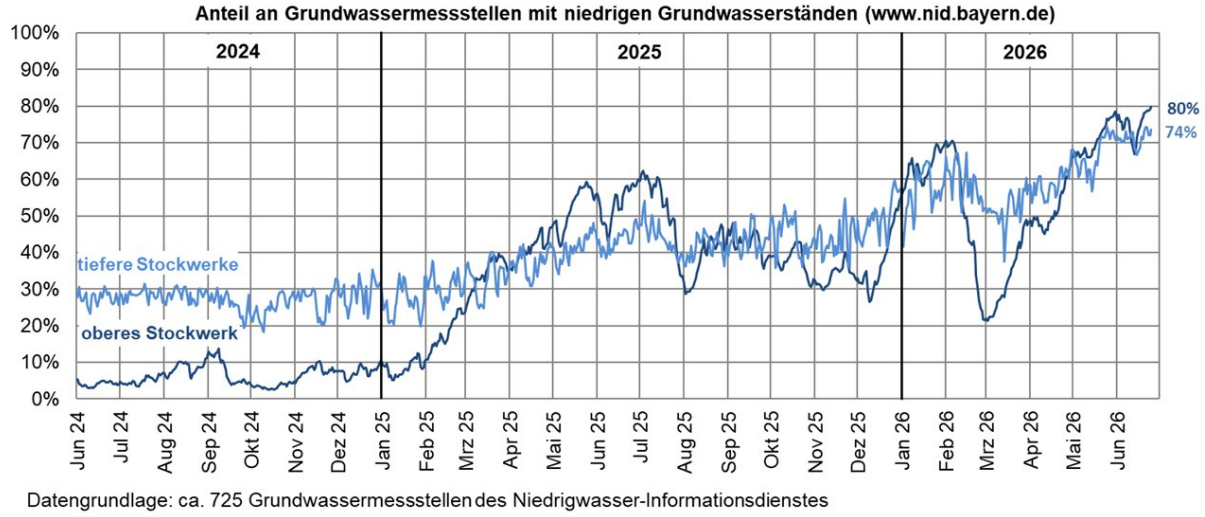

Fig. 28: 2-year time series of percentage of groundwater wells and wells with water levels classified as low, very low, or all-time low. Dark blue line indicates shallow wells, light blue deep wells.

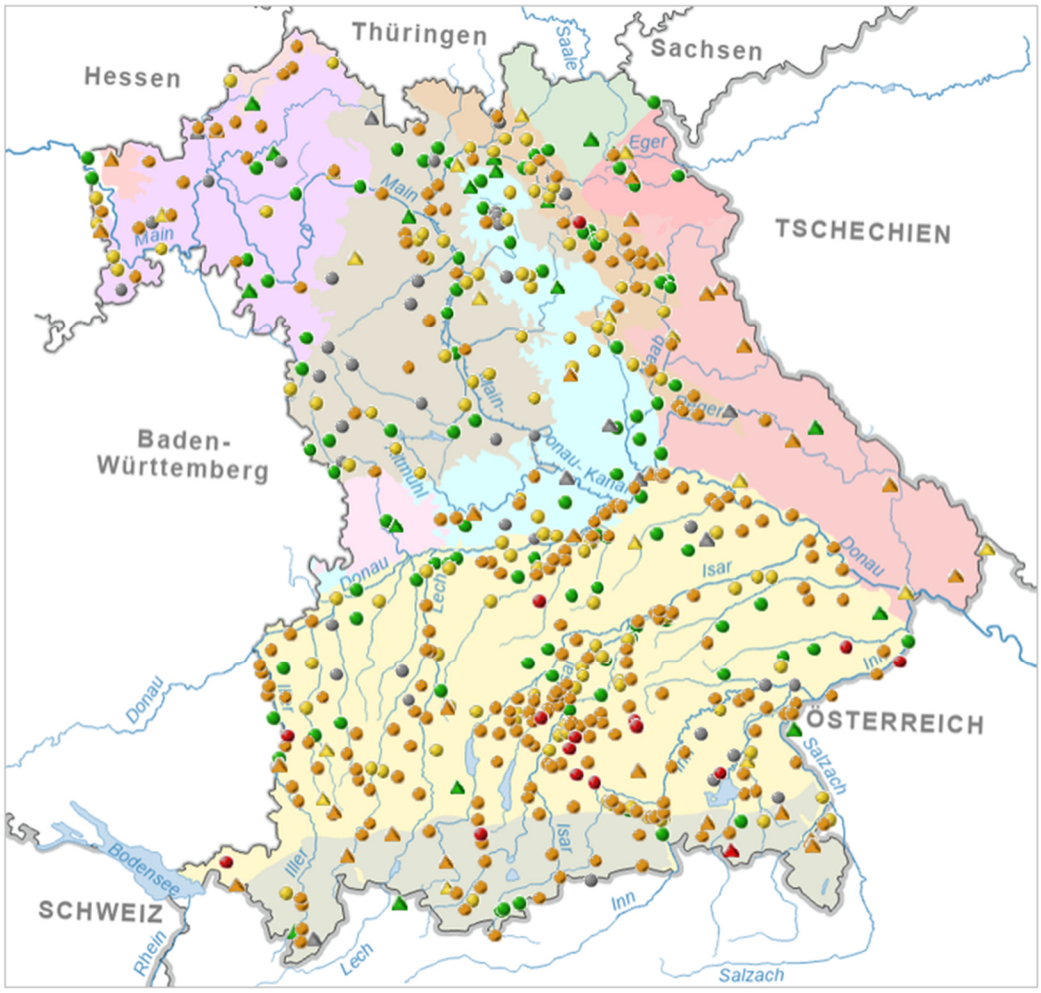

Fig. 29: Ground water levels and surface well discharge (daily averages) at 1st July 2026 (Classification: Green dots indicate normal conditions, yellow dots indicate low water levels (< 70th percentile), orange dots indicate very low water levels (< 90th percentile, red dots indicate all-time lows; Figure taken from https://www.nid.bayern.de/grundwasser).

3.6. Soil moisture

3.6.1. Topsoil drought development in Germany

Soil moisture conditions in the form of plant-available water (*in German: nutzbare Feldkapazität, nFK*) depleted substantially over the course of the heat wave. At the beginning of the heat wave over Germany on 16th June, 75 % of the country had already conditions under threshold dryness for vegetation stress (< 50% nFK), and 45 % of the country had conditions under vegetation stress (< 30 % nFK; Fig. 30a). By the end of the heat wave on 29th June, these numbers had increased to over 90 % and 75 % of the country, respectively (Fig. 30b). A general lack of precipitation resulted in decreasing soil moisture conditions throughout the heat wave, with the most rapid day-to-day depletion occurring at the beginning of the heat wave, when water was still available for evapotranspiration (Fig. 31). The maximum soil moisture depletion did not occur until the end of the heat wave.

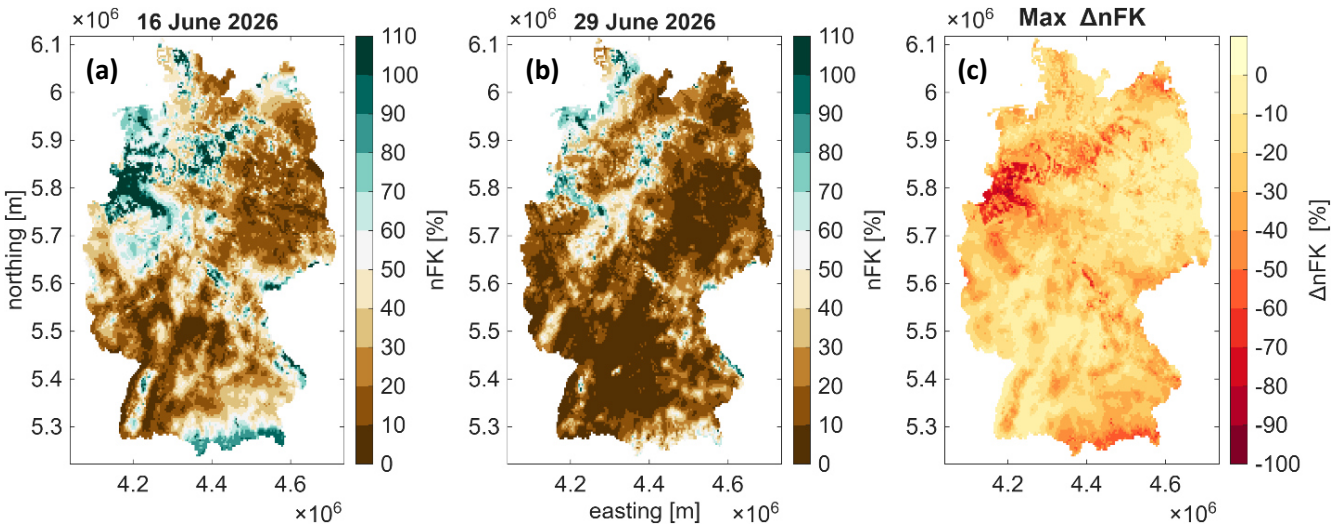

Fig. 30: Plant-available water (German: nutzbare Feldkapazität, nFK) (a) at the onset (16th June 2026) and (b) at the end (29th June 2026) of the heat wave in Germany, (c) as well as the maximum total depletion during the heat wave. In (a) and (b), conditions below 50 % indicate the beginning of vegetation stress, and conditions below 30 % indicate vegetation stress (Data sourced from the German drought monitor: https://www.ufz.de/index.php?de=37937, accessed 30th June 2026).

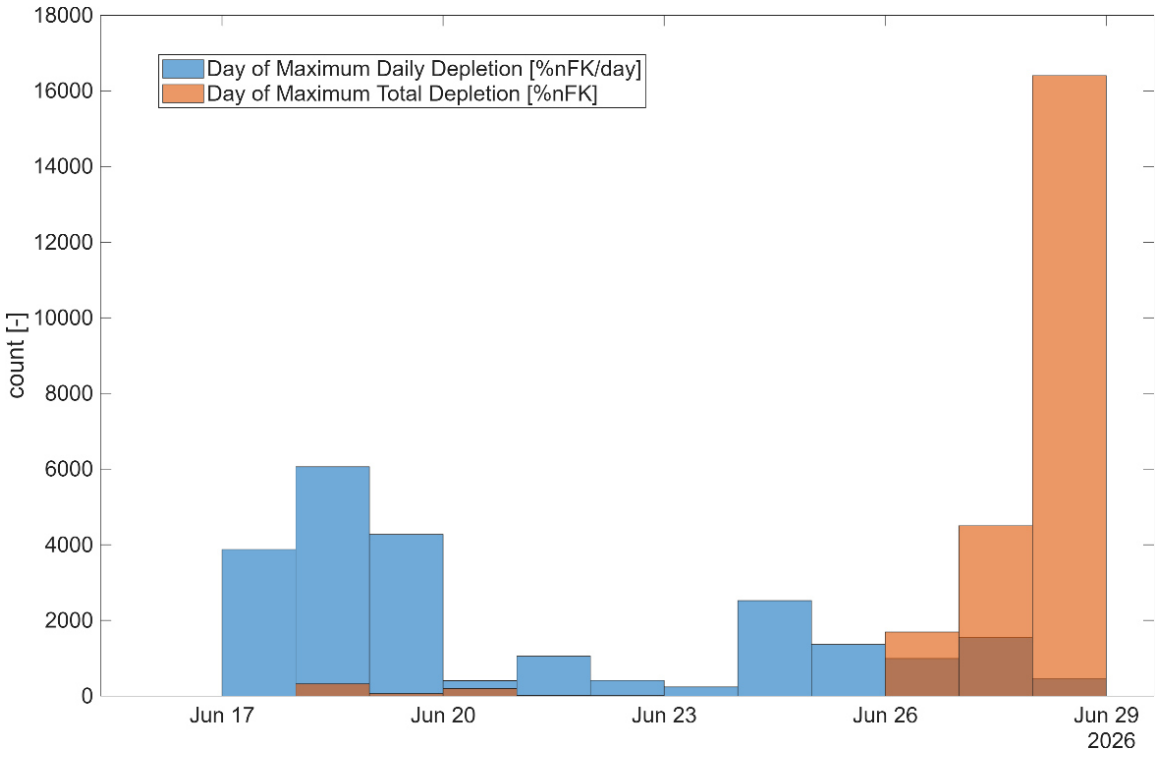

Fig. 31: Timing of maximum daily and maximum total soil moisture depletion during the German heat wave.

Indeed, longer-term soil moisture drought conditions were already quite critical at the beginning of the heat wave, particularly over southern Germany, because of the all-time low climatic water balance. The German drought monitor of the UFZ presents soil moisture drought conditions based on the previous month on a near-real-time basis (Zink et al., 2016; Boeing et al., 2022). The soil moisture data is calculated via a mesoscale hydrological model, which uses daily meteorological variables (precipitation, temperature, and potential evapotranspiration) to calculate major hydrological processes. This monitor classifies drought intensity into classes based on a soil moisture index (SMI) that describes the percentile rank of soil moisture dryness (lower is drier) in comparison to the years 1973 to 2023. Dryness begins when conditions are below the 30th percentile (lowest 30 % of the record), whereas drought conditions begin below the 20th percentile.

Despite a dry spring, topsoil (uppermost 25 cm of soil) conditions in much of the northern part of Germany had recovered to normal levels on 16th June (Fig. 32). By the end of the heat wave over Germany, the reduction of plant-available water resulted in largest changes in the soil moisture index over eastern Germany, where the SMI dropped by up to 45 percentile points. As a result, the overall area experiencing moderate (below the 20th percentile) to exceptional (below the 2nd percentile) drought events increased from 44 % to 54 %. Rapid expansions in drought area are not unprecedented; indeed, more intense and widespread expansions in topsoil-affected drought area occurred in 2025 (UFZ, 2025). However, such an event during the growing season can have consequences for agriculture, which is most dependent on topsoil conditions.

Interesting to note is the difference in the spatial distributions of the maximum changes in SMI and nFK: areas with largest changes in soil moisture do not coincide with those areas exhibiting the largest changes in SMI. This is a result of the near-normal soil moisture conditions at the beginning of the heat wave, meaning that a substantial depletion in plant-available water (ΔnFk) still results in generally acceptable SMI levels in the norther half of Germany. The situation in southern Germany was quite different—here, topsoil conditions were mostly already under extreme and exceptional drought conditions at the beginning of the heat wave. Despite further drying, the soil moisture conditions were already at low percentiles resulting in only little changes in the SMI.

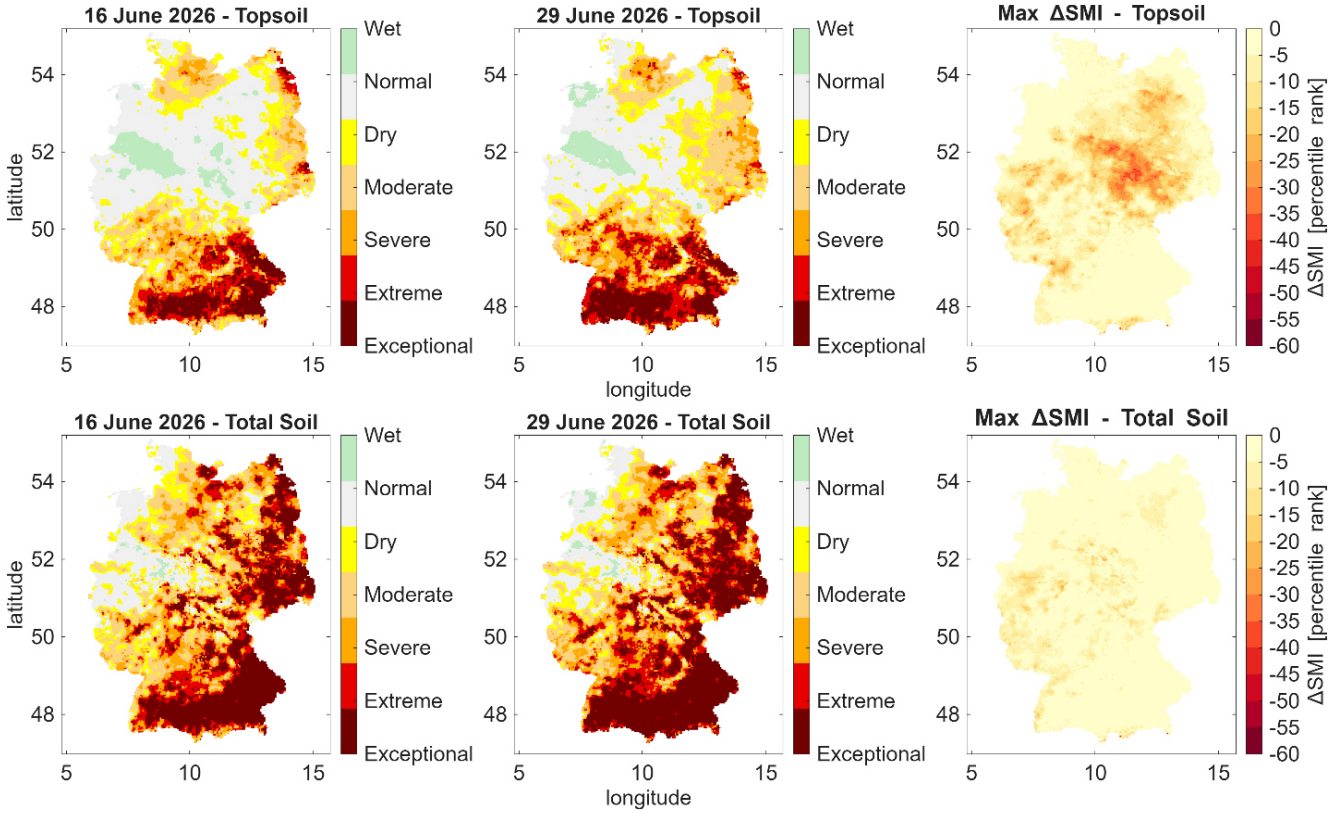

Fig. 32: The UFZ drought monitor shows conditions in the topsoil (0 to 25 cm depth) and the total soil column (up to 1.8 m depth) at the onset and end of the heat wave in Germany (16th to 29th June 2026). The change in soil moisture index *(SMI) represents the change in likelihood of occurrence (negative change means increasingly unlikely dryness; Data sourced from the German drought monitor:* **https://www.ufz.de/index.php?de=37937***, accessed 30th June 2026).*

Considering the total soil column (up to 1.8 m below the surface), 75 % of the country was already experiencing moderate to exceptional drought conditions by the onset of the heat wave. Until the end of the heat wave, this number increased to 79%. The area suffering from extreme to exceptional drought conditions increased from 55 % to 63 %. This continues along a general trend of increasing drought intensity since January, in part due to a relatively dry winter and spring.

Drought conditions in the total soil column are more persistent than in the topsoil, as the soil surface is more prone to rapid drying and can pull water from the deeper soil column to fulfil evaporative demand. Conversely, during rainfall events, the soil surface generally needs to be saturated before more water can infiltrate into the deeper soil layers. Thus, longer and more persistent rainfall over the course of months or even years are needed before moisture in the total soil column can return to normal, which will also impact streamflow and groundwater levels in the future.

3.6.2. Land-atmosphere coupling in the heat wave: Role of moisture limitation

Land-atmosphere (LA) coupling has been identified as a primary factor contributing to the disproportionate intensification of heat waves (Benson and Dirmeyer et al., 2021). A useful proxy to identify the role of LA coupling in the amplification of a heat extreme is to assess whether soil moisture (SM) falls below a critical value (critical SM), at which evapotranspiration strongly reduces, causing an increase in the sensible heat flux and thus in near-surface temperature (Klimiuk et al., 2026). Below critical SM conditions, the land-atmosphere system can enter a so-called hypersensitive regime, making unprecedented temperatures possible (Benson and Dirmeyer et al., 2021).

The share of moisture-limited (ML) days in Europe over the period from 13rd to 29th June is shown in Figure 33a,b, as computed from ERA5 (Herschbach et al., 2020), for the historical period 1985 to 2014 (a) and for 2026 (b). During the current heat wave, up to 100 % of days show ML conditions in Spain, France and Italy. In southern Germany, over 80 % of days show ML conditions, which is atypical for this time of year. The anomalies of the share in ML days reach 60 to 90 % over the mentioned regions (Fig. 33c). The anomaly pattern of the ML days and the average anomaly of daily maximum 2m temperature (Fig. 33d) show strong similarities, implying a substantial role of LA coupling in the unprecedented magnitude of the current heat wave.

The role of moisture limitation for the magnitude of the heat wave is well discernible in Figure 34, where the evaporative fraction EF = LE / (LE+H), which is the fraction of latent heat flux to the sum of latent and sensible heat fluxes (panels a-c), and daily maximum 2m temperature (panels d-f) are plotted against near-surface SM. The selected subregions represent 2° x 2° lon/lat boxes around the grid points with the strongest temperature anomalies in different countries (see Fig. 33d). The critical SM, shown as a dashed vertical line in Figure 34, was computed based on the 1985 to 2014 (May to September) values of EF and SM. EF tends to drop for soil moisture values below the critical soil moisture. It is especially seen in Figure 34b-c for subregions in France (FR) and Germany (DE). The role of LA coupling over the United Kingdom (UK; Fig. 34a) is less pronounced, and the uncertainty in the critical SM is large.

As can be seen from Figure 34e to 34f, the average temperature anomalies of 11 °C (FR) and 8.7 °C (DE) may be a direct consequence of the positive feedback that has transitioned the LA system to the hypersensitive regime. The prerequisite for initiating such feedback could be the coincidence of several factors. Particularly important for France was the May heat wave that preceded the event in June and caused already intense evaporation and soil desiccation (see the “movement” of the May data points towards the critical soil moisture in Figure 34b and e.

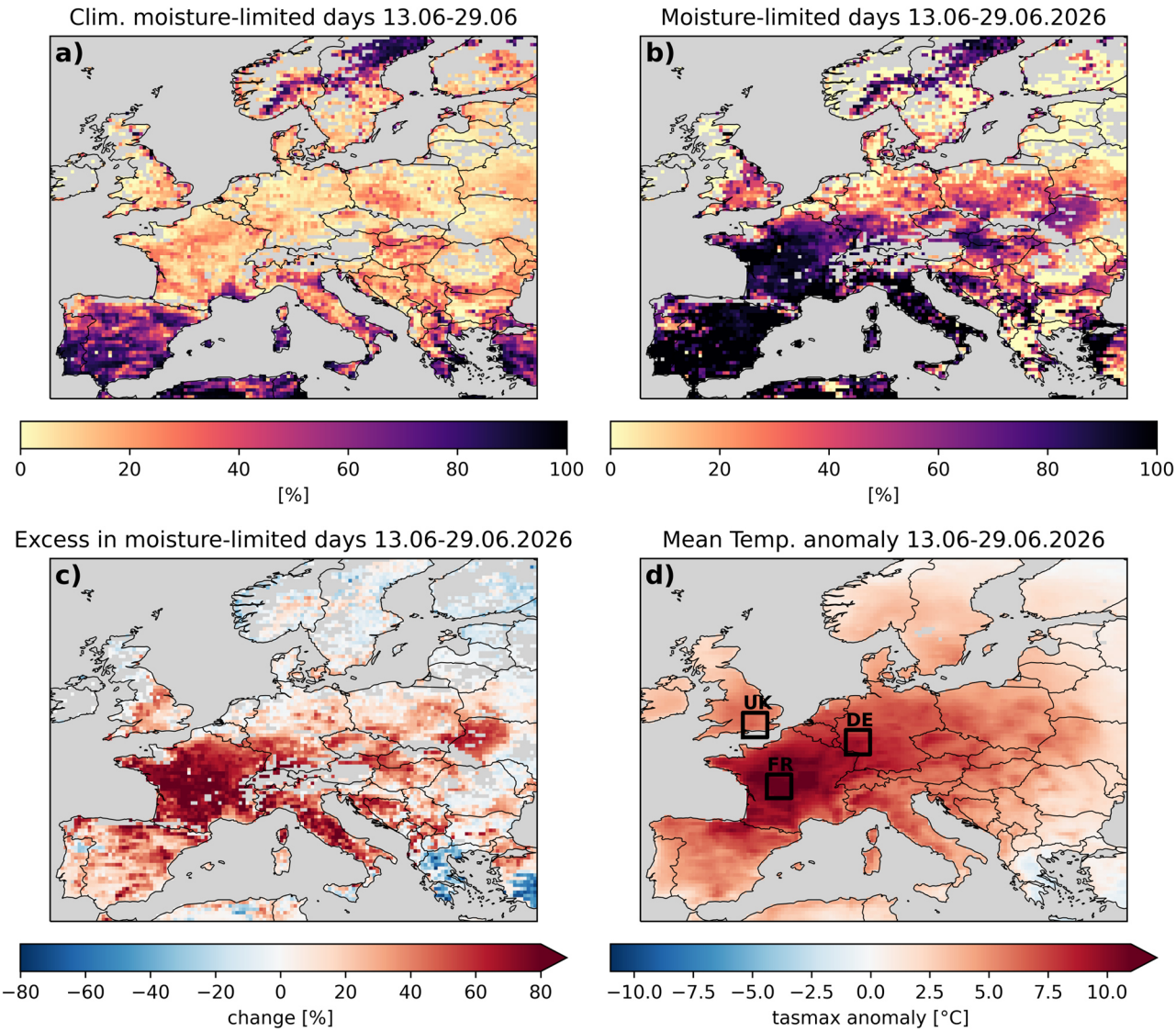

Fig. 33: (a) Average share of moisture-limited days over the period from 13rd to 29th June between 1985 and 2014; (b) Share of moisture-limited days over the heat wave period from 13rd to 29th June; (c) Anomaly of the share of moisture-limited days over the heat wave period from 13rd to 29th June; (d) Daily maximum 2m temperature anomaly over the period from 13rd to 29th June. Black boxes denote the 2° x2° longitude-latitude regions around the points of maximum temperature anomaly over the heat wave period in the United Kingdom (UK), France (FR), and Germany (DE).

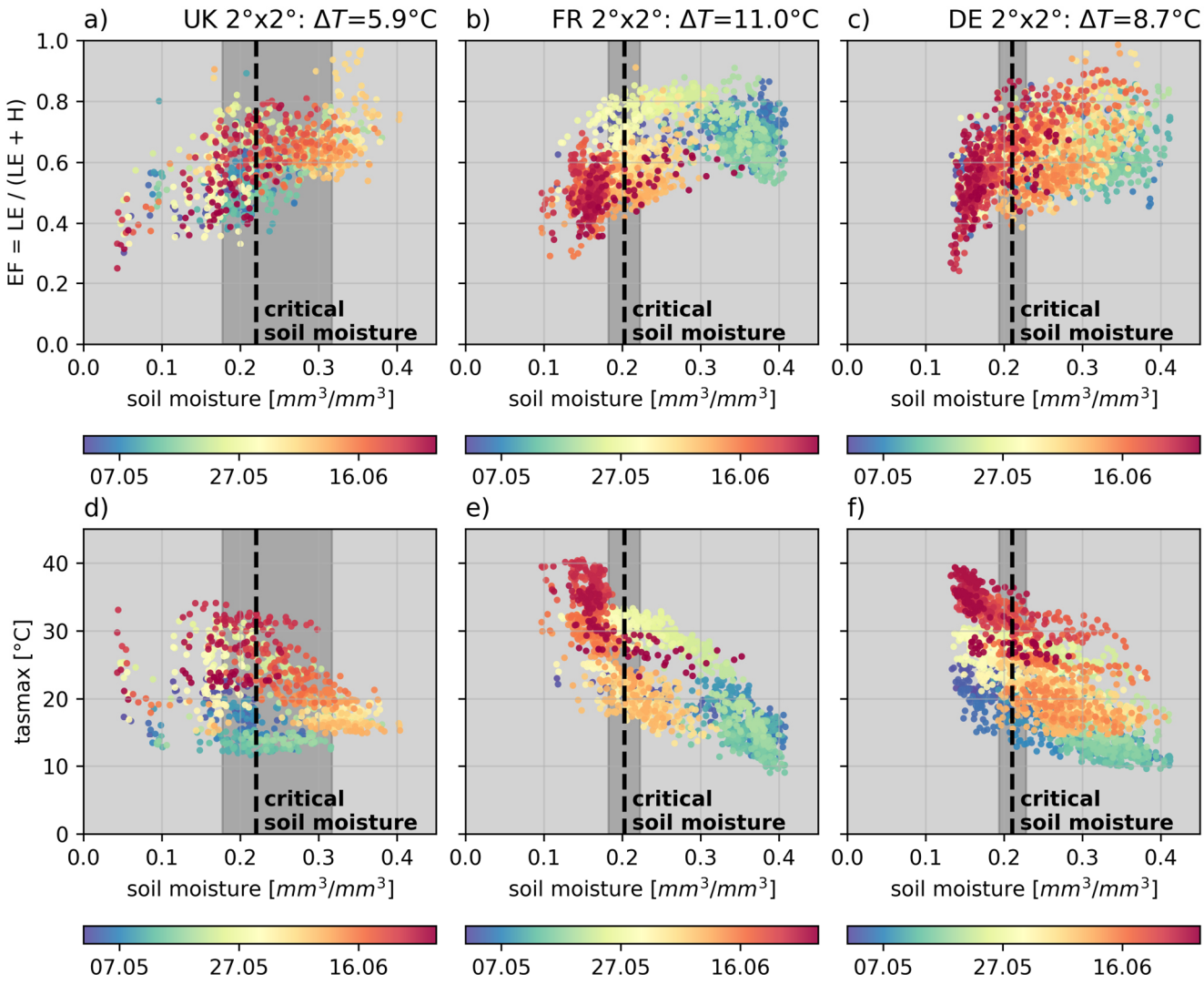

Fig. 34: (a-c) Daytime (06:00 to 18:00) evaporative fraction vs. near-surface soil moisture and (d-f) daily maximum 2 m temperature vs. near-surface soil moisture over the 2° x 2° boxes around the grid point of the highest temperature anomaly in (a, d) the United Kingdom, (b,e) France, and (c,f) Germany; the average anomaly of the daily maximum 2 m temperature is shown in the panel titles. The boxes are shown in Figure 33d. Shading corresponds to the date.

4. Impact: Effects on renewable energy

4.1. Meteorological anomalies and renewable energy generation

Beyond its direct meteorological impacts, the June 2026 heat wave also substantially affected the meteorological drivers of renewable electricity generation. Persistent high-pressure conditions altered solar radiation, land-surface temperatures, and wind speeds, thereby influencing photovoltaic and wind power generation as well as the overall balance of the German electricity system.

Methods

The analysis focuses on 13rd to 29th June, and uses data from the entire month of June for the preceding 15 years as reference. For solar radiation at the surface, the SARAH dataset based on geostationary satellite data from the SEVIRI sensor on Meteosat Second Generation (Pfeifroth et al., 2023) was used. Land-surface temperature was taken from the EUMETSAT LSASAF MLST (LSA-001) product based on the same satellite sensor at 12 noon German time. Wind speed at 100m altitude above ground was obtained from ECMWF ERA5 and ERA5T reanalysis products. ERA5T is the near-real-time extension of the ERA5 reanalysis, providing preliminary atmospheric data that are typically available within a few days and are later replaced by the final ERA5 product. All products were mapped onto a 0.05° grid for analysis.

The electricity figures additionally show the full heat wave window from 13rd to 29th June 2026. For the energy-system comparison, hourly SMARD data (SMARD, 2026) were used for realized electricity consumption, photovoltaic generation, and wind generation. Wind generation is onshore plus offshore where SMARD provides the regional offshore series.

The German electricity transmission system is operated by four transmission system operators (TSOs): 50Hertz, TenneT, Amprion, and TransnetBW. Their control areas provide the regional framework used here to analyse the impacts of the heat wave on renewable electricity generation and demand.

Findings

Solar radiation at the surface (Fig. 35a, Fig. 36) was increased by 31.2 % nationally (299.70 W/m^2 relative to 228.36 W/m^2 in the reference period). The 50Hertz area experienced a later increase, resulting in a less pronounced overall increase. At the same time, the land surface temperature (LST) and, consequently, the temperature of the PV installations increased markedly (Fig. 35b). Nationally, the temperature was 5.4 K above the reference value, particularly in the Amprion and TransnetBW areas. Concurrently, wind speed remained well below typical June values, in particular in the 50Hertz region, an overall reduction of 28.6 % for Germany (Fig. 37, Fig. 38).

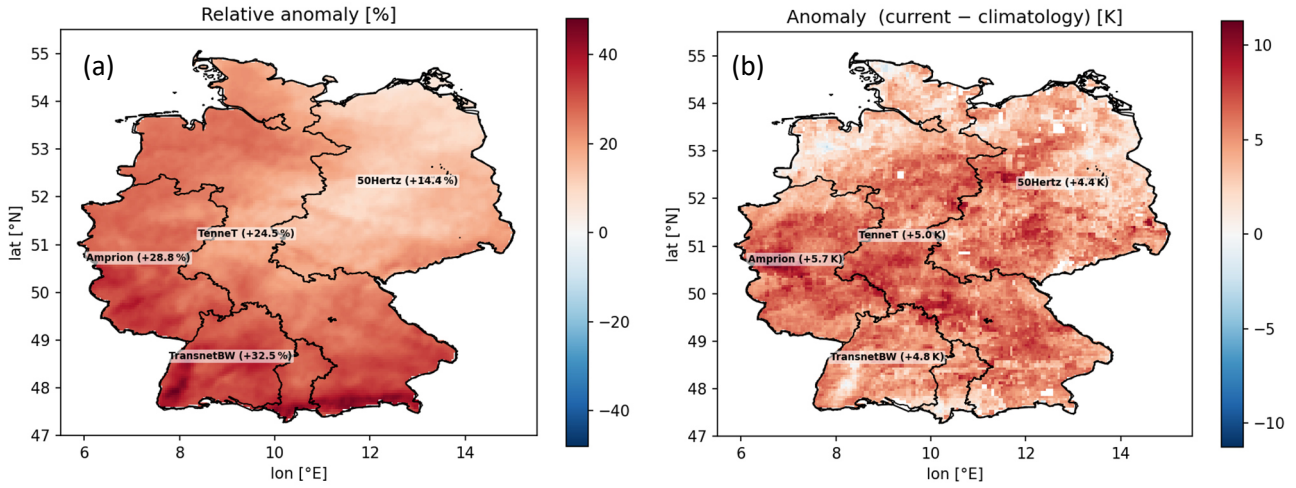

Fig. 35: (a) Relative anomaly of solar radiation incoming at the surface (SARAH dataset), (b) absolute anomaly of land surface temperature (LSASAF dataset) at local noon, both relative to the previous 15 years. The German areas covered by the four transmission system operators 50Hertz, TenneT, Amprion, and TransnetBW are marked on the map.

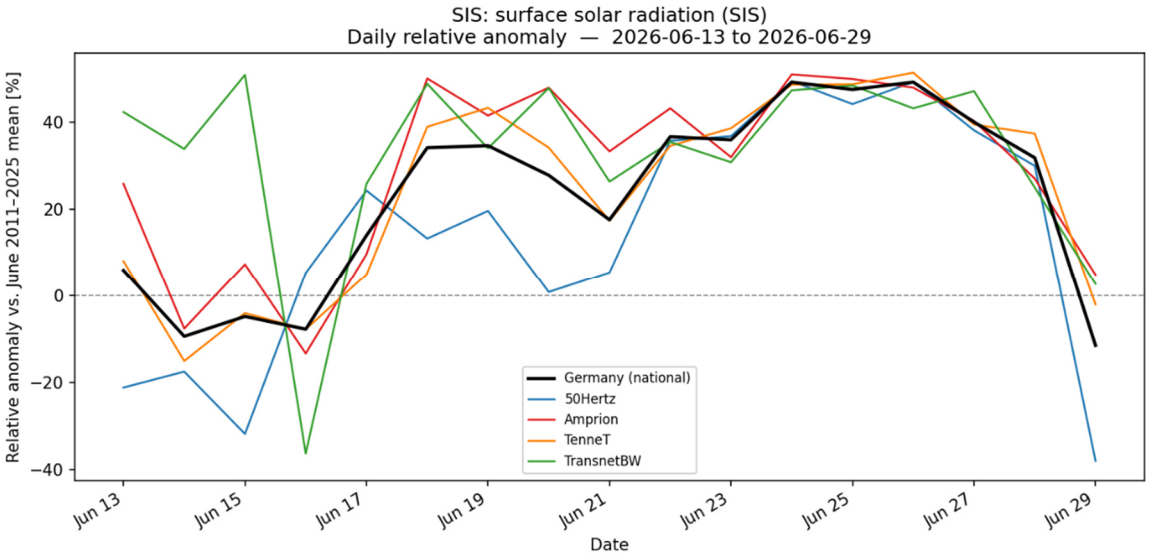

Fig. 36: Relative daily anomalies of surface solar radiation compared with the previous 15 years.

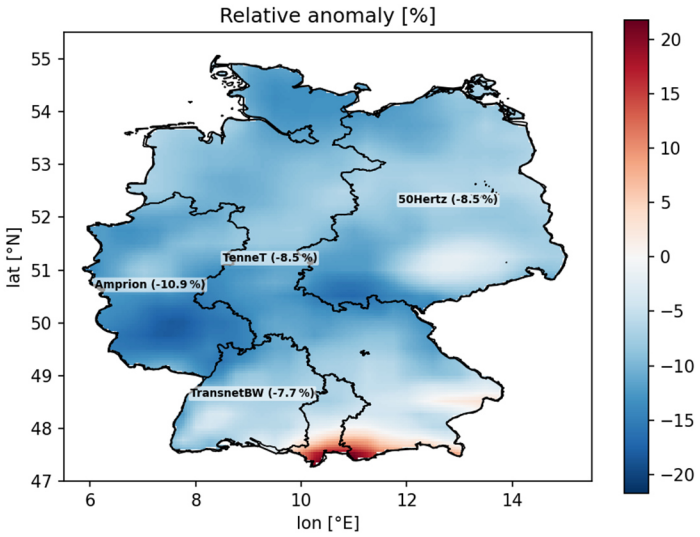

Fig. 37: Relative anomaly in wind speed 100 m above ground (all-hour mean) compared to the previous 15 years.

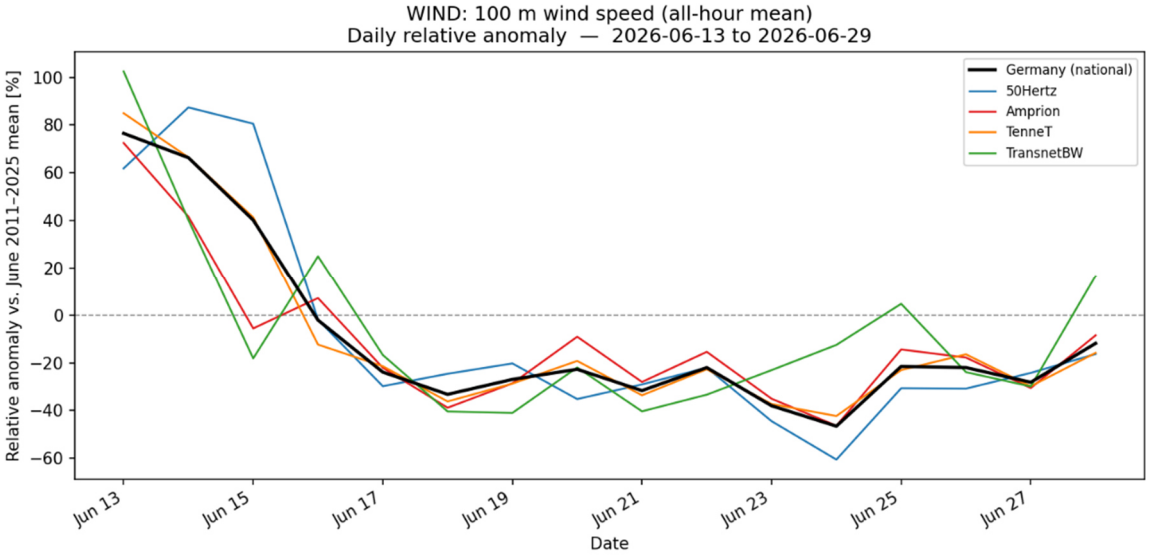

Fig. 38: Relative daily anomalies in wind speed 100m above ground (all-hour mean) compared to the previous 15 years.

The atmospheric blocking and stationary high-pressure systems characteristic of this heat wave (see Section 2) dictate not only the thermal environment but also the fundamental drivers of renewable energy generation. The combination of clear-sky conditions and stagnant air masses creates a stark dichotomy in generation potential: a vast surplus of solar resources paired with a severe deficit in wind. To quantify these effects on the energy grid, the meteorological anomalies were cross-referenced with realized generation and load data from the four German Transmission System Operator (TSO) zones (Fig. 39).

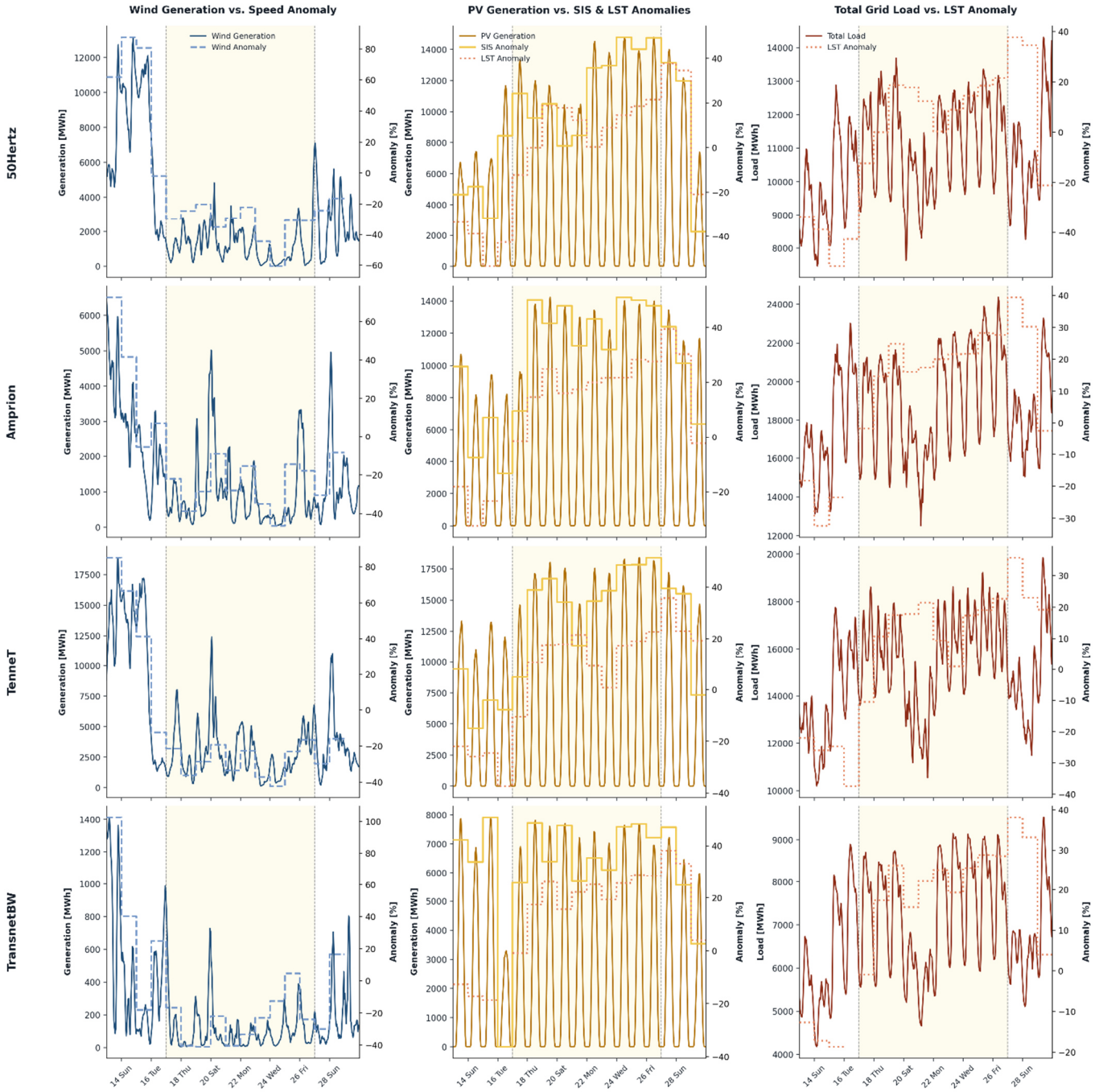

Fig. 39: Hourly renewable generation and load in Germany TSO zone during the heat wave combined with anomalies from wind, radiation and temperature (Data: SMARD, SARAH, EUMETSAT LSASAF MLST, ECMWF ERA5).

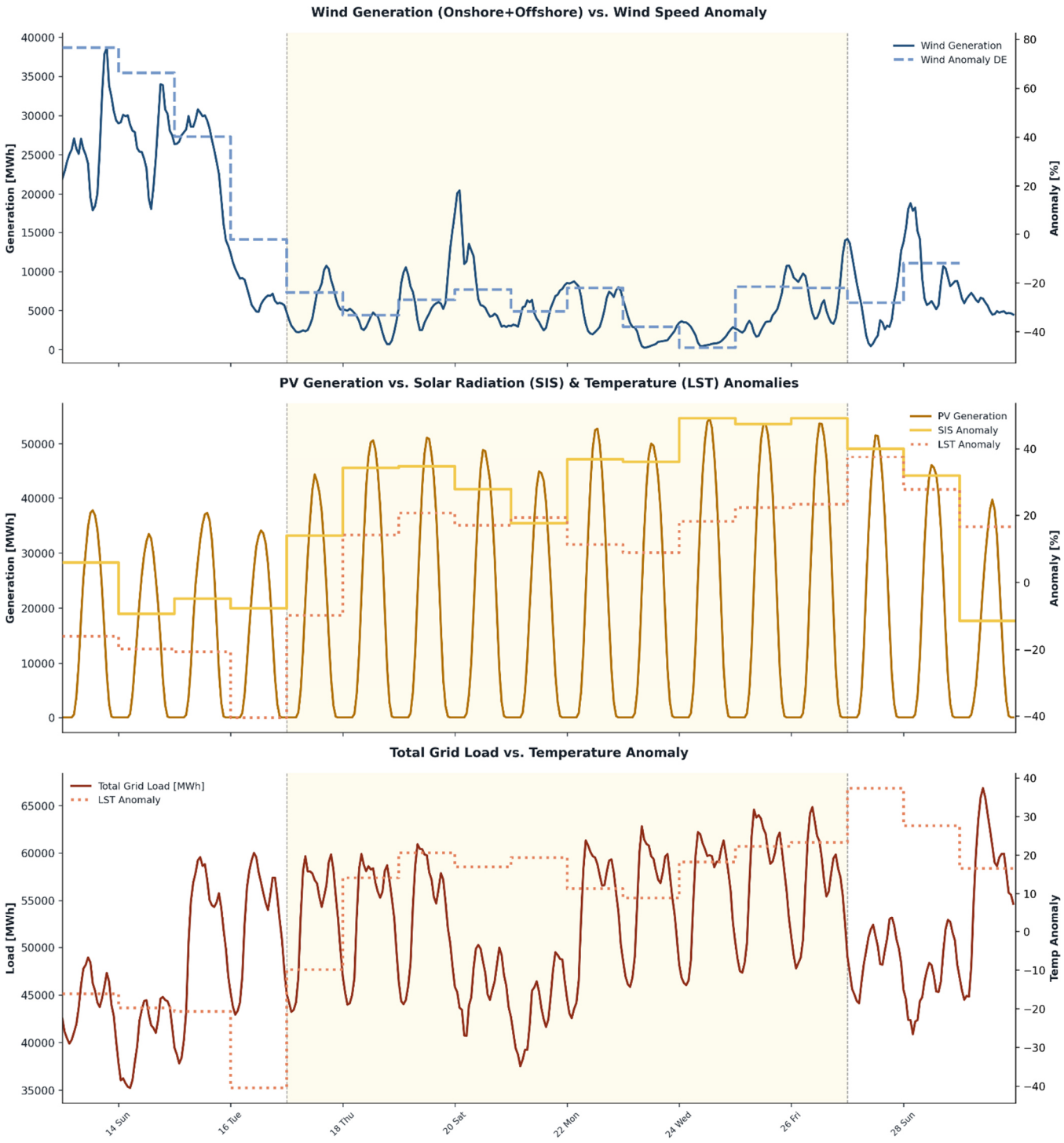

Fig. 40: Hourly renewable generation and load in Germany during the heat wave combined with anomalies from wind, radiation and temperature (Data: SMARD, SARAH, EUMETSAT LSASAF MLST, ECMWF ERA5).

From 13rd to 29th June, German wind generation averaged about 225 GWh/day, which was 32 % below the average from June 1st to 12nd. The drop was particularly strong in Amprion (-54 %) and TransnetBW (-56 %), with TenneT and 50Hertz clearly lower (-33 % and -7 %). These reductions in generation correlate well with the wind speed anomalies as illustrated in Figures 37 and 38.

Similar effects in solar radiation are mirrored in PV generation. Germany's daily PV generation during 13rd to 29th June averaged about 413 GWh/day, roughly 31 % above the 1st to 12nd June lead-in. The regional pattern is consistent with the radiation anomaly: PV output rose by about 44% in Amprion, 35 % in TenneT, 15 % in 50Hertz and 34 % in TransnetBW relative to the lead-in period from 1st to 12nd June. Higher module

temperatures can reduce PV efficiency, so the observed PV increase should be read as a net effect: stronger irradiance dominating, potentially offset by heat-related efficiency losses.

Despite the severe thermal anomaly, the heat-related load effect was far less prominent than the effects on wind and PV generation. Germany's average daily load increased by about 1.8% during 13rd to 29th June compared with 1st to 12nd June. This muted response indicates that cooling demand is less dominating in the German grid compared to other countries (compare to Section 4.2), without the severe demand spikes often associated with summer heat waves in southern Europe.

4.2. Impact on energy supply, demand, and prices

The June 2026 heat wave influenced electricity markets across Europe through simultaneous changes in electricity demand, renewable generation, and thermal power plant availability. This section examines how these interacting factors affected wholesale electricity prices, residual load, and the operation of the European power system during the event. All electricity and renewable energy data used for the analysis were sourced from the ENTSO-E transparency platform (Entso-e, 2026) and SMARD (2026).

4.2.1. High electricity prices were regional and concentrated in peak hours

The daily maximum price heatmap in Figure 41 shows that the heat wave did not affect every day equally. The most visible stress is a cluster around 18th June, 23rd and 24th June and again toward 29th and 30th June. Belgium, the Netherlands, Germany and Hungary show the highest peak prices, while France recorded an increase in average prices but a lower absolute maximum than its northern neighbors.

On 24th June, France with 433.43 €/MWh and Germany with 747.10 €/MWh reached their highest spot prices since January 2025. Analyses based on SMARD and ENTSO-E data show a daily average of 92.26 €/MWh for France in the heat wave time from 13rd June to 29th June, and a monthly average for June of 66.07 €/MWh, well above the May average of 52.2 €/MWh. In Germany, the average day-ahead price during the heat wave was 110.33 €/MWh, compared with 109.52 €/MWh for June as a whole and 97.54 €/MWh in May.

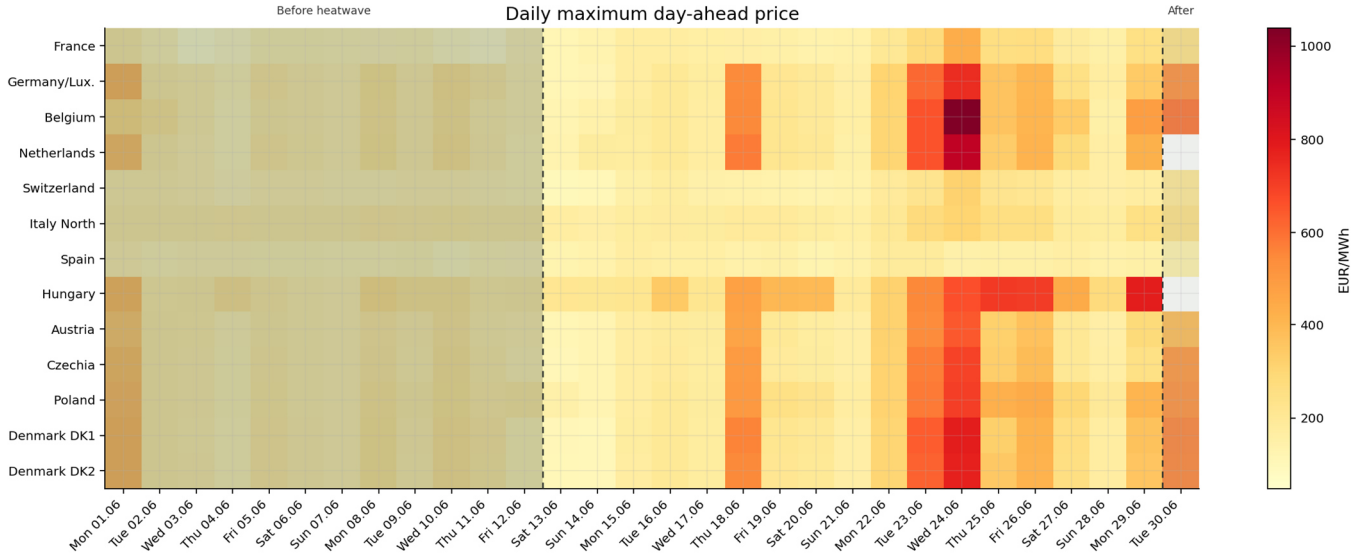

Fig. 41: Daily maximum 15-minute day-ahead electricity prices in selected European bidding zones during June 2026. The shaded periods are outside the heat wave window. The figure highlights the regional clustering of scarcity prices, especially around 24 June, and shows that coupled neighboring markets experienced simultaneous peak-price stress (Data: ENTSO-E Transparency Platform and SMARD).

Figure 42 distinguishes between load, solar, wind, and residual load in Germany. The heat wave effect stems from the combination of temperature-driven load and the daily profile: Solar reduces residual load around noon, but solar output drops in the evening. If wind remains weak at the same time, residual load can rise significantly and be reflected in the price. Residual load is the demand that remains after subtracting solar and wind generation. It is the load that must be met by dispatchable plants, imports, storage or demand response. This effect is visible during the hours of price peaks on 24th and 25th June. Observed wind generation cannot be

interpreted as a purely meteorological indicator. During hours of high solar output, negative prices or local grid congestion, wind farms may also reduce their output for market or system-management reasons. Since complete event-specific curtailment and redispatch data were not available at the time of writing, the analysis uses realized wind generation and cannot fully separate meteorological scarcity from curtailment effects.

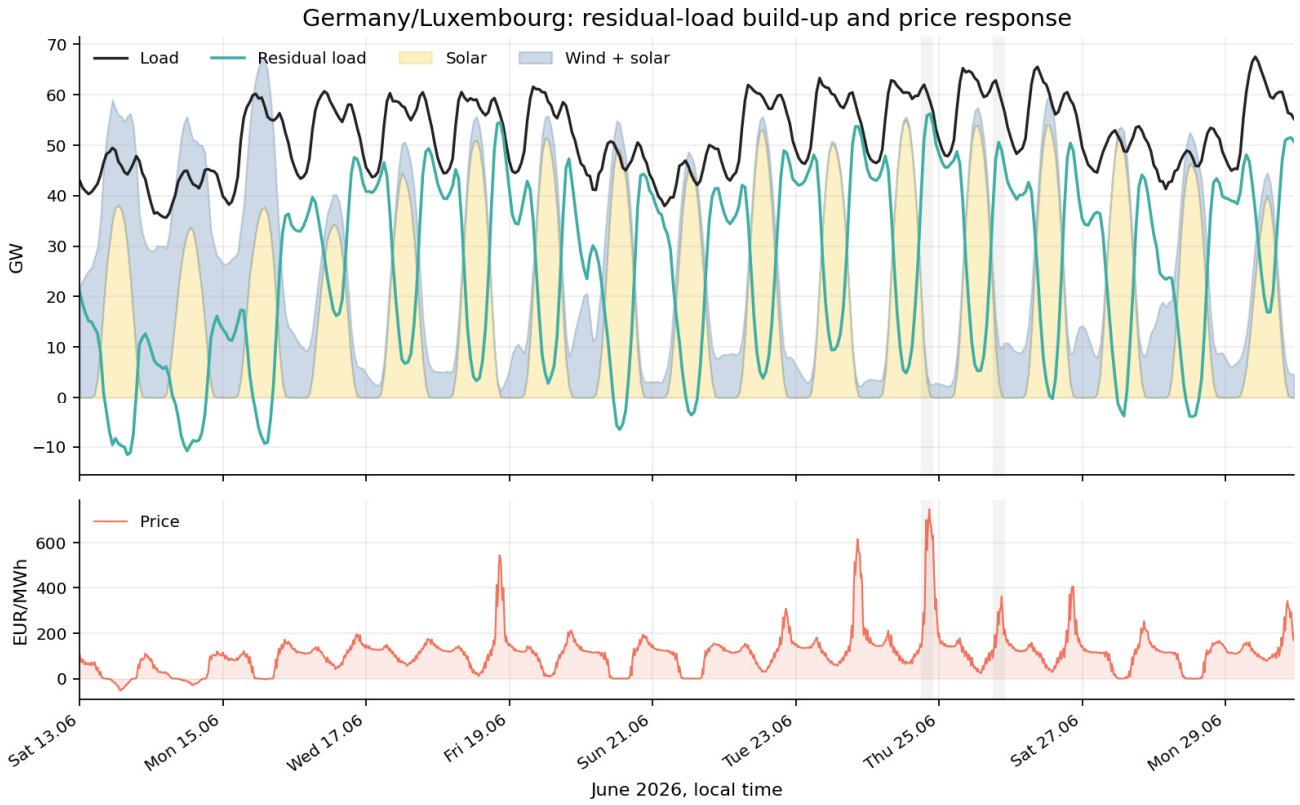

Fig. 42: Electricity load, wind and solar generation, residual load and day-ahead prices in Germany during the heat wave. Residual load is defined as electricity demand minus wind and solar generation. Solar generation reduced residual load around midday, whereas declining PV output, elevated evening demand and weak wind generation produced steep residual-load ramps and price peaks, particularly on 24th and 25th June (Data: ENTSO-E Transparency Platform and SMARD).

4.2.2. The heat wave changed the intraday- and residual load shape

One important market effect is the change in the intra-day shape. As shown in the German example midday prices were often moderated by solar output, but evening prices rose as solar output declined and cooling-related demand remained elevated. In the heat wave, Hungary had an average evening premium of 235 €/MWh, the Netherlands 183 €/MWh, Belgium 176 €/MWh, Germany 172 €/MWh and France 117 €/MWh.

The multiple profiles in Figure 43 shows that several countries had a steeper move from the midday trough into the evening peak during the heat wave. France, Spain and Italy show higher residual-load levels; Germany, Belgium and the Netherlands show particularly sharp evening reshaping. The heat wave hours are compared to the two weeks before the heat wave 1st to 12nd June.

The higher residual load in Germany cannot be attributed to cooling demand alone. Average electricity demand was higher during the heat wave than during the preceding two weeks, but the strongest market effects occurred when this demand increase coincided with lower wind generation and the evening decline in solar output. The observed price peaks therefore reflect a compound residual-load effect.

4.2.3. Wind shortfall made the evening residual load effect stronger

The heat map showing wind and load distribution in Figure 44 illustrates why similar heat conditions can lead to different price trends. Wind power generation is aggregated across onshore and offshore facilities. During the heat wave, several western and southern markets experienced lower wind coverage, precisely at the time when solar power was unable to meet evening peak demand. Belgium and the Netherlands are the most striking examples: During the event, the average wind/load share fell from 23% to 8% in Belgium and from 28% to 16%

in the Netherlands compared to the two preceding weeks. Although Germany continued to generate more wind power in absolute terms, the wind-to-load ratio there also fell by more than 6 percentage points, and in France by an average of more than 7 percentage points.

Low wind/load shares are particularly relevant during heat waves because, while solar reduces the load at midday, wind power would need to fill the gap in the evening hours after solar output declines. If that does not happen, the residual load increases.

Figure 45 compares the average wind and solar generation profiles during the event. Although the two technologies appear partly complementary in the daily mean, average profiles conceal the individual hours that determine system stress.

The difference in magnitude illustrates the potential benefits of short-term flexibility. Battery storage and demand response can absorb or shift electricity from solar-rich midday hours into the evening ramp. Their ability to mitigate price peaks nevertheless depends on their available power, energy capacity, state of charge, consumer participation and the duration of low-wind conditions. They can reduce the need for rapidly dispatchable generation but may not fully replace it during prolonged periods of low renewable output.

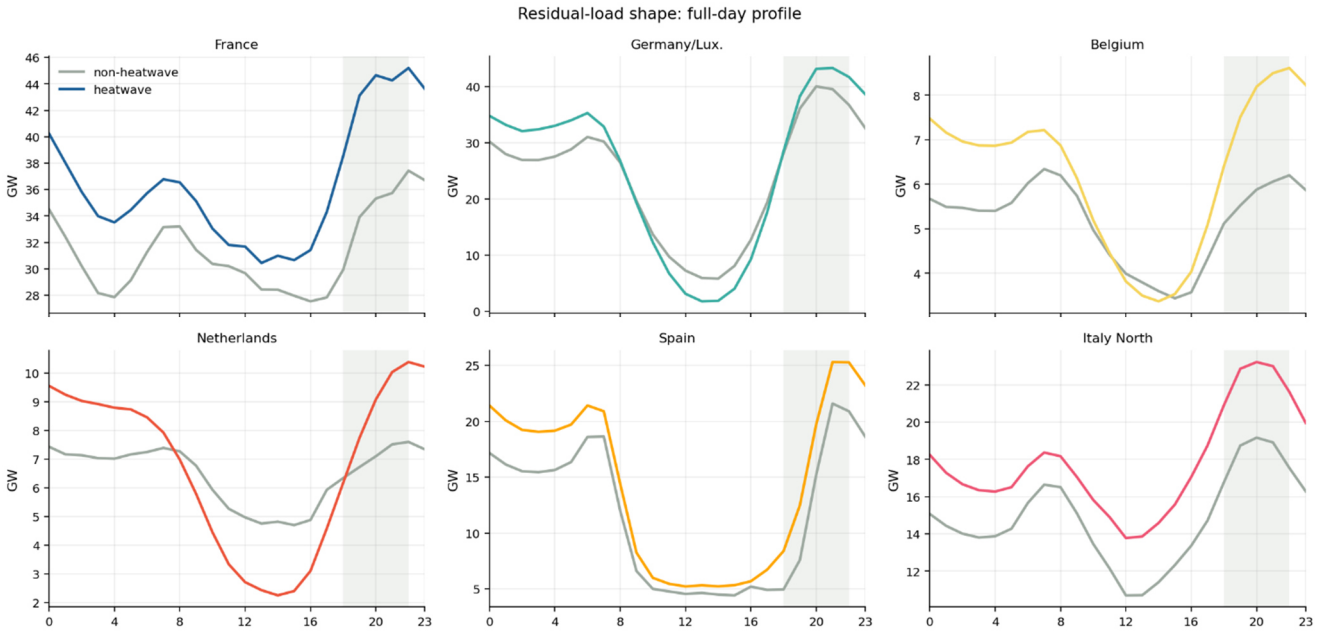

Fig. 43: Lines compare average residual-load profiles during the heat wave with non-heat wave June days (01.06 – 12.06). The grey band marks 18:00-22:00. The slope into the evening explains: when solar falls and wind is weak, the system must cover a larger dispatchable/import requirement within a few hours (Data: ENTSO-E Transparency Platform and SMARD).

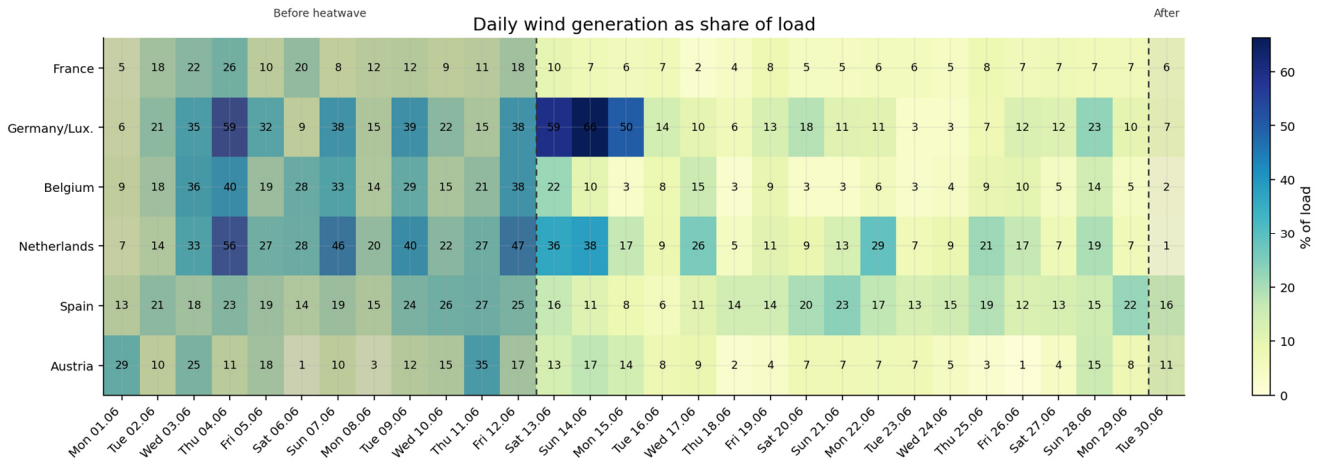

Fig. 44: Daily mean wind generation divided by daily mean load. Low shares indicate that less of the load was covered by wind. Low wind cover increases residual load and makes the evening ramp harder to absorb (Data: ENTSO-E Transparency Platform).

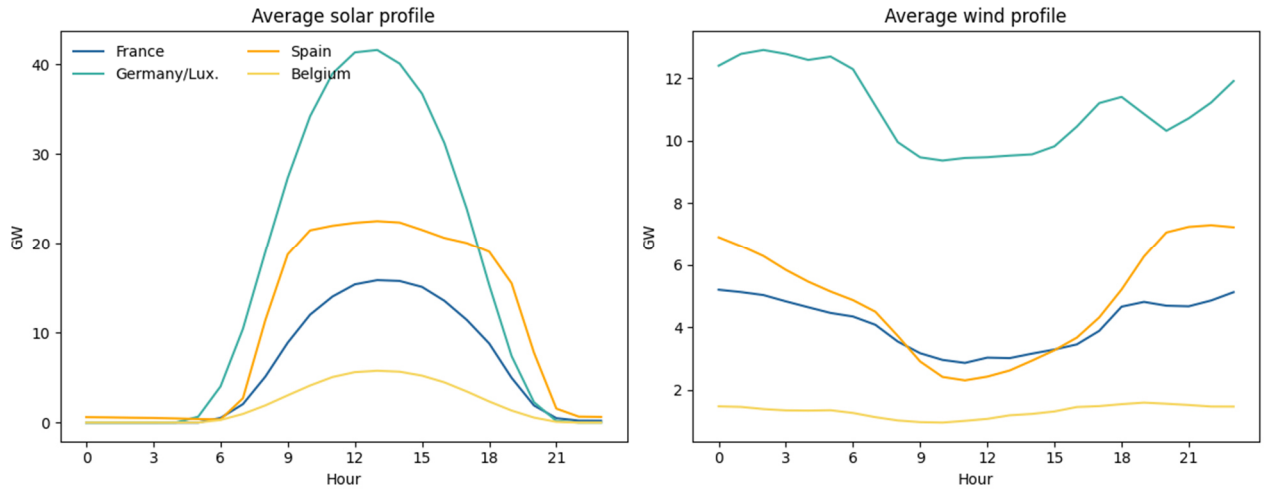

Fig. 45: Average hourly wind and solar generation profiles during the heat wave. The figure illustrates their broad temporal complementarity. Solar generation is several orders of substantially greater than wind generation (Data: ENTSO-E Transparency Platform).

4.2.4. Nuclear and fossil generation

The heat wave caused a noticeable but systemically manageable reduction in French nuclear output. Golfech 2 (1.3 GW) was shut down on 22nd June because the Garonne was expected to reach the site-specific limit of 28 °C. Nogent 2 was reduced from 1.3 GW to 0.4 GW from 23rd June, while Nogent 1 (1.3 GW) and Bugey 3 (0.9 GW) were shut down on 25 June because of rising temperatures in the Seine and Rhône. As Golfech 1 was already offline for maintenance, the entire Golfech site was temporarily unavailable. The effective capacity loss was estimated at 2.2 GW on 23 June and 4.4 GW on 25th June, corresponding to around 3.5 to 7 % of France's 63 GW nuclear fleet. These restrictions were triggered by environmental regulations limiting river temperatures and thermal discharges to protect aquatic ecosystems (EDF Group, 2026a,b,c; Connaissance des Énergies, 2026).

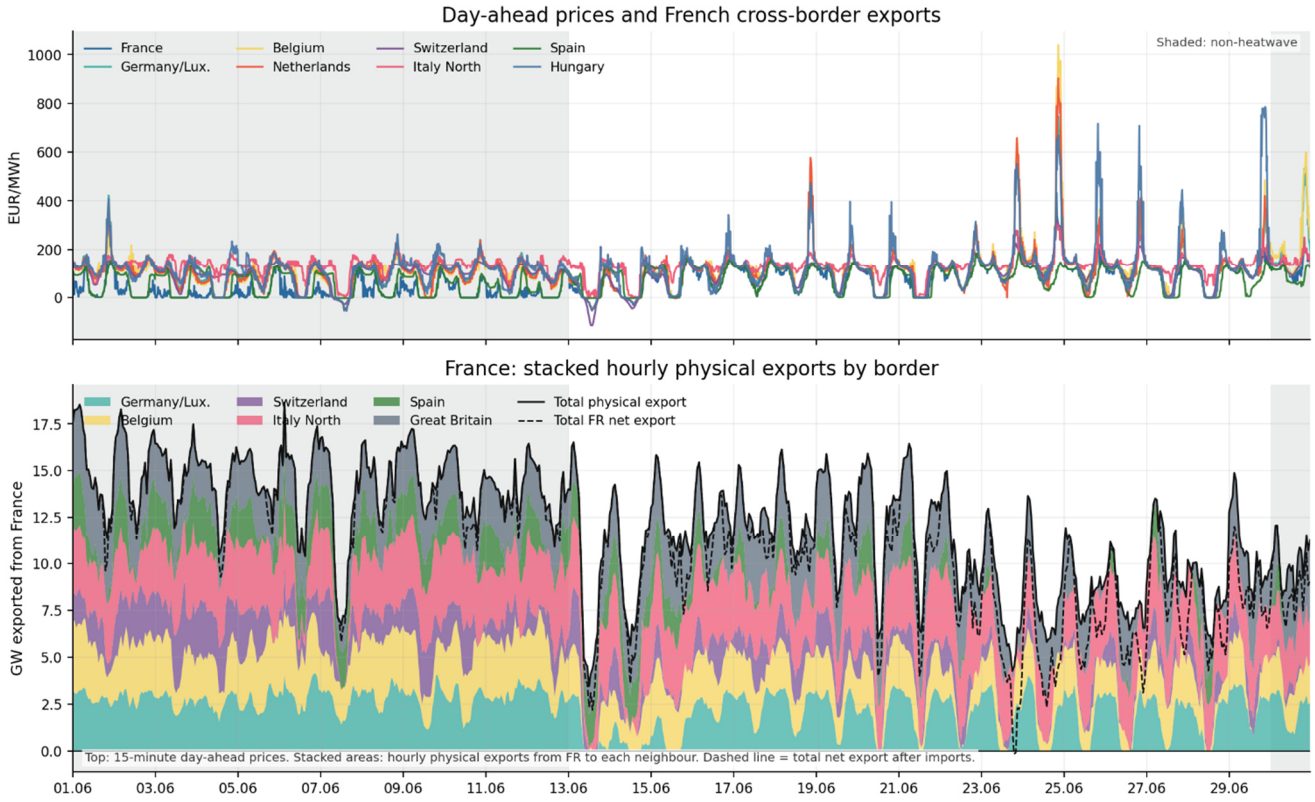

Fig. 46: French net electricity exports and day-ahead prices during June 2026. Net exports declined during the heat wave as domestic demand increased and nuclear availability was temporarily reduced, but France remained a net exporter. No stable one-to-one relationship between exports and prices is visible because both variables respond simultaneously to domestic residual load, generation availability and conditions in coupled neighboring markets. Data: ENTSO-E Transparency Platform.

Despite the reductions, security of supply was not endangered. On 22nd June, the French grid operator RTE stated that supply security did not require any special vigilance. French electricity demand during the heat wave would average 58 GW, remaining below the summer record of 60 GW set on 1st July 2025 (RTE, 2026). High solar output, continued generation from the remaining nuclear fleet, lower electricity exports and additional conventional and cross-border flexibility compensated for the shortfall. French net exports fell from around 10 to 15 GW to approximately 5 to 10 GW, as also seen in Figure 46.

France did not become a net importer during the event. Despite planned maintenance and heat-related nuclear restrictions, the system retained sufficient seasonal margin because summer demand remained substantially below winter peak levels. For comparison, the historical French winter peak reached 102 GW during the February 2012 cold spell. This seasonal difference helps explain why several gigawatts of nuclear unavailability remained manageable in June.

The United Kingdom reported heat-related restrictions at gas-fired plants. Five major gas-fired power plants were forced to reduce output as they struggled to cool when temperatures in the country reached 36 °C (FT, 2026; Guardian, 2026a,b).

Hungary temporarily relaxed cooling-water limits at Paks to prevent a power reduction of 640 MW to just 40 MW. The Danube's River temperature at the Paks nuclear plant reached 30.2 °C on Monday, exceeding a 29.5 °C intervention threshold (Reuters, 2026).

Nuclear and thermal constraints are important impact factors for the higher electricity prices. France is the main case where a nuclear reduction and a fossil increase are visible at the same time. France averaged about 1.6 GW less nuclear output and 1.7 GW more fossil output during the heat wave than in the 1 to 12 June baseline. This is consistent with a heat-related replacement channel, but it should be interpreted carefully: the aggregate data do not prove which unit replaced which megawatt-hour, and other flexibility sources like imports, hydro, storage and demand response also matter.

4.2.5. Load profile analysis in heat wave

On average, the load profiles of the countries distinguish the all-day load increase from time-of-day effects: Spain and Italy show a steeper increase in the evening, France shows higher load levels throughout much of the day, while the increase in Germany is less clearly driven by cooling demand.

RTE estimates that, during periods of high temperatures, each additional degree Celsius increases French electricity demand by approximately 0.7 to 1 GW, depending on the time of day. This sensitivity is around one-third of the effect associated with a one-degree temperature decrease during winter. For the June 2026 heat wave, RTE attributed an additional 10 to 14 GW of electricity demand at peak times to air-conditioning compared with an equivalent period with seasonally normal temperatures (RTE, 2026).

The load-profile comparison in Figure 47 is consistent with this mechanism but remains descriptive rather than causal. In addition to temperature-related cooling demand, the differences between the periods may reflect calendar effects, economic activity, behavioral changes and variations in behind-the-meter electricity generation. The reported load reflects the demand visible to the grid, not necessarily total electricity consumption. In countries with a large number of decentralized rooftop PV systems (particularly in Germany, Italy, and Spain) part of the additional cooling demand during sunny hours can be met directly behind the meter and therefore does not appear as a higher measured grid load. This can dampen the observed load response during the day in the event of heat waves. At the same time, this effect becomes system-relevant in the evening: As PV generation declines, the cooling demand that persists after sunset becomes more clearly visible to the grid and can contribute to a steeper rise in residual load.

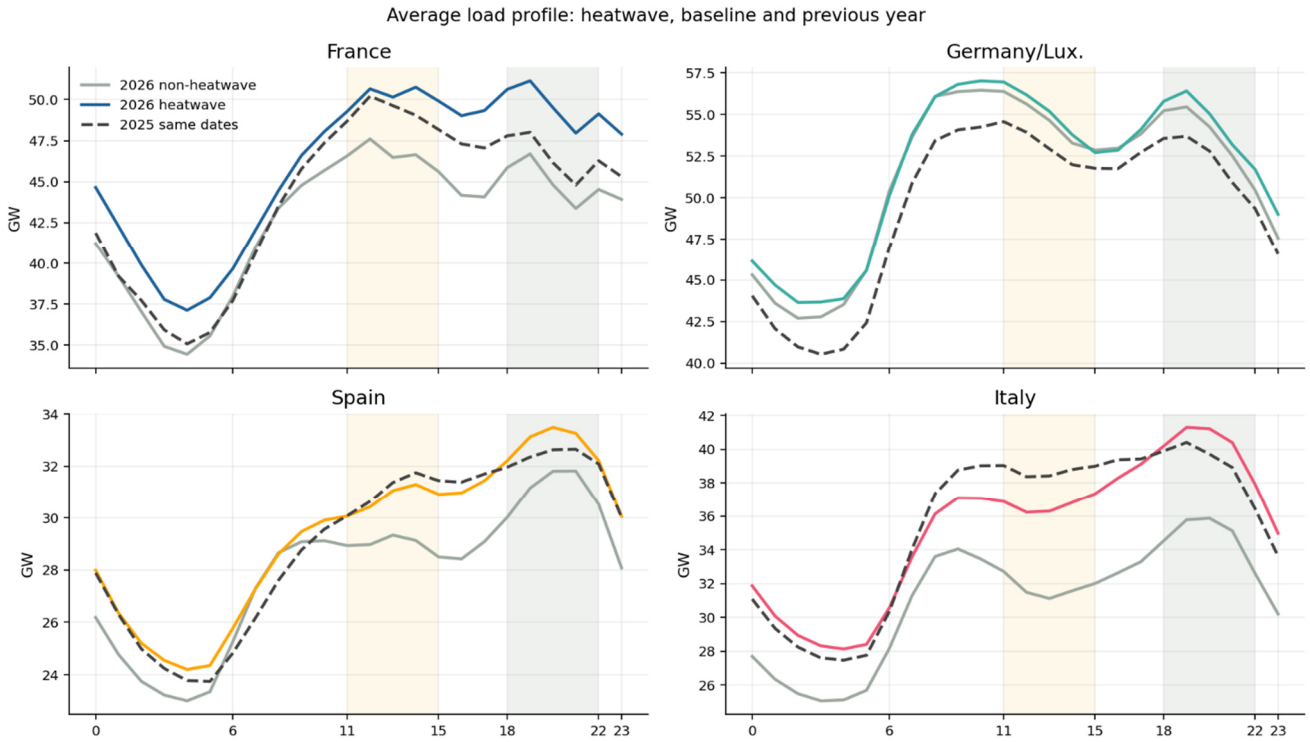

Fig. 47: Average hourly load profiles. Solid colored line: 13-29 June 2026; grey line: 2026 non-heat wave: 01-12 June 2026; dashed line: 13-29 June in the previous year 2025. Shading marks midday and evening hours. Data: ENTSO-E Transparency Platform.

5. Impact: Heat stress and health

The June 2026 heat wave had far-reaching implications for human health by exposing large parts of the European population to prolonged periods of exceptional heat. However, the severity of health impacts depends not only on outdoor air temperature, but also on local urban conditions, indoor environments, exposure duration, and individual vulnerability. This chapter therefore provides a multi-scale assessment of heat-related impacts, combining high-resolution observations from Karlsruhe with continental-scale population exposure analyses, building heat-transfer simulations, estimates of heat-related reductions in labor productivity, and the current understanding of heat-related mortality. Together, these complementary perspectives illustrate how the exceptional meteorological conditions of June 2026 translated into human heat exposure and associated health risks across a range of spatial scales.

5.1. Persistent heat stress and nighttime urban warming in Karlsruhe

The June 2026 heat wave produced pronounced spatial variations in thermal conditions across Karlsruhe. Located within the Upper Rhine Valley, one of the climatologically warmest regions in Germany, Karlsruhe is particularly prone to extreme summer heat and therefore provides a representative case study for analyzing urban heat-wave impacts. During the June 2026 heat wave, temperatures in the nearby DWD station Waghäusel-Kirrlach reached 41.4 °C (see Table 1), placing the region close to the new national record and highlighting the exceptional heat conditions in the Upper Rhine Valley. According to measurements from 96 urban monitoring stations (Stadt Karlsruhe, 2026), maximum air temperatures exceeded 40 °C at several locations during the event, with the highest observed value reaching 41.3 °C. The spatial distribution indicates that high temperatures were not restricted to the city center, although many of the hottest stations were located in densely built-up parts of the city. Lower maxima occurred mainly at sites with more vegetation or in more peripheral areas (Figure 48).

Heat exposure was also persistent. Many stations across the monitoring network recorded more than 240 hours (10 days) with a Heat Index of at least 27 °C, while the longest continuous period with a Heat Index of at least 27 °C lasted 71 hours.

The nighttime Urban Heat Island Intensity (UHII) was calculated as the temperature difference between urban stations and nearby vegetated reference sites, with positive values indicating warmer urban conditions. Figure 49 shows a clear tendency towards longer heat-stress duration at stations with stronger nighttime UHII. Median nighttime UHII values exceeded 2 °C at several urban stations, whereas vegetated reference locations generally showed values close to or below 0 °C. Many stations also experienced 10 to 13 tropical nights in a row, indicating that nighttime temperatures frequently remained above 20 °C and provided little opportunity for physiological recovery. This highlights the importance of limited nocturnal cooling as an additional component of heat-wave impacts.

The population count of the corresponding 100-m census cell (Statistische Ämter des Bundes und der Länder, 2024) was used as an indicator of local exposure around each station. Larger points in both figures therefore represent stations located in more populated grid cells. Several stations with both elevated nighttime UHII and long heat-stress duration were situated in comparatively populated urban cells, suggesting that the most persistent thermal burden coincided locally with areas of higher residential exposure. However, these values represent only the census cell containing the station and should not be interpreted as a city-wide estimate of the total number of exposed inhabitants.

Overall, the observations demonstrate that the June 2026 heat wave in Karlsruhe was characterized not only by exceptionally high daytime temperatures but also by prolonged heat exposure and pronounced nighttime urban warming. The coincidence of elevated nighttime UHII, extended periods of heat stress, and comparatively high local population densities indicates that densely built-up urban areas experienced the most persistent thermal burden. These findings underline the importance of considering both daytime heat and limited nocturnal cooling when assessing urban heat-wave impacts and identifying areas where adaptation measures may be most beneficial.

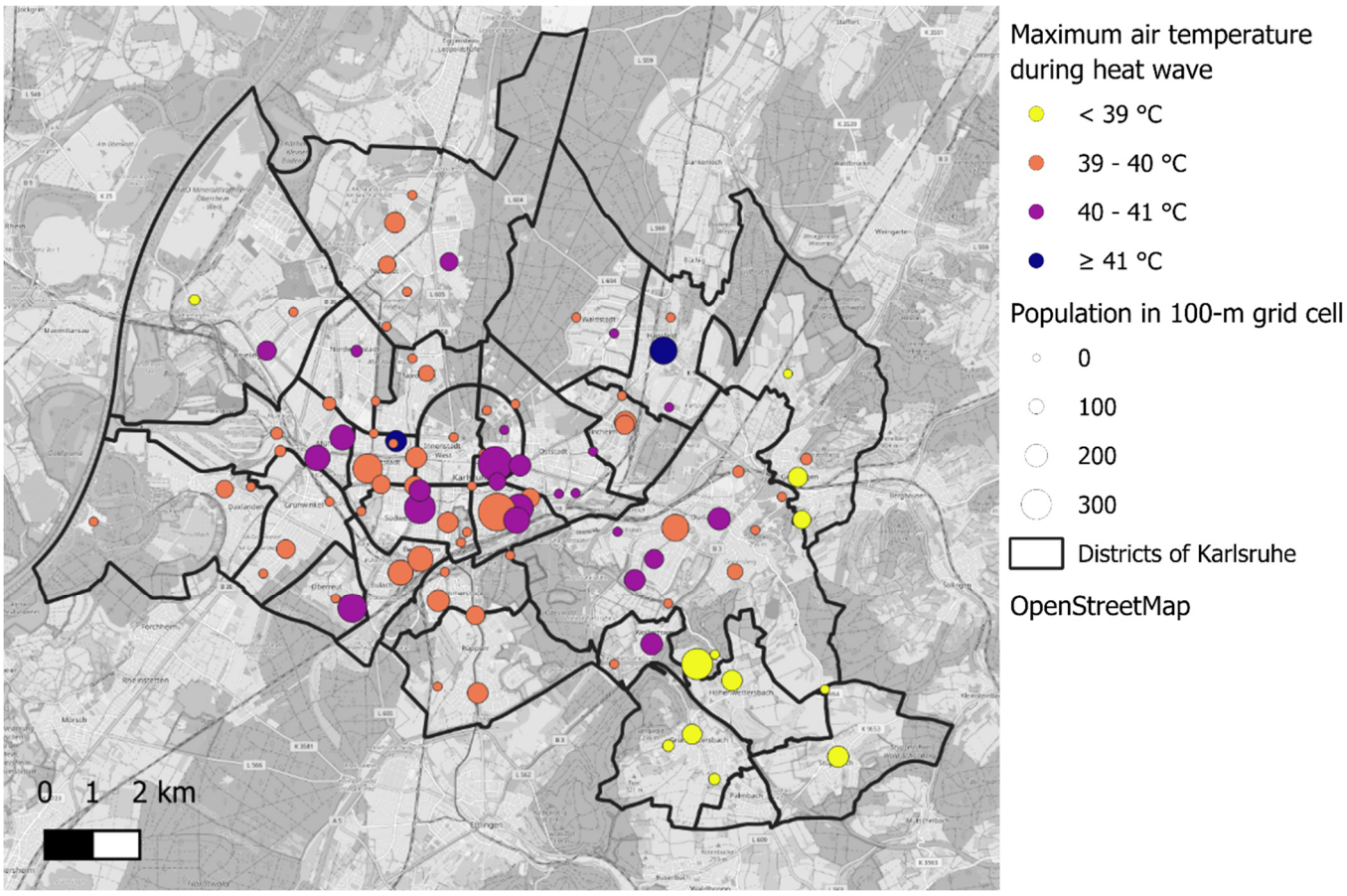

Fig. 48: **Maximum air temperature observed at monitoring stations in Karlsruhe during the June 2026 heat wave. The size of each point represents the population within the corresponding 100-m grid cell.**

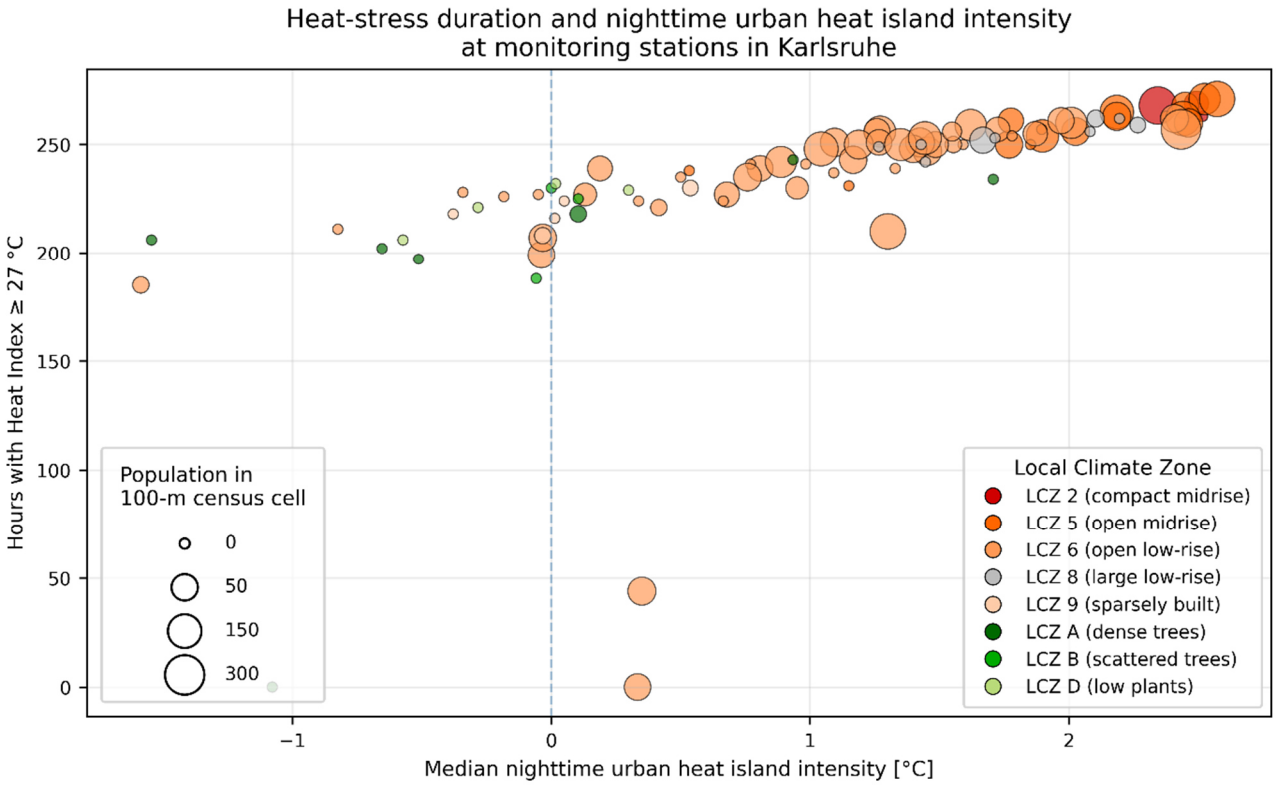

Fig. 49: **Relationship between median nighttime urban heat island intensity (UHII) and the cumulative number of hours with a Heat Index of at least 27 °C. Marker size represents population in the corresponding 100-m census grid cell, and marker color indicates Local Climate Zone (Demuzere et al., 2022).**

5.2. European population exposure assessment

The following assessment quantifies acute human heat exposure across mainland Europe during the June 2026 heat wave event by combining high-resolution population data with hourly ERA5 reanalysis data from 13rd June to 28th June and historical climate data.

Methodology

The spatial population distribution is derived from the Global Human Settlement Layer (GHSL 2020 Pop) at a native resolution of 1 km. Hourly surface air temperatures (2 m) are extracted from the ERA5-Land reanalysis (approx. 9 km resolution). Acute heat hazards and duration metrics are evaluated across increasing temperature increments (30 °C to 44 °C in 1 °C increments). Cumulative exposure is quantified as the absolute population experiencing sustained thermal durations across six duration classes (1-10 h, 10–24 h, 24-48 h, 48-72 h, 72-120 h, and >120 h). Daily maximum temperatures (Tasmax) are compared against a 30-year historical reference period (1960 to 1990) using the ERA5 reanalysis on single levels at a resolution of approximately 25 km.

Limitations

While reanalysis datasets provide continuous spatial and temporal hazard tracking, interpreting absolute temperature thresholds requires accounting for two well-documented physical limitations inherent to gridded geospatial climate modelling. ERA5-Land calculates surface energy balances over grid cells measuring approximately 9 km × 9 km (~81 km²). In complex terrain such as rift valleys (e.g., the Upper Rhine Valley) and topographic basins (e.g., the Stuttgart Basin), the model assigns a single mean surface elevation to the entire grid box.

Air temperature drops systematically with altitude. When a 9 km grid cell spans a low-lying valley floor flanking hillsides, the model averages these elevations. If the grid cell's mean elevation is higher than the true valley elevation, the reanalysis surface temperature is artificially suppressed, resulting in lower recorded temperatures than those actually observed by weather stations. Similarly, weather station records measure local thermodynamic extremes that low-resolution climate models do not capture. Thus, an ERA5-Land grid cell represents an area-weighted spatial average combining urban concrete, sunlit agricultural fields, and shaded forests. Consequently, ERA5-Land systematically underestimates absolute peak records at weather stations during extreme afternoon maxima. On average, this typically leads to an underestimation of about 2 °C, which correlates well with the provided ERA5-land maxima and the recorded station maxima (see Section 5.1). Furthermore, ERA5-Land incorporates static land-cover parameterizations but lacks a dynamic urban canopy model capable of resolving microclimatic air trapping, anthropogenic heat emissions, and narrow street canyon geometry. During sustained summer heat waves, this means that urban cores absorb shortwave radiation during the day and slowly re-emit it at night, keeping nocturnal temperatures elevated above physiological recovery thresholds. Similarly, rural dilution occurs because city centers rarely fill an entire 81 km² grid box. The extreme thermal trapping of dense urban infrastructure is diluted by the surrounding suburban gardens, rural vegetation, and open land. As a result, gridded reanalysis models fail to capture peak urban heat island intensities and substantially underestimate heat exposure duration.

In this assessment, ERA5-Land serves as a conservative indicator of regional background heat exposure rather than a microclimatic record at the point level. Since historical baselines (ERA5 single levels) undergo the same topographic and spatial averaging, relative metrics such as temperature anomalies remain methodologically robust and structurally consistent across comparative spatial evaluations.

Findings

The June 2026 European heat wave manifested as an exceptional, continent-wide thermal event, driven by intense daily maximum temperature anomalies ranging from +8 °C to +12 °C above the 1960 to 1990 climatological baseline in Western, Southern, and Central Europe. As illustrated in Figure 50, the spatial distribution shows that physical heat exposure (≥ 30 °C) engulfed nearly the entire population of the mainland outside of the high alpine and northern Scandinavian zones. This exposure lasted for over 120 hours in France, Italy, Spain, and Central Europe. As temperatures rose above 36 °C, widespread and severe thermal stress

occurred around densely populated continental corridors subjecting tens of millions of individuals to sustained, multi-day physiological stress.

At the most acute hazard thresholds (≥ 40 °C), extreme heat exposure concentrated heavily within classic southern European hotspots, most notably southern and inland Spain, southern France, and central/southern Italy, where populations endured critical multi-hour peak exposures. Even a larger proportion of Europe experienced temperatures of at least 40 °C for a sustained amount of time when taking the above-described limitations into account.

Figure 51 shows the spatial distribution of heat exposure duration across Europe between 13rd and 28th June 2026. The longest periods of sustained heat occurred across large parts of Southern and Western Europe, whereas shorter exposure durations predominated in Northern Europe. This spatial pattern is reflected in the national demographic breakdowns (Fig. 52), which illustrate a distinct geographical divergence in exposure duration: while Northern European populations experienced predominantly transient heat spikes within the shorter duration brackets (1 to 24 h), major demographic cores across Southern and Western Europe shifted heavily into prolonged, multi-day thermal stress windows (>72 to >120 h), with regional hotspots and urban heat island effects further amplifying local exposure.

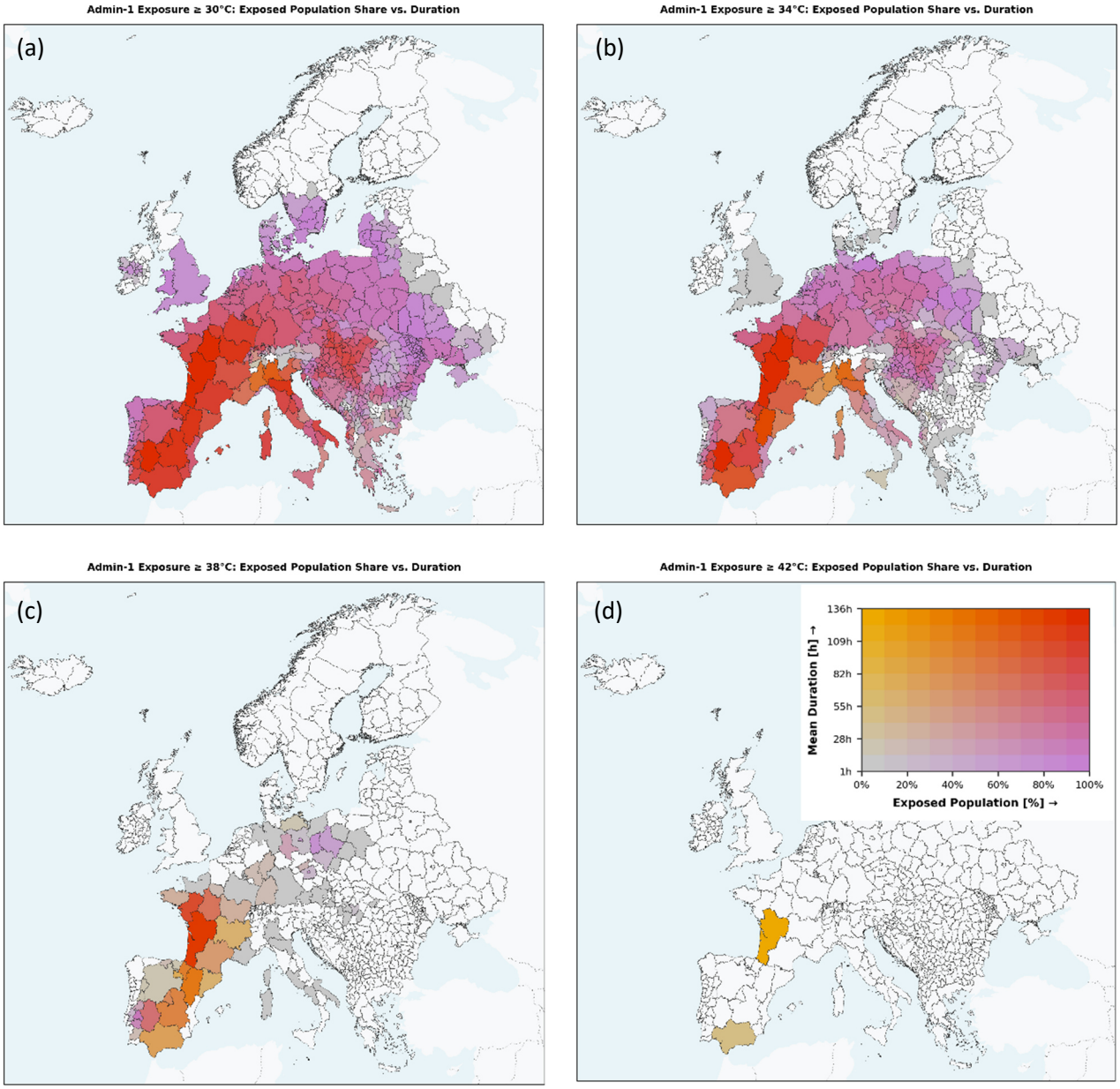

Fig. 50: **Heat exposure intensity maps based on admin-1 regional aggregation. It shows the share of population exposed to certain duration of temperature above threshold: (a) ≥ 30 °C, (b) ≥ 34 °C, (c) ≥ 38 °C, and (d) ≥ 42 °C.**

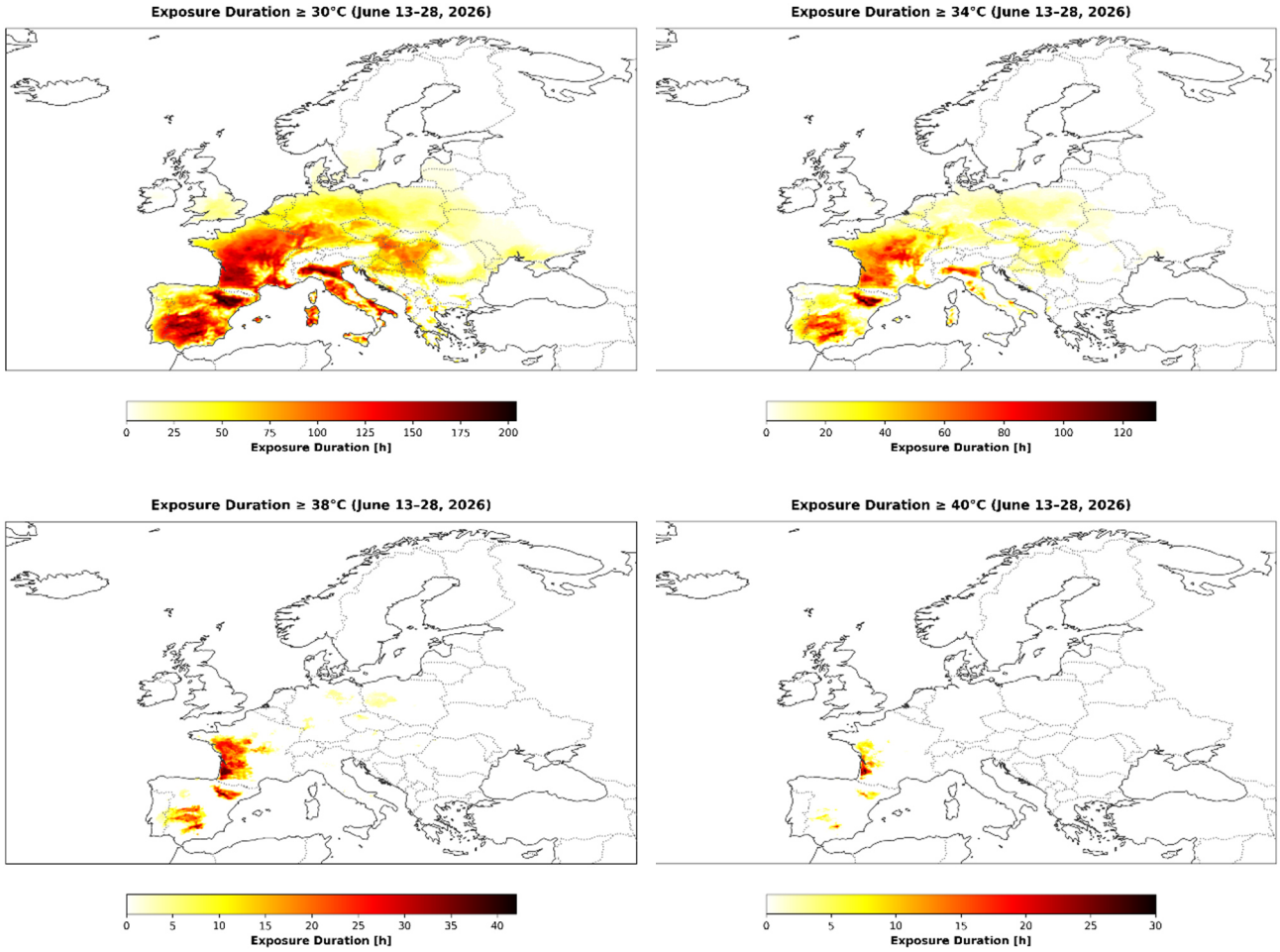

Fig. 51: Spatial distribution of heat exposure duration from June 13rd to 28th using ERA5-Land.

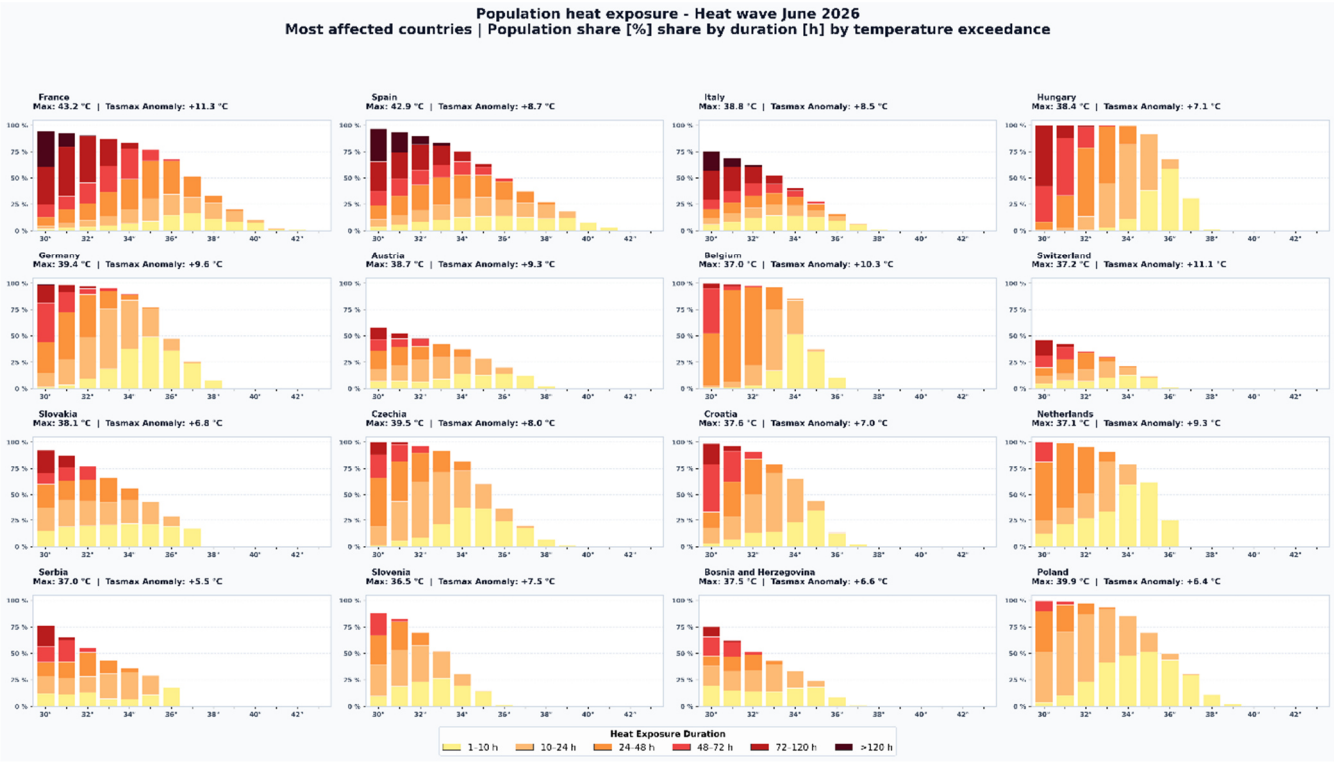

***Fig. 52:* Charts on heat exposure for different affected countries. Bar charts show share of population exposure to temperatures above certain thresholds and their total duration between June 13th and June 28th 2026. Daily maximum temperature anomaly (tasmax), weighted by population density, in comparison to 1960-1990 baseline (Data source: ERA5-Land, retrieved on 3rd July 2026).**

Table 3: Total exposed population in Europe (incl. UK, Ukraine, Serbia, etc.) by temperature and duration. Population is given in millions.

°C	1-10 h	10-24 h	24-48 h	48-72 h	72-120 h	> 120 h	Total_Exposed >= 1 h
>30 °C	66.6	88.1	108.4	81.7	92.5	44.8	482.1
>32 °C	101.4	108.1	106.3	41.5	51.9	4.5	413.7
>34 °C	117.8	104.8	50.7	26.9	8.2		308.4
>36 °C	87.9	48.6	26.0	1.6	0.04		164.2
>38 °C	25.4	12.2	3.9				41.5
>40 °C	6.1	1.2	0.1				7.4
>42 °C	0.39	0.06					0.45

Table 3 summarizes the total exposed population across Europe, including non-EU countries like the United Kingdom, Ukraine and Serbia. It shows that more than 480 million people experienced at least 30 °C and more than 160 million people even above 36 °C. Peak temperatures above 40 °C affected at least 7.5 million people. Those temperature numbers are locally further exaggerated due to topographic and urban heat island effects.

5.3. Building heat-transfer model for indoor heat exposure during the heat wave

The June 2026 heat wave was characterized not only by exceptionally high outdoor temperatures, but also by persistent hot days and warm nights (as mentioned above), substantially increasing the risk of indoor overheating. As people spend most of their time indoors, indoor thermal conditions are a key determinant of heat exposure and associated health risks. To illustrate the potential impact of the heat wave on residential buildings, a dynamic, multi-zone building simulation was conducted for a representative residential building in the Karlsruhe region. The simulation used observed weather conditions during the heat wave and compared typical older and modern building standards under identical passive cooling strategies.

Methodology

RoomFlex (Cheng et al., 2026a) is used to describe building instances in a format that supports rapid multi-zone model generation and heat wave analysis. Based on the structural parameter tables used by RoomFlex, the simulated heat transfer mechanisms include heat conduction through walls, surface convective heat transfer, solar heat gain, and heat losses from infiltration and ventilation. RoomFlex provides a Python-based, topology-driven GUI that represents a multi-zone building as a set of orthogonal zone volumes and exports a face-level parameter table for automated Modelica model generation. The workflow and the three-zone virtual building are shown in Figure 53. The building used here is based on the residential resilience case study reported by Cheng et al. (2026b). Zones 101 and 102 are on the first floor, while Zone 201 is on the second floor. Zone 101 connects to Zone 102 via an open internal door and to Zone 201 via the staircase.

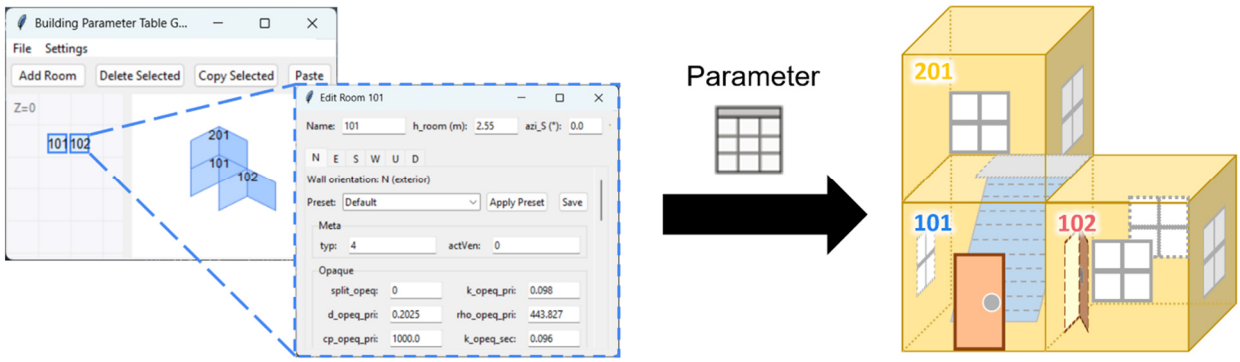

Fig. 53: RoomFlex GUI workflow and three-zone virtual building geometry.

Case Study

The selected analysis window extends from the week preceding the heat wave onset to the most recent available data, from 8th June to 1st July 2026. The 200-m KITmast (located near the city of Karlsruhe) dataset provides measured outdoor temperature (2 m) and global horizontal irradiance (GHI), but direct normal irradiance (DNI) is not directly available. Therefore, DNI is approximated by decomposing GHI into direct and diffuse components.

First, solar altitude and zenith angle are calculated from the timestamp, the geographic coordinates of Karlsruhe, and the local time zone (Reda & Andreas, 2004). Extraterrestrial horizontal radiation is then estimated and used to compute the clearness index K_t, defined as the ratio of measured GHI to extraterrestrial horizontal radiation. The diffuse fraction is estimated using the Erbs model (Erbs et al., 1982), yielding diffuse horizontal irradiance (DHI). After that, DNI is derived from the horizontal radiation balance:

$$DNI = \frac{GHI - DHI}{\cos(\vartheta_z)},$$

where ϑ_z is the solar zenith angle. During nighttime, at very low solar altitudes, or when measured radiation values are negative due to sensor zero-offset noise, DNI is set to zero. This method does not replace measured DNI, but it provides a physically consistent approximation for facade irradiance and solar heat-gain calculations when only GHI measurements are available.

Two building scenarios are modeled with identical geometry and internal airflow paths. The New Building scenario represents a low-energy-demand demonstration building corresponding to KIT-LLEC, featuring higher thermal insulation performance (Langner et al., 2025). The Old Building scenario uses envelope heat-transfer coefficients (U-values) based on the TABULA DE.N.SFH.05.Gen standard (TABULA, 2016). Windows 102E and 201S are used for natural ventilation: they open only when the indoor temperature exceeds 25 °C and the indoor-outdoor temperature difference exceeds 2 K. Roller shutters close automatically when direct solar radiation exceeds 300 W/m².

The main heat wave period spans approximately Days 10 to 21. During this period, outdoor dry-bulb temperatures frequently reach 35-40 °C, and direct solar radiation repeatedly rises to 800-1000 W/m².

Findings

Before the heat wave, indoor temperatures generally remain in the low 20s to about 25 °C. Once high outdoor temperatures and intense radiation persist for several days, all zones show heat accumulation and insufficient nighttime recovery.

- **The New Building performs better than the Old Building, although the extent of improvement is limited.** In the New Building scenario, Zones 101 and 201 reach approximately 41-42 °C, while Zone 102 peaks around 36-37 °C (Fig. 54). In the Old Building scenario, Zones 101 and 201 rise to about 43-44 °C, and Zone 102 reaches approximately 37-38 °C (Fig. 55). The better-insulated envelope reduces heat transfer from the hot outdoor environment and slightly lowers peak temperatures. However, once heat accumulates indoors, the same insulation slows heat dissipation. The old building is therefore more susceptible to rapid envelope heat gains, but the new building still cannot maintain safe or comfortable conditions with the tested passive strategy alone.
- **The three zones exhibit distinct thermal behavior.** Zones 101 and 201 are tightly coupled via the staircase and therefore show highly consistent temperature trends. Zone 101 tends to be among the warmest areas because it is located in the building core, has fewer direct paths for heat dissipation, and is influenced by thermal storage in surrounding construction. Zone 201 can reach similar or slightly higher peaks due to upper-zone heat accumulation and solar exposure. Zone 102 has larger and faster diurnal temperature fluctuations because it has more exterior windows and the 102E ventilation opening.

- **Under both scenarios, window operation varies with zone temperature.** Compared with the New Building scenario, the Old Building generally requires longer ventilation periods under the same control logic, especially for window 201S. Window 102E operates more intermittently. During the hottest afternoon periods, the windows may close even when indoor temperatures are high because outdoor air is no longer cooler than indoor air. This prevents additional heat from entering but limits ventilation's ability to remove accumulated indoor heat.

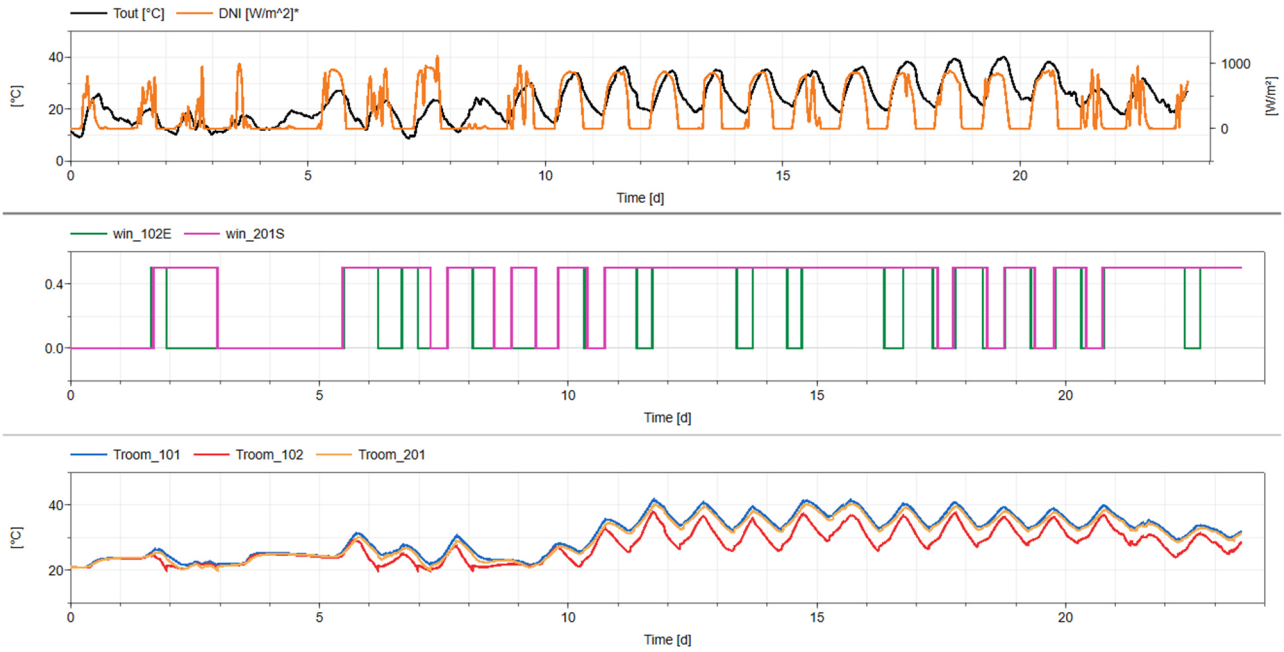

Fig. 54: New Building heat wave simulation results: outdoor weather, window states, and zone temperatures.

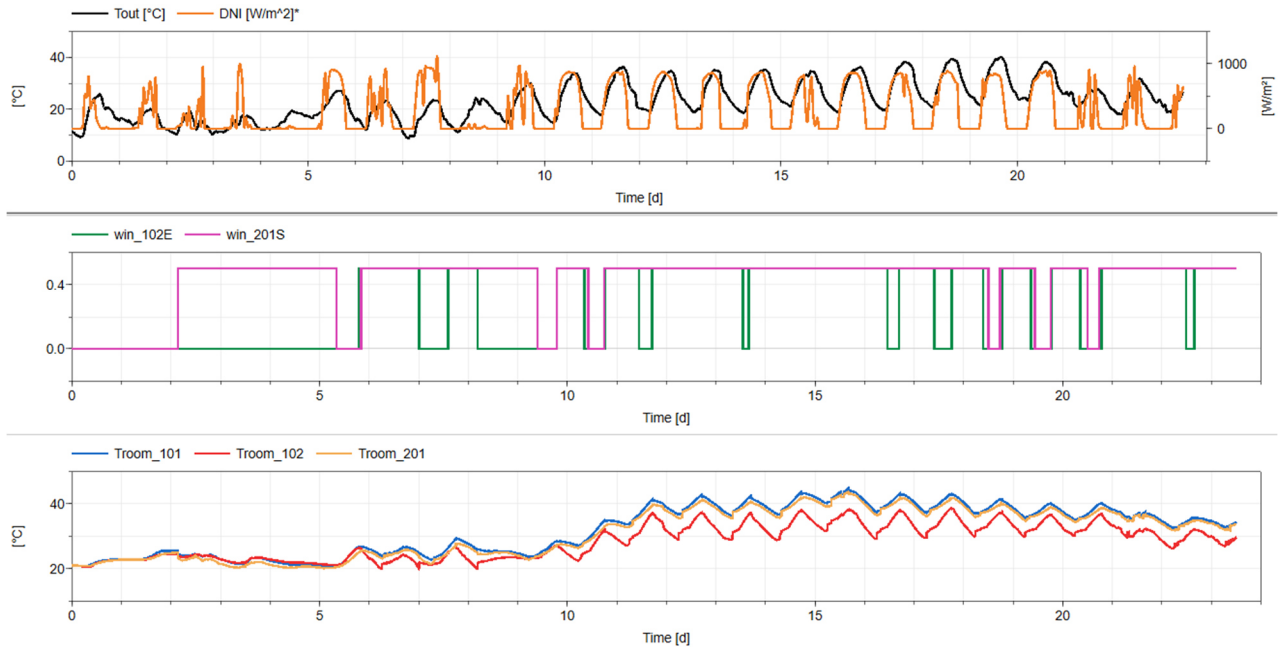

Fig. 55: Old Building heat wave simulation results: outdoor weather, window states, and zone temperatures.

Discussion

The results are consistent with Taylor et al. (2023), who emphasize that new buildings are neither inherently more heat-resistant nor inherently more prone to overheating than older ones. Heat wave performance depends on solar heat gain control, thermal mass, nighttime heat dissipation capacity, ventilation opportunities, and occupant behavior, rather than on insulation level alone.

From an indoor environmental quality and health perspective, the simulated temperatures are severe. Indoor temperatures consistently above 30 °C indicate significant thermal discomfort, impaired sleep recovery, reduced attention, and increased physiological strain. Consecutive hot days and warm nights limit the body's ability to dissipate heat and cool down, increasing the risk of dehydration, heat exhaustion, heatstroke, and worsening pre-existing medical conditions. WHO (2026) identifies heat as an important health hazard that can exacerbate cardiovascular disease, diabetes, mental health conditions, asthma, and kidney stress.

For the Old Building, priority should be given to envelope retrofit, exterior shading, reduction of solar gains through exposed windows, and controllable ventilation paths that support effective night cooling. For the New Building, the envelope already provides some benefit, so the main improvement should be heat-wave-oriented operation: earlier shutter closure before solar peaks, stronger night ventilation whenever outdoor air is cooler than indoor air, and a backup active-cooling strategy for extreme days.

5.4. Heat stress and labor productivity

The recent heat wave has led to significant disruptions and even excess deaths. In comparison, its effect on labor productivity is less severe, but still a concern. Figure 56 outlines the potential effect on that dimension. The horizontal axis is the wet-bulb globe temperature (WBGT), a heat-stress index combining air temperature, humidity, and radiant load. The vertical axis is the estimated productivity loss relative to cool conditions. WBGT is not the same as the air temperature reported by a thermometer or in a forecast, and interpreting it as such is misleading. In hot and dry air, the WBGT can be significantly lower than the shaded air temperature, because the large wet-bulb depression lowers the index. Germany's national record of 41.8 °C (DWD, 2026a,b), for example, corresponds to a shade WBGT around 30 °C relatively dry air, and to about 33 °C only where work was fully exposed to the sun (in more humid conditions, the WBGT would be higher at the same air temperature). A WBGT of 33 °C already represents severe heat stress for a working body, because it folds in humidity and radiant load.

The red band in Figure 56 shows the distribution of estimated peak-day WBGT across the region, not a single value. Substantial uncertainty surrounds these values, and those of the labor-productivity estimates, so plausible ranges are given as broad indicative benchmarks. Heavier work generates more metabolic heat, so its curve rises earliest. Within the red band, the central estimate for heavy outdoor work rises from about a third of output at WBGT 30 °C to two-thirds near WBGT 33 °C, with moderate work at roughly 15 to 46 % and light or indoor work at 2 to 3 %. Where the band is wide, the central value is broadly indicative. The relationship is physiological rather than an economic forecast. A loss for a firm or the wider economy also depends on how many people work outdoors, at what hours, and with what adaptation.

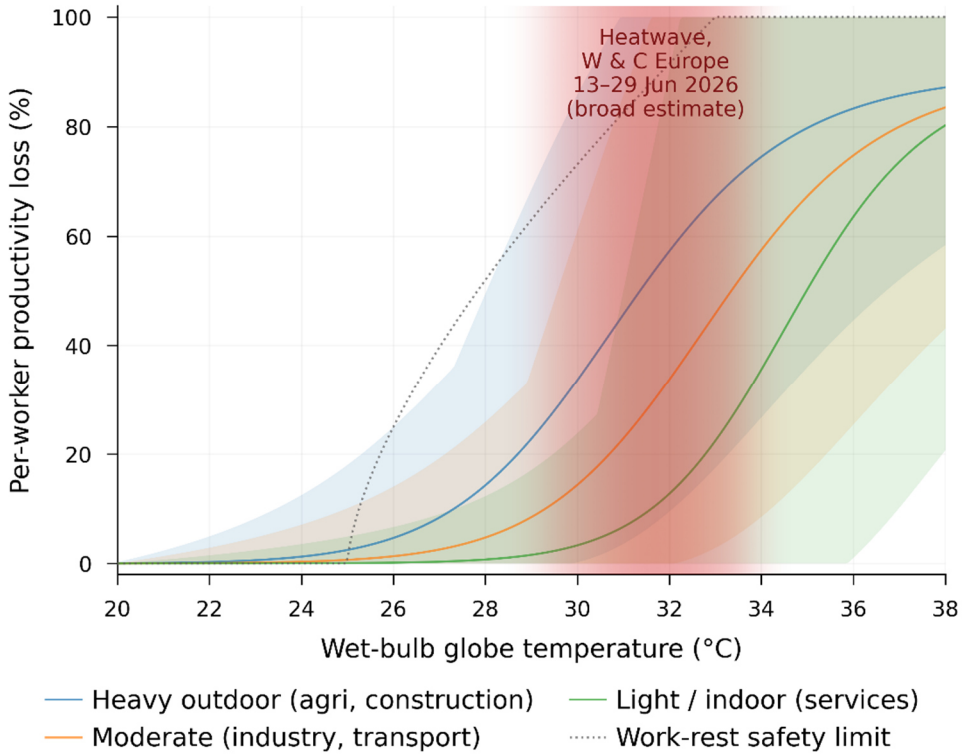

Fig. 56: Per-worker productivity loss against wet-bulb globe temperature (WBGT) for three work-intensity classes, with the West and Central European heat wave of 13–29 June 2026 marked. Each central line is the Hothaps labor work-capacity curve for that class and re-baselined to zero loss at a cool reference of WBGT 20 °C, so the axis reads loss relative to cool conditions. The shaded band around each line spans the published range for that class, from a Hothaps curve with a 10 % capacity floor to an ISO 7243 benchmark implying total work stoppage by WBGT 33 °C. Adapted from (Foster et al., 2021, 2022; Szewczyk et al., 2021; Lemke and Kjellstrom, 2012; Liljegren et al., 2008; Dunne et al., 2013; García-León et al., 2021). The dotted grey line is the Dunne work-rest safety limit (Dunne et al., 2013), a different quantity shown for comparison. The red band marks the WBGT potentially reached across the region on peak days (estimated). Shading is darkest at the median of 31.7 °C, the central estimate of what workers experienced under typical mixed sun and shade, and fades across the plausible envelope from about 28 °C, for deep shade in the coolest country, to about 35 °C, for full sun in the hottest.

5.5. Heat-related mortality

Heat waves are among the deadliest natural hazards. During the European summers of 2022 to 2024, the combined heat-related death toll was estimated to be over 180,000 (Janoz et al., 2025). In 2022, the weekly heat-related death toll peaked at over 11,000 (Ballester, 2023). For the June 2026 heat wave, reliable estimates are not yet available; mortality data take time to collect and validate, meaning that heat-related mortality cannot be estimated immediately. Nonetheless, the occurrence of high temperatures in June, at the beginning of summer, means that this heat wave is again expected to be associated with a high heat-related death toll across Europe.

The additional stress from extreme heat can exacerbate underlying health conditions (Ebi et al., 2021). In particular, the elderly and people with chronic health conditions are among the most vulnerable to heat. This event highlights the need for healthcare systems to adapt to our changed climate. For example, by providing facilities which operate at temperatures comfortable both for patients and staff, whilst also ensuring sufficient capacity to manage increased demand during heat waves.

The health risk posed by heat increases non-linearly. This means that during heat waves, each additional degree increase in temperature results in a disproportionately larger increase in deaths. During heat waves we typically see a displacement in mortality, also known as the harvest effect, where there is initially higher mortality amongst vulnerable groups, followed by a period of reduced mortality. In parallel, the heat-related stress placed on the human body cumulates over time. This is amplified by elevated nocturnal temperatures, which limit recovery during the night. Thus, during particularly severe events, even younger and healthier individuals may experience serious health impacts.

Another important factor is the timing of a heat wave. Early-season heat waves are associated with higher mortality, partly because humans are not yet acclimatized to extreme heat (Gasparrini et al., 2016). This event occurred unusually early in the season, potentially amplifying its health impacts. Furthermore, this heat wave coincided with the period of peak incoming solar radiation around the summer solstice, which likely enhanced daytime heat exposure, particularly at higher northern latitudes.

The health impacts, particularly the mortality of heat waves like this one, highlight the growing human cost of climate change and the urgent need to adapt healthcare systems. Community support is also important, for example by checking on and assisting vulnerable people during heat waves.

6. Impact: Transport infrastructure

The heat wave placed significant stress on the transport infrastructure of Western and Central Europe, but the severity and nature of impacts varied considerably between countries and transport modes. While there were warnings and precautionary measures, such as travel warnings, taken in all countries, operational and infrastructure failures are mostly reported in Germany, the United Kingdom, France, and Belgium, with a focus on train infrastructure.

Germany experienced the most severe impacts on road infrastructure. Extreme air temperatures, combined with intense solar radiation, caused road surface temperatures to exceed 60 °C, leading to substantial thermal expansion of pavement materials. Around one-third of the German motorway network still consists of older concrete pavements, which are particularly susceptible to this type of thermal stress and can fail through sudden pavement buckling ("blow-ups"). Consequently, multiple motorway sections were affected, particularly along the A2 in Saxony-Anhalt and Brandenburg, where blow-ups forced full motorway closures and emergency repairs [1]. Additional lane closures and precautionary speed restrictions were imposed on several other major federal highways [1]. Germany also experienced rail disruptions, most notably in North Rhine-Westphalia, where an RE5 regional train carrying around 475 passengers had to be evacuated near Bonn after technical systems, including air conditioning, brakes, and the compressor, failed during extreme heat on Friday, 26th June. The following day, several major Rhein-Ruhr-Express regional lines in the same area were temporarily suspended as a precaution against further heat-related failures [2]. Due to the high population density in the affected region and the short-term nature of the service suspension, the disruption was expected to have a significant impact on travelers. The presence of a nationwide heat-related rail travel advisory, which provided passengers with greater flexibility to defer or cancel journeys, may have mitigated the overall number of directly affected passengers [3].

In the **United Kingdom**, the principal transport impacts occurred on the rail network. Following a rare Red Extreme Heat Warning issued by the Met Office, Network Rail imposed widespread speed restrictions across large parts of the country to mitigate risks of track buckling and overhead line failures [4]. Numerous train operators reduced services, cancelled connections or advised passengers to travel only if essential. International services operated by Eurostar were also affected, with cancellations reported on routes linking London with Paris and Brussels [5]. Despite the severe operational disruption, no comparable heat-related failures of motorway infrastructure were reported.

France also experienced substantial rail impacts. SNCF introduced speed restrictions on sections of the network to reduce the risk of rail deformation. Over 70 long-distance and Intercité train services were canceled until 22nd June, including connections involving the travel axes: Paris-Clermont-Ferrand and Paris-Orléans-Limoges-Toulouse [6]. Taken together about 10% of trains in the Paris region were cancelled to prevent overheating the tracks [7]. By 24th June 2026, regional TER services in Nouvelle-Aquitaine were being suspended daily between 10:00 and 18:00, with the restriction scheduled to remain in place through 27th June 2026 [8]. Nouvelle-Aquitaine is regularly among the French regions most affected by summer heat waves, and its older rail infrastructure is considered particularly vulnerable to extreme temperatures and thermal expansion of rails.

In **Belgium**, rail operators reduced services significantly, canceling approximately 100 train connections per day, including many commuter trains during the peak of the heat wave [9]. Next to infrastructure issues, the lack of air conditioning in old trains led to their cancellation [9]. While Belgium was placed under high-level heat alerts and activated national heat response measures, there were no widely reported cases of motorway damage or major road closures caused by extreme temperatures.

In contrast, transport infrastructure impacts in the **Netherlands, Switzerland, Austria, Portugal, and Spain** were generally more limited [10]. Although these countries experienced exceptionally high temperatures and, in several cases, record-breaking heat (Section 2.7), there were comparatively few reports of major infrastructure failures, extensive service suspensions or emergency transport closures. Transport operators primarily relied on precautionary measures, increased infrastructure monitoring and travel advisories. The Netherlands stood out for issuing its highest heat warning level and activating transport preparedness measures during its first

recorded “super-heat wave” [11], while Switzerland and Austria reported concerns regarding potential heat-related stress on rail infrastructure [12]. Spain and Portugal experienced some of the highest temperatures recorded during the event, but transport impacts were largely overshadowed by concerns about wildfire risk and public safety [13, 14]. Overall, these countries experienced severe meteorological conditions but comparatively limited direct impacts on transport infrastructure compared with the more significant road and rail disruptions reported in Germany, France, the United Kingdom and Belgium.

Compared with road and rail transport, impacts on aviation and waterborne transport were limited across Europe. Airports generally remained operational throughout the heat wave, although airlines and airport operators reported an increased risk of delays, schedule adjustments and operational disruptions associated with extreme temperatures or related thunderstorms [5, 15].

Similarly, no major heat-related disruptions to maritime transport or inland waterways were widely reported during the late-June 2026 heat wave. Unlike previous low-water events on major European rivers such as the Rhine, the available reporting on this episode focused predominantly on road and rail transport rather than navigation constraints. Overall, waterborne transport remained comparatively resilient during the event, with no significant navigation restrictions or widespread service interruptions identified across the countries.

7. Sources & references

[1] Ballester, J., Quijal-Zamorano, M., Méndez Turrubiates, R.F. et al. (2023): Heat-related mortality in Europe during the summer of 2022. *Nat. Med.,* 29, 1857–1866, https://doi.org/10.1038/s41591-023-02419-z.

[2] Benson, D. O., Dirmeyer, P.A. (2021). Characterizing the Relationship between Temperature and Soil Moisture Extremes and Their Role in the Exacerbation of Heat Waves over the Contiguous United States. *J. Clim.*, 34(6). https://doi.org/10.1175/JCLI-D-20-0440.1.

[3] BFG (2026): Niedrigwasser-Bericht für Periode 19. bis 25.06.2026, available: https://www.bafg.de/SharedDocs/Downloads/DE/bfg_niedrigwasserbericht/2026/260625_nw_bericht.pdf?__blob=publicationFile&v=2 (Accessed 01 July 2026).

[4] Boeing, F., Rakovec, O., Kumar, R., Samaniego, L., Schrön, M., Hildebrandt, A., Rebmann, C., Thober, S., Müller, S., Zacharias, S., Bogena, H., Schneider, K., Kiese, R., Attinger, S., Marx, A. (2022): High-resolution drought simulations and comparison to soil moisture observations in Germany, *Hydrol. Earth Syst. Sci.,* 26, 5137-5161, https://doi.org/10.5194/hess-26-5137-2022.

[5] Cheng, H., Çakmak, H. K., Hagenmeyer, V. (2026a). JanusBM: A dual-fidelity multi-zone white-box building modeling framework. arXiv. https://arxiv.org/abs/2603.23015.

[6] Cheng, H., Hagenmeyer, V., Çakmak, H. K. (2026b). Enhancing resilience in residential buildings: Assessing comfort under blackout scenarios with a modular multi-zone white-box modeling approach. In Proceedings of the 2026 ACM Sustainability Week (pp. 352-356). ACM. https://doi.org/10.1145/3765611.3813757.

[7] Connaissance des Énergies (2026): EDF réduit la production de plusieurs réacteurs nucléaires durant la canicule, available: https://www.connaissancedesenergies.org/afp/canicule-un-reacteur-arrete-des-baisses-de-production-dans-deux-autres-260623 (Accessed 02 July 2026).

[8] DWD (2026a): Deutschlandwetter im Juni 2026 | Trockener und sehr sonniger Juni 2026 endet mit historischer Hitzewelle, Pressemitteilung 29.06.2026, Deutscher Wetterdienst, Offenbach, Germany, available: https://www.dwd.de/DE/presse/pressemitteilungen/DE/2026/2020260629_deutschlandwetter_juni_news.html?nn=495078 (Accessed 02 July 2026).

[9] DWD (2026b): Vorläufiges höchstes Maximum, Post Mastadon, Deutscher Wetterdienst (DWD), available: https://social.bund.de/@DeutscherWetterdienst/116838683797051418 (Accessed 02 July 2026).

[10] Demuzere, M., Kittner, J., Martilli, A., Mills, G., Moede, C., Stewart, I. D., van Vliet, J., Bechtel, B. (2022): A global map of local climate zones to support earth system modelling and urban-scale environmental science*. Earth Syst. Sci. Data.*, 14, 3835–3873, https://doi.org/10.5194/essd-14-3835-2022.

[11] Dunne, J., Stouffer, R., John, J. (2013): Reductions in labour capacity from heat stress under climate warming. *Nature Clim. Change*, 3, 563–566, https://doi.org/10.1038/nclimate1827.

[12] Ebi, K.L. et al. (2021): Hot weather and heat extremes: health risks. *Lancet*, 398, 10301, 698-708. https://doi.org/10.1016/S0140-6736(21)01208-3.

[13] EDF Group (2026a): Actualités des unités de production de la Centrale nucléaire du Bugey - 29/06/2026, Groupe EDF, available: https://www.edf.fr/actualites-des-unites-de-production-de-la-centrale-nucleaire-du-bugey (Accessed 02 July 2026).

[14] EDF Group (2026b): Adaptation de la production de l'unité n°2 en raison des conditions climatiques - 23/06/2026, Groupe EDF, available: https://www.edf.fr/la-centrale-nucleaire-de-golfech/les-actualites-de-la-centrale-nucleaire-de-golfech/adaptation-de-la-production-de-l-unite-ndeg2-en-raison-des-conditions-climatiques (Accessed 02 July 2026).

[15] EDF Group (2026c): Adaptation de la production des unités de production de la centrale de Nogent-sur-Seine en raison des conditions climatiques - 23/06/2026, Groupe EDF, available: https://www.edf.fr/adaptation-de-la-production-des-unites-de-production-de-la-centrale-de-nogent-sur-seine-en-raison-des-conditions-climatiques (Accessed 02 July 2026).

[16] Entso-e (2026): Transparency Platform, available: https://transparency.entsoe.eu/ (Accessed 02 July 2026).

[17] Erbs, D. G., Klein, S. A., & Duffie, J. A. (1982). Estimation of the diffuse radiation fraction for hourly, daily and monthly-average global radiation. *Sol. Energy,* 28, 293-302, https://doi.org/10.1016/0038-092X(82)90302-4.

[18] Faranda, D., Messori, G. et al. (2024): A statistical physics and dynamical systems perspective on geophysical extreme events, *Phys. Rev. E*, 110, 041001, https://doi.org/10.1103/PhysRevE.110.041001.

[19] Fischer, J., Groenemeijer, P., Holzer, A., Feldmann, M., Schröer, K., Battaglioli, F., … Gatzen, C. (2025). Invited perspectives: Thunderstorm intensification from mountains to plains. *Nat. Hazards Earth Syst. Sci.,* 25, 2629–2656, https://doi.org/10.5194/nhess-25-2629-2025.

[20] Foster, J., Smallcombe, J.W., Hodder, S. et al. (2021): An advanced empirical model for quantifying the impact of heat and climate change on human physical work capacity. *Int. J. Biometeorol.,* 65, 1215–1229, https://doi.org/10.1007/s00484-021-02105-0.

[21] Foster, J., Smallcombe, J.W., Hodder, S. et al. (2022): Quantifying the impact of heat on human physical work capacity; part III: the impact of solar radiation varies with air temperature, humidity, and clothing coverage. *Int. J. Biometeorol.,* 66, 175–188. https://doi.org/10.1007/s00484-021-02205-x.

[22] FT (2026): Electricity prices soar as Europe battles heatwave, Financial Times, 25 June 2026, available: https://www.ft.com/content/5609310d-923b-47d0-b690-37a1c89e6097?syn-25a6b1a6=1 (Accessed 02 July 2026).

[23] García-León, D., Casanueva, A., Standardi, G. et al. Current and projected regional economic impacts of heat waves in Europe. Nat Commun 12, 5807 (2021). https://doi.org/10.1038/s41467-021-26050-z.

[24] Gasparrini, A., Guo, Y., Hashizume, M., Lavigne, E., Tobias, A., Zanobetti, A., Schwartz, J., Leone, M., Michelozzi, P., Haidong, K., Tong, S., Honda, Y., Kim, H., Armstrong, B.G. (2016): Changes in Susceptibility to Heat During the Summer: A Multicountry Analysis, *Am. J. Epidemiol.*, 183, 1027-1036, https://doi.org/10.1093/aje/kwv260.

[25] Grams, C. M. (2026): A life cycle definition of year-round weather regimes in the North Atlantic European region, EGUsphere [preprint], https://doi.org/10.5194/egusphere-2025-6385.

[26] Guardian (2026a): Great Britain's grid operator warns again over power supplies in heatwave, The Guardian, 26 June 2026, available: https://www.theguardian.com/business/2026/jun/26/great-britain-grid-operator-power-supplies-heatwave-neso-electricity (Accessed 02 July 2026).

[27] Guardian (2026b): Great Britain's grid operator pays £10m for extra power to avoid supply crunch tonight, The Guardian, 25 June 2026, available: https://www.theguardian.com/business/2026/jun/24/ heatwave-great-britain-grid-operator-extra-electricity-power-plants (Accessed 02 July 2026).

[28] Hersbach, H., Bell, B., Berrisford, P., Hirahara, S., Horányi, A., Muñoz-Sabater, J., Nicolas, J., Peubey, C., Radu, R., Schepers, D., Simmons, A., Soci, C., Abdalla, S., Abellan, X., Balsamo, G., Bechtold, P., Biavati, G., Bidlot, J., Bonavita, M., De Chiara, G., Dahlgren, P., Dee, D., Diamantakis, M., Dragani, R., Flemming, J., Forbes, R., Fuentes, M., Geer, A., Haimberger, L., Healy, S., Hogan, R. J., Hólm, E., Janisková, M., Keeley, S., Laloyaux, P., Lopez, P., Lupu, C., Radnoti, G., de Rosnay, P., Rozum, I., Vamborg, F., Villaume, S., and Thépaut, J.-N. (2020): The ERA5 global reanalysis, *Q. J. Roy. Meteorol. Soc.,* 146, 1999–2049, https://doi.org/10.1002/qj.3803.

[29] Hersbach, H., Bell, B., Berrisford, P., Biavati, G., Horányi, A., Muñoz Sabater, J., Nicolas, J., Peubey, C., Radu, R., Rozum, I., Schepers, D., Simmons, A., Soci, C., Dee, D., Thépaut, J-N. (2023): ERA5 hourly data on single levels from 1940 to present. Copernicus Climate Change Service (C3S) Climate Data Store (CDS), https://doi.org/10.24381/cds.adbb2d47 (Accessed on 05 July 2026).

[30] Janoš, T., Quijal-Zamorano, M., Shartova, N. et al. (2025): Heat-related mortality in Europe during 2024 and health emergency forecasting to reduce preventable deaths. *Nat. Med.,* 31, 4065–4074, https://doi.org/10.1038/s41591-025-03954-7.

[31] Kautz, L.-A., Martius, O., Pfahl, S., Pinto, J. G., Ramos, A. M., Sousa, P. M., Woollings, T. (2022): Atmospheric blocking and weather extremes over the Euro-Atlantic sector – a review, *Weather Clim. Dynam*., 3, 305–336, https://doi.org/10.5194/wcd-3-305-2022.

[32] Klimiuk, T., Sanchez-Benitez, A., Ludwig, P. et al. (2026): Regional nudged storylines for the European hot and dry summers 2018–2022: response of evapotranspiration regimes to climate change. *Clim. Dyn.,* 64, 315, https://doi.org/10.1007/s00382-026-08205-0.

[33] Kunz, M., Kottmeier, C., Lähne, W., Bertram, I., Ehmann, C. (2022): The Karlsruhe temperature time series since 1779. *Meteor. Z.,* 31, 175–202, https://10.1127/metz/2022/1106.

[34] Langner, F., Kovačević, J., Spatafora, L., Dietze, S., Waczowicz, S., Çakmak, H. K., Matthes, J., & Hagenmeyer, V. (2025). Experimental evaluation of model predictive control and fuzzy logic control for demand response in buildings. *Appl. Energy,* 401, 126666, https://doi.org/10.1016/j.apenergy.2025.126666.

[35] Lebeaupin, C., Ducrocq, V., Giordani, H. (2006), Sensitivity of torrential rain events to the sea surface temperature based on high-resolution numerical forecasts, *J. Geophys. Res*., 111, D12110, https://doi.org/10.1029/2005JD006541.

[36] Lemburg, A., Fink, A.H., Lima, M.M., Pinto, J.G. (2026): Lagrangian analysis of two flavours of Central European heatwaves: Formation under omega blocking versus initiation by subtropical ridges. *Q. J. R. Meteorol. Soc*., e70199, https://doi.org/10.1002/qj.70199.

[37] Lemke, B., Kjellstrom, T. (2012): Calculating Workplace WBGT from Meteorological Data: A Tool for Climate Change Assessment, *Ind. Health*, 50, 267-278, https://doi.org/10.2486/indhealth.MS1352.

[38] Liljegren, J. C., Carhart, R. A., Lawday, P., Tschopp, S., Sharp, R. (2008): Modeling the Wet Bulb Globe Temperature Using Standard Meteorological Measurements. *J. Occup. Environ. Hyg.,* 5, 645–655. https://doi.org/10.1080/15459620802310770.

[39] Lima, M. M., Sousa, P. M., Fuentes-Alvarez, T., Ordóñez, C., García-Herrera, R., Barriopedro, D., ... Trigo, R. M. (2026). STABLE: An open-source atmospheric blocking and subtropical ridge detection system. Environmental Modelling & Software, 195, 106729, https://doi.org/10.1016/j.envsoft.2025.106729.

[40] Miglietta, M.M., Mazon, J., Motola, V. et al. (2017): Effect of a positive Sea Surface Temperature anomaly on a Mediterranean tornadic supercell, *Sci. Rep*., 7, 12828, https://doi.org/10.1038/s41598-017-13170-0.

[41] Mohr, S., Wandel, J., Lenggenhager, S., Martius, O. (2019): Relationship between atmospheric blocking and warm-season thunderstorms over western and central Europe. *Q. J. R. Meteorol. Soc*., 45, 3040–3056, https://doi.org/10.1002/qj.3603.

[42] NIZ (2026): Lagebericht NIZ BaWü, issued 29.06.26, 14:00, available https://niz.baden-wuerttemberg.de/lageberichte/oberflaechengewaesser (Accessed 02 July 2026).

[43] NID (2026): Niedrigwasser-Lagebericht Bayern, issued 26.06.26, 15:10, available https://www.nid.bayern.de/lage/archiv/217 (Accessed 02 July 2026).

[44] Pfeifroth, U., Kothe, S., Drücke, J., Trentmann, J., Schröder, M., Selbach, N., Hollmann, R. (2023): Surface Radiation Data Set – Heliosat (SARAH) – Edition 3, Satellite Application Facility on Climate Monitoring, https://doi.org/10.5676/EUM_SAF_CM/SARAH/V003.

[45] Reda, I., Andreas, A. (2004): Solar position algorithm for solar radiation applications. *Sol. Energy*, 76, 577-589. https://doi.org/10.1016/j.solener.2003.12.003.

[46] Reuters (2026): Hungary grants Paks nuclear plant temporary exemption from cooling water rules, Reuters, 29 June 2026, available: https://www.reuters.com/business/energy/hungary-grants-paks-nuclear-plant-temporary-exemption-cooling-water-rules-2026-06-29/ (Accessed 02 July 2026).

[47] Russo, S., Sillmann, J., Fischer, E. M. (2015): Top ten European heat waves since 1950 and their occurrence in the coming decades. *Environ. Res. Lett.*, 10, 124003, https://10.1088/1748-9326/10/12/124003.

[48] RTE (2026): Canicule : la sécurité d'approvisionnement en électricité n'appelle aucune vigilance particulière, available: https://www.rte-france.com/actualites/canicule-securite-approvisionnement-electricite-appelle-aucune-vigilance-particuliere (Accessed 02 July 2026).

[49] SMARD (2026): SMARD – Strom- und Gasmarktdaten, available: https://www.smard.de/home (Accessed 02 July 2026).

[50] Sousa, P. M., Barriopedro, D., García-Herrera, R., Woollings, T., Trigo, R. M. (2021). A new combined detection algorithm for blocking and subtropical ridges, *J. Climate*, 34, 7735-7758, https://doi.org/10.1175/JCLI-D-20-0658.1.

[51] Stadt Karlsruhe (2026): Datenlizenz Deutschland Namensnennung – Version 2.0, available: https://www.govdata.de/dl-de/by-2-0 (Accessed 03 July 2026).

[52] Statistische Ämter des Bundes und der Länder (2024): Zensus 2022 – Bevölkerungszahl in 100-m-Gitterzellen. Stichtag: 15 May 2022. Licensed under Datenlizenz Deutschland – Namensnennung – Version 2.0.

[53] Szewczyk et al. (2021): Heat stress, labour productivity and adaptation in Europe—a regional and occupational analysis*, Environ. Res. Lett.,* 16, 105002, https://doi.org/10.1088/1748-9326/ac24cf.

[54] TABULA (2016): Typology approach for building stock energy assessment, available: https://webtool.building-typology.eu/#bm (accessed 6 July 2026).

[55] Taylor, J., McLeod, R., Petrou, G., Hopfe, C., Mavrogianni, A., Castaño-Rosa, R., Pelsmakers, S., Lomas, K. (2023): Ten questions concerning residential overheating in Central and Northern Europe. *Build. Environ.,* 234, 110154, https://doi.org/10.1016/j.buildenv.2023.110154.

[56] UFZ (2025): Dürre-Jahresrückblick 2025. Presse: Im Fokus „Wasser in Deutschland: Dürren und Hochwasser", Helmholtz-Zentrum für Umweltforschung (UFZ), Leipzig, Germany, available https://www.ufz.de/index.php?de=52518 (Accessed 03 July 2026).

[57] WHO (2026). Heat and health, World Health Organization, https://www.who.int/news-room/fact-sheets/detail/climate-change-heat-and-health (accessed 6 July 2026).

[58] Zink, M., Samaniego, L., Kumar, R., Thober, S., Mai, J., Schäfer, D., Marx, A. (2016): The German drought monitor, *Environ. Res. Lett.,* 11, 07400, https://doi.org/10.1088/1748-9326/11/7/074002.

Further sources (for the Section 2 "Meteorological information"):

- https://www.ncei.noaa.gov/erddap/search/index.html?page=1&itemsPerPage=1000&searchFor=OISST
- https://cds.climate.copernicus.eu/requests?tab=all
- https://www.meteociel.fr/
- https://www.mtwetter.de/
- https://www.theguardian.com/environment/2026/jul/03/weather-tracker-heatwave-breaks-june-temperature-records-across-europe
- https://www.theguardian.com/world/2019/jun/28/france-on-red-alert-as-heatwave-forecast-to-reach-record-45c
- https://wmo.int/media/news/record-breaking-heat-spreads-through-europe
- https://abcnews.com/Health/wireStory/france-records-1000-additional-deaths-extreme-heat-breaks-134291463
- https://www.dmi.dk/nyheder/2026/varme-og-uvejr-ny-dansk-varmerekord-sat-i-baade-oedum-og-odense

Further sources (for the Section 6 “Impact: Transport infrastructure”):

[1] L. Walcher, „ADAC,“ 28 06 2026. [Online]. Available: https://www.adac.de/news/reise-hitzewelle-deutschland/.
[2] „WDR,“ 27 06 2026. [Online]. Available: https://www1.wdr.de/nrw/verkehr/verkehrsthemen/re5-bonn-evakuierung-100.html.
[3] „Deutsche Bahn,“ 27 06 2026. [Online]. Available: https://www.deutschebahn.com/de/presse/Newsblog-12829716.
[4] G. Topham, „The Guardian,“ 22 06 2026. [Online]. Available: https://www.theguardian.com/business/2026/jun/22/rail-passengers-travel-heatwave-train-services-chiltern.
[5] „BBC,“ 26 06 2026. [Online]. Available: https://www.bbc.co.uk/news/live/c7vy8ql6rgnt.
[6] „Sortira Paris,“ 18 06 2026. [Online]. Available: https://www.sortiraparis.com/en/news/in-paris/articles/347633-canicule-71-trains-canceled-several-connections-from-paris-affected-until-monday.
[7] „Le Monde,“ 23 06 2026. [Online]. Available: https://www.lemonde.fr/en/international/article/2026/06/23/heat-wave-why-high-temperatures-are-wreaking-havoc-on-europe-s-trains_6754790_4.html?srsltid=AfmBOoqzF5RF7GAAMmGUG9gS6yYm40W7609Qq3eNDaymm9Mk4US8TrE1.
[8] „BMF TV,“ 24 06 2026. [Online]. Available: https://www.bfmtv.com/economie/entreprises/transports/quasiment-plus-aucun-ter-ne-roulera-en-nouvelle-aquitaine-jusqu-a-vendredi-a-cause-de-la-canicule_AV-202606240589.html.
[9] „ED News,“ 24 06 2026. [Online]. Available: https://ednews.net/en/news/country/737697-belgium-issues-nationwide-heat-alert.
[10] L. Cech, „Railmarket,“ 24 06 2026. [Online]. Available: https://railmarket.com/news/insights/58982-european-passenger-railways-shift-to-heat-response-mode.
[11] „NL Times,“ 27 06 2026. [Online]. Available: https://nltimes.nl/2026/06/27/netherlands-records-first-regional-super-heatwave-since-2020-ell-hits-304-degc.
[12] „Swissinfo,“ 25 062 2026. [Online]. Available: https://www.swissinfo.ch/eng/climate-solutions/the-heat-is-also-affecting-rail-services/91646516.
[13] „Euronews,“ 23 06 2026. [Online]. Available: https://www.euronews.com/2026/06/23/spain-faces-toughest-day-of-heatwave-red-alerts-and-san-juan-bonfires-cancelled.
[14] „Portugal News,“ 23 06 2026. [Online]. Available: https://www.theportugalnews.com/news/2026-06-23/weather-warning-issued-in-portugal-due-to-heatwave/1044409.
[15] „Frankfurter Rundschau,“ 29 06 2026. [Online]. Available: https://www.fr.de/frankfurt/unwetter-am-flughafen-frankfurt-100-fluege-annulliert-94374457.html.

Contact

CEDIM Head Office	CEDIM Spokesman	KIT Public Relations
Dr. Susanna Mohr	Prof. Dr. Michael Kunz	Christian Könemann
E-mail: info@cedim.de	E-mail: kunz@kit.edu	E-Mail: christian.koenemann@kit.edu

Subscribe to CEDIM FDA mailing list: https://www.cedim.kit.edu/english/3668.php

After registering, you will receive emails whenever the CEDIM FDA Task Force publishes a new report. Rest assured that the information you provide will be used exclusively for this purpose.